Evaluation of hygrothermal ageing damage in structural foam cored marine sandwich materials and the potential of thermoelastic stress analysis for its detection

E-M Lembessis

SCHOOL OF ENGINEERING SCIENCES
FACULTY OF ENGINEERING
UNIVERSITY OF SOUTHAMPTON

MPhil Thesis
June 2008

Preface

Abstract

This work seeks to address concerns voiced in the marine industry over the confidence of design safety factors applied to sandwich cores following reported failures in service and the introduction of new lower standards for linear foams. Design calculations largely define the safety factor for the sandwich structure based upon the performance characteristics of the laminate skins with only basic criteria for the core, in terms of section modulus, moment of inertia, core shear and density, all intended to limit skin buckling at the compressive face. Typically, the core is the most vulnerable component of the sandwich, and is assigned the lowest factor of safety with no allowance for change in the material properties over time. Much of the research on durability and the effects of environmental ageing into the degradation of sandwich materials has been generated by the aeronautical industry and has focused upon laminate composites with environmental exposure specific to flight. Further information is required by marine designers to address the knowledge gap in the estimation of risk posed by the altered response of aged cores, especially in light of the special dispensation offered to linear foams of equivalent density.

The approach adopted by this work was an experimental investigation into the effects of ageing on two medium density foam types, typical of the marine industry; a cross-linked C70.130 and a linear R63.140. Their responses to exposure and ageing were chronicled by changes in weight and fracture toughness. Fracture toughness values were obtained for a progression of mixed modes from pure tensile to pure shear, mapping the deterioration of mechanical properties over a period of accelerated ageing using a sharp edge-crack CTS-type specimen with the same configuration for all modes.
Mechanical testing revealed increasing brittle behaviour for both foam and micrographs depicted evidence of pitting and leaching of material from the cell of the R63.140. Long-term environmental exposure was simulated by

hygrothermally ageing within temperature-controlled tanks at 60°C. Cyclic conditioning indicated that periods of interruption and drying had little effect on total moisture uptake, but freeze/thaw cycles had the potential to be very damaging. The linear foam, employed for its excellent resistance to crack propagation and slam impact loading, exhibited the greatest deterioration in properties, and almost twice that of the cross-linked foam.
The superior resistance to moisture and subsequent property retention of the cross-linked foam, can be related to its smaller cell size, measured as more than half that of the linear foam despite being of the same density.

The potential and limitations of thermography to assess the response of closed-cell structural foams to damage sustained during service in the marine environment. Thermoelastic Stress Analysis (TSA), an advanced form of thermography, was the assessment technique selected as it provides non-contact, full-field data in real-time. Data from TSA was used to show the difference in behaviour between aged and unaged foams in response to local stress from a sharp edge-crack, and the different responses of linear and cross-linked foams. An established method for the extraction of crack-tip stress intensity factors from TSA data was attempted for foam, though limitations of the application arose from the local architecture of the foam cells, struts and cell walls; the foams method of stress redistribution through local cellular distortion; and the formation of interacting high stress pockets in advance of the crack-tip stresses.

Keywords: TSA, foam, hygrothermal ageing, Cedip, fracture toughness

Preface

Contents

Preface

Tables and Figures

Chapter One

Chapter Two

Preface

Symbols

Symbol	Meaning	Units
K_e	Effective stress intensity	
ρ^*	Foam density	
ρ_s	Density of solid	
T_g	Glass transition temperature	°C
ψ	Kinking angle	°
P_{max}	Maximum load applied	N
σ_Y	0.2% offset tensile yield strength	N/m^2
K_Q	Conditional fracture toughness	$MPa.m^{0.5}$
P_Q	Conditional load	N
Δ	change	
α	Angular rotation of specimen within loading rig	°
a	Crack length	m
$F_{I,II}$	Geometric function	
$K_{IC,IIC}$	Fracture toughness	$MPa.m^{0.5}$
t	Specimen thickness	
w	Specimen width	m

Acknowledgements

With many thanks to Airex for donating the material tested free of charge.

With thanks to all the technical and admin support staff at the University of Southampton.

With tremendous thanks to the academic staff at the University of Southampton, most especially to my supervisors.

Chapter One

Introduction

1.1 Introduction to Sandwich Composites and Marine Applications

The essence of a sandwich construction is to mimic the principle of increased stiffness and strength through the manipulation of moment of inertia of the cross-section that has been exploited by the classical girder 'I-beam' shape in order to evade the corresponding penalty in weight. In a sandwich composite, this cross-sectional manipulation is effected by dividing the customary glass fiber/epoxy laminae composite into an inner and outer face, separated by a light yet rigid core. The inner and outer faces or 'skins' resist the bending stresses, whilst the low density core resists the shear stresses and buckling of the panel in compression'[1]. Figure 1- 1 illustrates the I-beam principle and the allure of sandwich construction by tabulating the effect upon relative strength, stiffness and weight exhibited by the section due to increasing separation between the laminate faces.

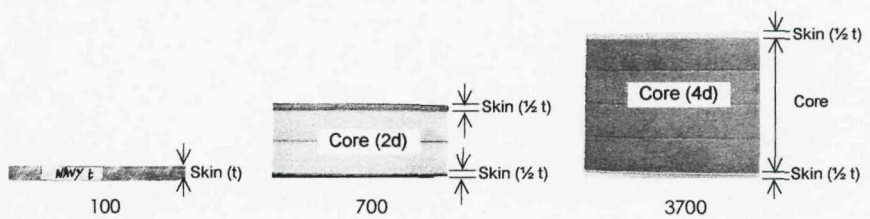

RELATIVE STIFFNESS	100	700	3700
RELATIVE STRENGTH	100	350	925
RELATIVE WEIGHT	100	103	106

Figure 1- 1 Property advantages of a sandwich composite; two skins separated by a lightweight core.

The single skin laminate is assigned a thickness of t, which is then divided by a light core of thickness d, but of negligible strength. As the moment of inertia I (proportional to stiffness), approximates to $td^2/4$, and d is

considerably greater than t, a large increase in stiffness results[2]. Sandwich composites offer an opportunity for design optimisation primarily through increased stiffness and strength without the consequence of increased weight as illustrated by Figure 1- 1. In a marine application this may translate as increased buoyancy, fuel efficiency or speed, as capitalised upon by lifeboats and sailing yachts respectively, while its material properties of insulation and low radar cross-section have been exploited for Naval applications (both surface and submersible). The largest sandwich hulls being the 72m Visby Corvette[3] and a 75m superyacht, Mirabella V, representative of current confidence limits in deflection and fatigue of sandwich construction[4].

1.2 Understanding Production Methods, Common Faults and Typically Reported Service Failures

While many recreational yacht hulls are still single skinned with stiffener reinforcement and only sandwich cored decks, sandwich designs in racing yachts are commonplace and the use of sandwich composites for motor boats is rapidly increasing. The closed-mould vacuum processing methods available to sandwich composites and the economics of mass production emphasising design simplification, durability, maintainability and environmental concerns[5] have encouraged large scale boatbuilders such as Toyota and Genmar to invest in $40M highly automated robotic plants capable of producing up to 60,000 hulls annually[6].

The specifics of production are tailored to a hull design and its scale of production, but the basic principle of the modern vacuum methods used remains the same: The fabrics that are to form the skin (carbon or more typically glass fibre) are layered in a dry state over the foam core sheets with the desired orientation and encapsulated by a vacuum bag from which all the air is removed. Under constant pressure a resin matrix is drawn through the dry fibres, infusing the skin and core in one. Uniform resin flow and distribution is assisted by a surface mesh (later peeled away), and by breather holes, grooves or scoring in the core used to contour the rigid foam to

the curvature of the hull shown in Figure 1- 2, which has been formed by a mould built over a non porous wooden plug geometrically equivalent to the end hull-form.

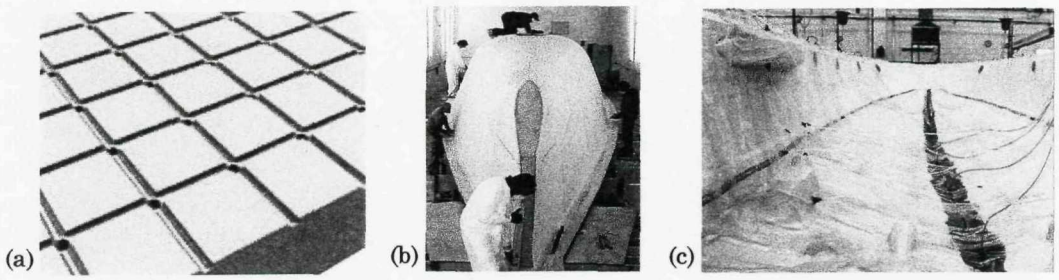

Figure 1- 2 (a) Grooves and breather holes in core for resin flow and air escape. (b) Gap filling and fairing of core prior to infusion of exterior skin of small-scale yacht built over a male plug (c) Resin infusion commencement in a female mould. It is important to optimise flow distribution uniformity especially around integral hull components.

Gaps within the core are filled to ensure structural continuity or the shear properties of the sandwich are greatly diminished. A microballoon filler with similar strength and elasticity properties to the core is preferable to allowing the infusing resin to fill the voids. Resin filled scoring results in hard spots between the faces making the panel considerably less resistant to impact. The mould is commonly female for large scale sandwich designs but the expense is forgone in favour of building over a male plug for small and custom builds as builders find resin flow easier to control over a convex surface.

In practice, vacuum infusion has greatly improved production quality and computer simulation tools allowing an infusion to be planned and problem areas anticipated, coupled with an improved understanding of sandwich philosophy in key areas such as joints have contributed to the lowered status of design as a root cause of service failures as cited by industry professionals[2-7] in the following ranking of industry concerns:

1. Inherently poor shear strength of core,
2. Moisture absorption in core and thermal radiation effects degrading material properties over time,
3. Weak or degraded bond strength of the skin/core interface. (criticism mainly restricted to skin/core bonding as a separate stage),

4. Inappropriate application of sandwich composite design and construction philosophy,
5. Quality of manufacture.

Despite the improvements in quality of construction, unless special attention is afforded to the preparation of an infusion flow, it is common for voids to not be fully infused. This invites an additional risk of damage from moisture accumulation and may cost the hull a significant penalty in weight, conflicting with one of the primary design requirements of a sandwich structure.

1.3 Limitations of Design Guidelines

The principal concern of core shear strength stems from statistics that record the most frequently reported failure mode for yachts, both recreational and those raced during the Whitbread, Vendee Globe and America's Cup challenges[8], as well as other high-speed light craft such as rescue craft and fast ferries as localised shear failure of the core with subsequent delamination of the skin. The effects are illustrated in Figure 1- 3. Recreational craft further reported delamination following localised core failure due to small-area impact or collision as common.

(a) 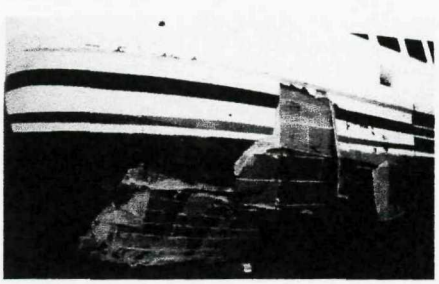 (b) 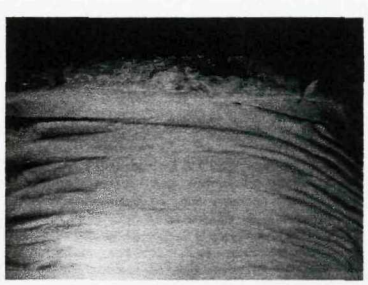

Figure 1- 3 (a) Core shear and delamination failure modes of hull following slamming impact loads.
(b) Scallop striations in core are illustrative of shear failure[9].

Industry points to such incidents as examples when voicing its frustrations over design optimisation in the literature, isolating design formulations for the greatest criticism and asserting that they are based upon test methods that do not fully incorporate slamming, fatigue, impact and environmental

effects[10] and so become proportionately unreliable with increasing vessel size[11,12,13]. In response, classification societies such as the American Bureau of Shipping (ABS), have recently reviewed and improved the requirements for high speed (HSC)[14,15] and Naval craft[16] though not yet for sailing yachts[17,18], and while the specifics vary with each rule-making body, there is a common approach. In general terms a design guideline stipulates a minimum section modulus and moment of inertia for a sandwich section dependent on the material and position within the hull with limitations on the core density and thickness and emphasis on the skin thickness. The new minimum density cited in the ABS HSC guidelines for the most vulnerable hull position is 120kg/m^3 for cross-linked PVC and 80-90kg/m^3 if the core is a linear PVC, commonly selected for its energy absorption properties and excellent resistance to crack propagation. Linear PVC receives further dispensation in shear strength safety margins with a permitted a design load of 55% the core shear strength ($0.55\tau_u$), as opposed to the 40% of cross-linked PVC cores ($0.4\tau_u$). The subscript *u* is a relic of the ABS HSC and Naval rules prior to their 2001 and 2006 revisions respectively, and refers to *ultimate* shear strength as derived from the *maximum* load per unit area sustained by the material in shear.

Figure 1- 4 illustrates sample load-extension curves for linear PVC and non-linear cores with characteristics of plastic and brittle behaviour respectively from which τ_u is calculated. The use of *ultimate* rather than *yield* shear strength in design calculations has the potential to diminish the safety margin of core materials that exhibit more plastic than brittle behaviour. In the latest ABS rule revisions for HSC and Naval craft, the τ_u term has been redefined as *minimum* shear strength and provided in a table against material type and density but remains uncorrected in other rules such as those applied to offshore yachts. In addition to which, the truncated safety margin of linear cores is based upon 4-point bend strength retention experiments conducted on virgin specimens under laboratory conditions at

room temperature (as for all specified material properties) with no specific accommodation for any potential long-term environmental effects.

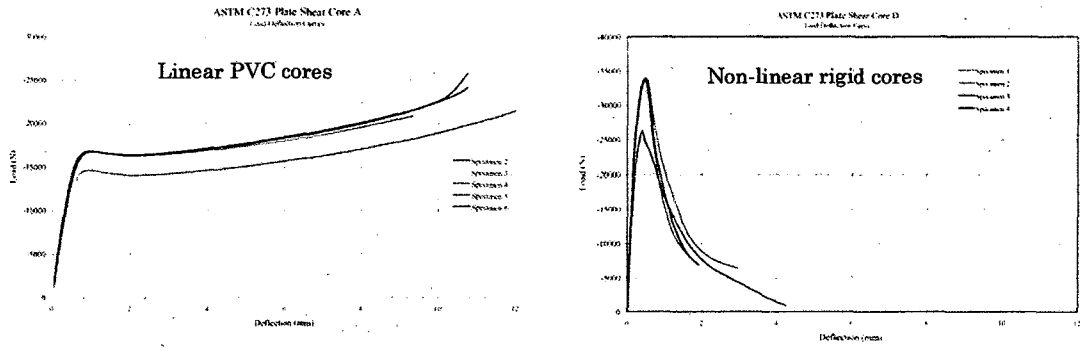

Figure 1- 4 Load extension curves for shear strength determination of (a) linear PVC cores showing plastic behaviour and (b) non-linear cores exhibiting brittle behaviour[19]

Safe design optimisation is complicated further by the introduction of ISO 12215 (small craft), a mandatory standard in Europe for craft smaller than 24m that legally supersedes classification guidelines. In a review conducted by ABS in 2004, the ISO Standard was unfavourably compared to current ABS standards, citing insufficient commitment to quality control, diminished safety margins and structural requirements as some key concerns. With respect to the core, the new ISO guidelines offer no minimum density requirement, but instead minimum mechanical properties, which for the hull are similar to those associated with cores of density 60 to 80kg/m^3 as opposed to the 100 and 120 kg/m^3 stipulated by ABS[20]. Design formulations in general are further contested in the literature on a broader basis with references to wave loading, frequencies and other hydrodynamic effects. The specifics of these arguments whilst beyond the scope of this work are worth noting as it is argued that the design hull pressures for both high speed marine vehicles[21] and sailing vessels[22] are frequently exceeded in unexceptional service conditions.

1.4 The Service Environment and Loadings on a Foam Core

Comparative measurements and impact velocities recorded by Manganelli and Wilson on a full-scale[23,24] and a 1/7th scale model[10] of an Open '60 showed

that impact velocities greater than 2.5m/s are regularly observed in service and loading is deemed dangerously close to the design limits and safety margins currently adopted for these structures assuming the structure is not weakened further still from production faults or in-service short or longer-term damage.

The core in a sandwich moulded hull must be able to transmit these loads across to the encapsulating laminate faces to maintain the integrity of the structure. Figure 1- 5 illustrates the complex shape and loading pattern of a typical sandwich composite yacht hull with possible modes of failure.

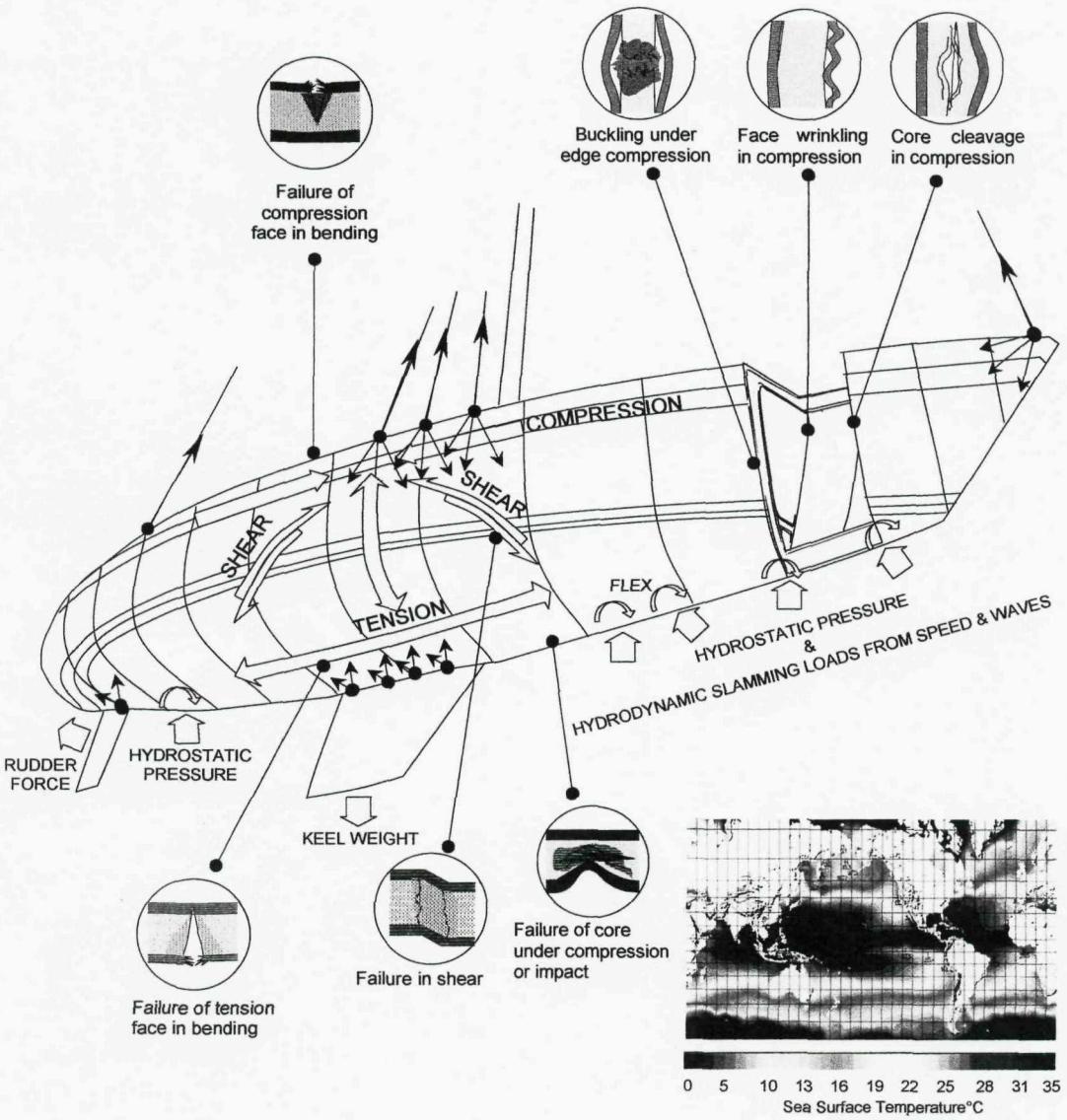

Figure 1- 5 Complex loadings on a sandwich yacht hull with potential failure modes[25]. Insert showing global sea surface temperature (°C) 3/11/2005[26].

Core materials may be at further risk from environmental factors such as moisture or thermal radiation, which may alter the material properties in either the short and long-term and where core density and composition may be pivotal. The range of service temperatures the sandwich is exposed to, is intimated by the sea surface temperatures shown in Figure 1- 5 and the Classification society rules assertion that the core must "possess good strength retention at 60°C"[16]. In practice, temperatures of 65°C are frequently recorded on the surface of white decks in Florida, and temperatures close to the 80°C softening point of a polymer core are not infrequent, while the dark pigmentation of Naval craft and some recreational yachts has resulted in deck temperatures up to 113.8°C[27]. In addition to the effects of elevated temperature upon the bulk material and mechanical properties of the sandwich, its vulnerability to moisture uptake and thermal cycling fatigue is also increased. Subsequently, seasonal exposure to freeze/thaw conditions may invite deeper microcracks and further accelerate material ageing.

1.5 Motivation for Research

The severity of environmental effects upon the core, and the implications, if any, for the design safety margin of the core are uncertain as much of the open literature is focused upon the high performance laminate skins used in the aero industry. It is clear that current design rules are inadequate to describe all the relevant material properties required for a safe yet optimised design. It is necessary to improve understanding of core behaviour to the effects of a service environment, and its response to defects such as cracks under the complex mixed-mode loading seen in service. In understanding the tolerance of the core to such damage at different stages of its service life, it may then be possible to assist designers in structural optimisation and increase confidence in the design safety margins.

In order to accomplish these aims an experimental approach is obviously necessary and raises the issue of instrumentation for damage evaluation. Conventional instrumentation such as strain gauges are bonded the specimen

surface with a resin, and relate changes in the electrical resistance experienced by its foil backing as it is moved small distances closer or further apart, to the stress experienced at the particular location to which they are adhered. The difficulty lies in the delicate and highly flexible structure of individual foam cells which may oblige the bonded gauges to relay information about the bond rather than the cell response. The application of Thermoelastic Stress Analysis (TSA), a thermographic technique is proposed as an approach in order to exploit its non-contact, non-destructive, full-field characteristics. Recent technological developments have made thermography more widely available, making it a valuable diagnostic tool for marine surveyors[28]. Figure 1- 6 illustrates the application of thermography, producing results far more accurate than a tapping hammer hitherto reliant upon the particular experience and judgement of an individual surveyor. It has additionally provided successful results in locating areas of moisture penetration where previous exploratory drilling for moisture meter readings led to unreliable results.

(a) (b) (c)

Figure 1- 6 (a) Thermal image of a boat hull exterior showing an anomaly in an otherwise uniform structure. (b) Detected anomaly marked on hull for examination. (c) Partial core sample from marked area reveals lack of bond between core and outer skin[29].

TSA supersedes thermography by combining Kelvin's principle that relates a slight change in volume of a body to a slight change in its temperature, with high resolution infra red detectors to allow this reversible *thermoelastic* effect to be quantitatively measured and proportionally related to the change in the sum of the principal stresses[30]. TSA with an early IR detector has successfully identified the stress distribution across a sandwich T-joint, and demonstrated the consequences of an unfilled space[31], however, new advances in detector technology and software analysis mean there is the potential to obtain far more detailed and novel insight into core behaviour.

1.6 Research objectives

Designers seeking to safely optimise a boat's design are hampered by the uncertainty associated with core behaviour after a period in service. The design safety margin applied to the core is determined primarily from the material response during mechanical testing, commonly ASTM C273[32], a plate shear-strength test. Additional tests may subject a material to a four-point-bend arrangement and determine shear criteria based upon shear strength retention at the fatigue half-life[33]. Excellent shear-strength retention properties of linear PVC foams have slimmed the design safety margins for a core of this material. These decisive mechanical tests are conducted upon virgin materials at room temperature where the possible effects of environmental exposure are omitted at this stage[34,35,36]. As design safety margins are being progressively shaved to accommodate new materials and new design standards, it remains unclear what portion of the design safety margin, if any, should remain in reserve to defend against potential environmental consequences.

The blanket objective of this work is to contribute to the debate.

More specifically this work seeks to:

1. Assist designers in the development of safety margins, by determining the degree of significance the exposure to a marine environment may have upon the core, and by implication, the durability of a sandwich hull built to current design standards. Using experimental observation, identify the portion of design safety margin consumed, if at all, by environmental effects, and consequently comment on the effectiveness of safety margins for the material types and densities commonly used in the marine industry.
2. Assist marine designers in the optimisation process by evaluating the latest developments in TSA for the potential to provide information on the response of a sandwich core to environmental damage over its service-life.

1.7 Novelty

To accomplish the first objective, an experimental approach is necessary based upon the identification of critical performance characteristics and properties that can serve as degradation indicators. From the volume of literature available in open publication, it is evident laminate skins related to the aeronautics industry have dominated ageing research, leaving a gap for foam cores, and with investigations of the fracture behaviour of hygrothermally aged cores in mixed loading modes yet to be published in open literature, the approach is novel. Additionally, in the event that significant change to the core properties and behaviour is evidenced during testing, the procedure may be of unique interest to designers seeking to develop predictive service life tests.

In order to accomplish the second objective listed above, it is necessary to address a number of new challenges for the TSA user:

1. Identify the differences in response, if any, between virgin and environmentally aged core materials to variants of cyclic loading such as frequency using TSA,
2. Evaluation of a damage site of an aged foam core in pure and mixed-mode loading conditions using TSA,
3. Evaluation of the potential for extracting quantitative stress intensity factors of a crack-tip from TSA data,

1.8 Report Layout

The work is structured into nine chapters. Chapter Two, *the literature review* presents a critical review of work in open publication relevant to the changes in material properties experienced by foam cores exposed to a marine environment, their response to damage such as a crack, and information applicable to the application of TSA. Chapter Three briefly describes the *experimental approach* to the research and explains in greater detail what must be done and why, in order to accomplish the research objectives. Chapters Four and Five form the basis for the first objective, and contain the

experimental arrangements and results relating to the *hygrothermal ageing* and *mechanical testing* of foams respectively. Chapter Six describes the practical issues and problems associated with TSA in the approach to the second research objective and presents the *TSA results* for the foam materials selected. A general *discussion* of the experimental results in the thesis follows in Chapter Seven. Chapter Eight presents recommendation for future work, and the *conclusions* are summarised in Chapter 9.

References

[1] Barkley,G. "A practical guide to the materials and survey procedures for FRP marine laminates" Lloyd's Register Technical Association, Paper no.2, 1991-1992

[2] Du Plessis,H., "Fibreglass boats", 3rd edition,Adlard Coles Nautical, 2002

[3] Mouritz, A.P., Gellert, E., Burchill, P., Challis, K., "Review of advanced composite structures for naval ships and submarines", Composite Structures 53, 21-41,(2001)

[4] Vosper Thorneycroft Shipbuilders; www.vosperthornycroft.co.uk

[5] Boating Industry International Magazine, "World-Wide Consolidation" May 2002

[6] Boating Industry International Magazine, "Genmars Vision" July 2000

[7] Belgrano,G."Structural Solutions" CEO SP Technology, Seahorse International, Aug 1997.

[8] "Composites I & II" Seahorse, May No. 159 (p49), & June No.160 (p34), 1993

[9] Shenoi,R., Wellicome, G. "Composite materials in marine structures" Vol.2 Practical considerations. Cambridge University Press, 1993.

[10] Manganelli,P., Wagemakers,B., Wilson,P., "Investigation of slamming loads using slam patches on a scale model of an open60' class yacht" Int. J. Small Craft Technologies p47, RINA 2003.

[11] Fan,M., Pinchin,P., "Structural design of high speed craft – a comparative study of classification requirements", Int. Conf. on Fast sea Transportation, p27-33, 1997

[12] Koelbel,J., "Comments on the structural design of high speed craft" Marine Technology,vol.32, No.2, p77-100, 1996

[13] Speer,T., " High speed craft and the design learning curve" 5th Int. conf. High Speed Marine Craft. 1996

[14] American Bureau of Shipping "Guide for building and classing motor pleasure yachts" February 2000

[15] American Bureau of Shipping "Guide for building and classing high speed craft" October 2001

[16] American Bureau of Shipping "Guide for building and classing high speed Naval craft" 2006

[17] American Bureau of Shipping "Guide for building and classing reinforced plastic vessels" 1978

[18] American Bureau of Shipping "Guide for building and classing offshore racing yachts" 1994

[19] High Modulus "A study of the effect of slamming on sandwich panels" Technical Note 2, Internal publication, January 2007

[20] Currie,R. "An assessment of ISO 12215 small craft hull construction with classification society rules" Int. Conf. Small Craft Regulations, RINA, London, October 2004

[21] Olsson,K., Lonno,A "Sandwich construction- recent research and development" Proc. 1st Int. Conf. Sandwich construction Vol.2 Florida,USA, March 1991.

[22] Joubert,P. "Strength of bottom plating of yachts" J. of Sip Research, Vol.26No.1, p45-49,March 1982.

[23] Manganelli, P., Wilson, P., "An experimental investigation of slamming on ocean racing yachts" Proc. 15th Chesapeake Sailig Yacht Symposium, Annapolis, January 2001.

[24] Manganelli,P., "Experimental Investigation of slamming loads on offshore sailing yachts" Internal report, ship Science, School of engineering Sciences, University of Southampton 2002.

[25] Larson, L., Eliason, R., "Principles of Yacht Design" Second Edition, Adlard Coles Publishing, 2002.

[26] National Oceanic and Atmospheric Administration, U.S. Department of Commerce. www.noaa.gov

[27] Greene,E., "Marine Composites" ISSC,

[28] Predmesky,R., Zaluzec, M. "Non-destructive Testing for AmericaOne" Open Paper, Ford Motor Company,Dearborn,MI.

[29] Coakley,S. "Non-destructive evaluation of composite structures using thermal imaging" Composites Fabrication, American Composites Manufacturers Association, May 2004

[30] Dulieu-Barton, J., Stanley,P . "Development and applications of thermoelastic stress analysis" J. Strain Analysis, 33(2),p93-104,1998

[31] Dulieu-Barton,J., Earl,J., Shenoi,R. "Determination of the stress distribution in foam cored sandwich construction composite tee joints" J.Strain Analysis Vol36 (6), p545-560, 2001

[32] ASTMC273-00 "Standard test method for shear properties of sandwich core materials", American Society for Testing of Materials (ASTM), July 2000

[33] Det norske Veritas (DnV), "Classification rules for High speed and light craft", 2003Edition
[34] Cheng,Y., "New special service craft rules" Lloyds Register, London, UK, internal paper no.6., 1995-6
[35] Det norske Veritas (DnV), "Examination of criteria for panel deflection in DnV's rules for high speed and light craft" technical report no.96-2014, 1996
[36] Clark,S., S., "Long-term behavior of FRP structural foam-cores sandwich beams", PhD thesis, Southampton University,1997

Chapter Two

Literature Survey

2.1 Introduction

Chapter One described the objectives of this work, discussed the motivation behind it, and placed the approach to it within context. The intention of this chapter is to identify information useful in the implementation or understanding of results in this work and establish the areas in which this work may provide a new contribution. The literature survey begins with an introduction to the core materials used in this work and includes the manner by which ageing damage of the core is initiated, the effects of ageing damage on the structural performance of the core and the methods used to accelerate and characterise the damage. The survey is concluded with a gap analysis summarising the distribution literature within open publication, to graphically illustrate the knowledge gap within.

2.2 The Foam Core, Structure and Formation

The structural foam cores selected for large-scale marine applications are most commonly known as PVC foams, though are actually a hybrid of PVC and polyurea. The original formulation of a PVC foam involved an isocyanate blend, and was created by Dr Lindermann for the Kriegsmarine in support of Germany's war effort, with rumours of early applications in E-boats and the Bismarck. Following WWII, the formula acquired by the French as a war reparation, was licensed out to companies in Sweden, Switzerland, and Germany. The original recipe has since spawned many variations and refinements, though the two main suppliers of PVC marine structural foams

remain as the US based DIAB Inc., and the Swiss Alcan-Airex[1]. It is then unsurprising, that much of the reserch funded by the US relates to the Divinycell group of materials from DIAB, while European interests are largely served by Airex.

Though other structural foams have been developed from a number of thermoset and thermoplastic polymers including polyurethane (PU), polystyrene (PS), styrene acrylonitrile (SAN), polyetherimide (PEI) and polymethacrylimide (PMI), it is the PVC group which dominates the marine market. Two types of PVC foam are available; cross-linked, and linear (both originally formulated by Lindermann). Linear PVC foams behave in a more ductile, elastic manner than cross-linked varieties and are favoured for areas of impact along the hull. The codes used by the two major suppliers to describe their cross-linked and linear products are H and HD (DIAB), C70 and R63 (Airex) respectively. Both companies have supplied cores for the two largest sandwich craft built as discussed in Chapter One, using linear PVC below the waterline as supplied by Diab for the Visby corvette and Airex for Mirabella V out of Southampton, UK. Though trade publications and fabrication professionals consider the highest quality linear foam available to be the Airex R63[2], foam formulations and production methods are constantly revised with major changes announced by DIAB for 2007.

Accordingly, the Airex R63 and C70 foams, rather than the DIAB cores were used in this work. Many foam types are typically integrated into a hull design in an effort to match the design requirements to specific foam properties, e.g. the R82 range is a PEI based foam selected for its thermal stability and used around fire hazard zones. The typical type and positioning of Airex foams as a reflection of the design requirements within a marine sandwich is shown in Figure 2- 1, where the suffix designates the density of the core in kgm^{-3}. With regard to the to environmental ageing interests of this work, the key structural foams at greatest risk would be those parts of the hull most frequently wetted and are primarily C70.130 and R63.140. The core design requirements for the hull are shown in Appendix 2A.

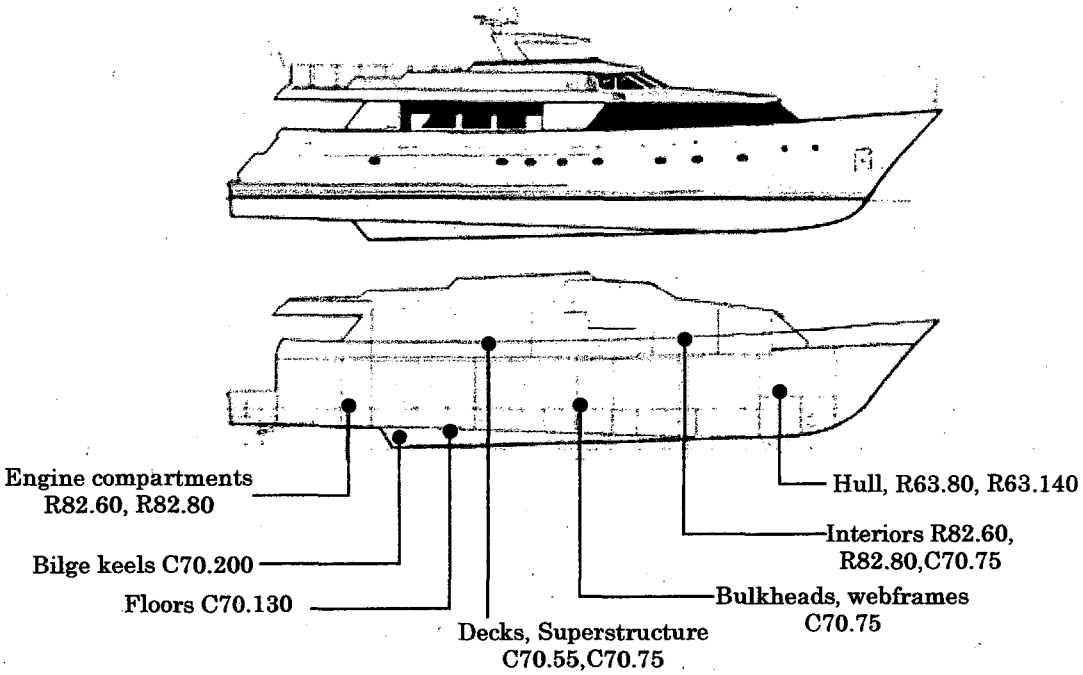

Figure 2- 1 Typical foam core types and positioning within a marine craft[3]

The single most important structural characteristic of the foam is its relative density, that is the ratio between density of the foam, to that of the solid from which it is made, however, the composition, cell size and shape are also significant factors[4]. These differences in composition and production cause differences in behaviour and materials properties and are issues to be considered before direct comparisons are made between similar *classifications* of foams such as the DIAB H, and the Airex C70 ranges. These differences must be remembered when surveying results in the literature, as the majority of published research appears to have been conducted using DIAB rather than Airex materials. For the higher densities of 130kgm^{-3} though some anisotropy exists, the cell geometry can be considered globally isotropic, and approximated as a tetrakaidecahdron[5]. The cell shape is illustrated in Figure 2- 2.

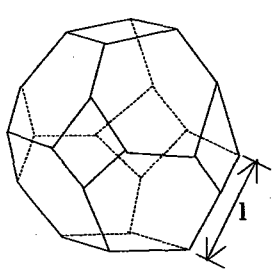

Number of Faces, f = 14
Number of edges, n = 36
Number of vertices, v = 24
Cell volume = 11.31 l^3
Surface area 26.80 l^2
Edge length = 3l
ρ^*/ρ_s=1.18 t/l

Figure 2- 2 Cell shape Tetrakaidecahedron [5].

The microstructure of DIAB closed cell cores is illustrated in the SEM micrographs below[6].

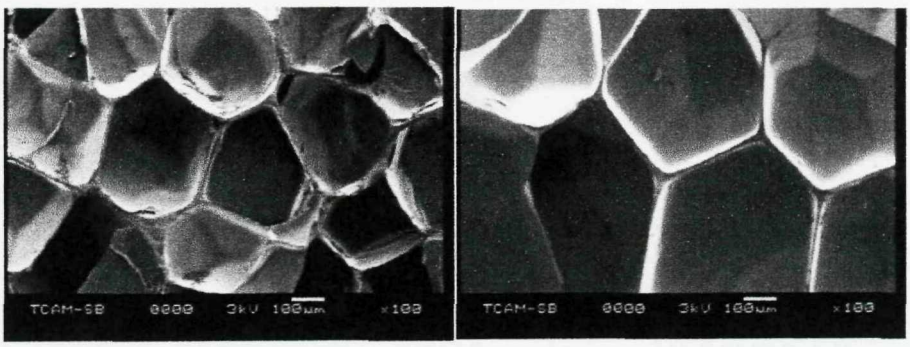

(a) (b)

Figure 2- 3 SEM micrographs of DIAB cores(a) HD130 (b) H130

Manufacturers are secretive of their foaming processes and chemical composition so only a generalised overview can be provided here. The foam cells are formed by mixing selected liquid polymers, additives and blowing agents such as CO_2 into molds[7], to allow a partial cure under high heat and pressure[8]. The resulting mass, also known as an amoeba or embryo, is demolded, placed in a second mold and re-heated again with hot water or steam in an expansion chamber. This activates the blowing agent and controls the gas expansion pressure to produce foam panels approximately 1.4 x 3m and up to 20-50 mm thick (depending on sheet density), containing closed, gas-filled bubbles or cells. The bubbles grow and stabilize as the polymer is solidified by cross-linking or cooling[9], before undergoing 'reticulation' where the faces of the closed-cells are ruptured to give an open-cell foam across the faces of the foam sheet to assist in surface bonding. Foams can be manufactured in densities ranging 30 kg/m^3 to 300 kg/m^3 by varying the ratio of the polymer ingredients to blowing agents and adjusting gas pressure. The gas, though carefully controlled does tend to elongate in the direction of rise in the face of viscous forces from the polymer melt and some anisotropy will arise[10]. The gas that is under pressure within the foam, remains so for most foams, but may escape from the closed cells over time and migrate migrates to voids or unbonded areas in the laminate and is termed *outgassing*. Though the underlining problem may be the sandwich production technique, outgassing has been blamed for accelerating

delamination and blistering in marine construction, especially in parts made at elevated cure temperatures with epoxy resin systems or finished in dark colours[11]. Airex R63 is reported to be devoid of outgassing due to its specialist processing stage where no excess gasses remain within the core.

2.3 The Sandwich in a Marine Environment

Despite encapsulation within laminate faces, the core of a sandwich is still vulnerable to hygrothermal ageing damage under service conditions as determined from surveyors and industry professionals in Chapter One.

The significance of ageing damage in cores has been discussed by Berggreen and Simonsen[12] in an investigation of the causes of debond failure modes and damage tolerance in marine sandwich hulls, with an emphasis on minesweepers. It was concluded that the commonly experienced failure mechanisms of a vessel in service such as face wrinkling, are highly imperfection sensitive, with a considerable influence on residual strength factors. Berggreen and Simonsen presented a common approach to ageing damage in sandwich structures, with a reliability index for an ageing structure, showing it to be reduced as the sandwich ages, but regained with repair when the reliability index reaches the minimum acceptable. Figure 2-4 shows the effect of the same sudden damage to the structure indicated for two different times during the structural lifetime, and shows structural integrity is suddenly reduced and the reliability index lowered. Damage is seen to be non-critical in the first damage case but critical to the second, as the reliability instantly drops below the acceptable minimum. These approaches to damage tolerance however, assume that that the degradation mechanisms are reversible or repairable.

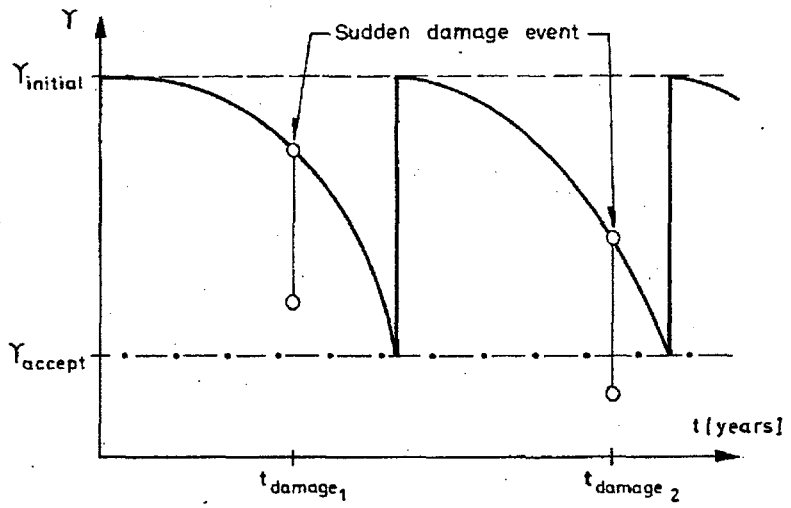

Figure 2- 4 The structural reliability index vs the ageing of the structure with a sudden damage event indicated and its effect upon reliability. (Berggreen and Simonsen)

The general degradation mechanisms that must be considered include the microstructural and compositional changes[13], time-dependent deformation and damage accumulation, moisture attack, accelerating effects of elevated temperature and the synergistic effects among them.

The more critical damage mechanisms are schematically illustrated in Figure 2- 5, which represents a three-dimensional view of a marine sandwich composite where features have been exaggerated to clarify the damage mechanism. The structure can be subdivided into layers comprising of the gel coat-a protective layer most commonly an isopthalic polyester approximately 0.5mm thick, a laminate skin which bonds of a fibre reinforcement within a resin matrix to the core.

The skin in Figure 2- 5 depicts fibres in cross-ply and woven roving formations, which are typically E-glass but may be carbon or aramid for high performance and weight-critical applications. The most economical matrix for use is an orthophthalic polyester resin which come to be superseded by the isophthalic polyester group for their superior water resistance, both of which are outperformed by epoxy resins[14]. The destructive mechanisms are labelled as 1-14 in Figure 2- 5 indicated by a bracket when referred to in the text.

Moisture is a major destructive influence and can access the sandwich core not only through gross damage (1), but more commonly via diffusion mechanisms[15,16,17,18,19,20,21,22,23,24,25] through the skin (2). All polymers are permeable to some extent due to their long chain molecular structure, allowing water molecules to diffuse into interstitial sites of the polymer molecule and bond to the polar groups of the polymer causing the resin to swell[26]. The increased distance between polymer molecules weakens intermolecular forces, reducing the glass transition temperature of the polymer to produce a plasticising effect[27,28,29], freeing the molecules to rotate and translate, making T_g dependent upon chain flexibility[30,31,32]. Figure 2- 6 schematically displays the typical bond structures of constituent materials of the sandwich shown in Figure 2- 5.

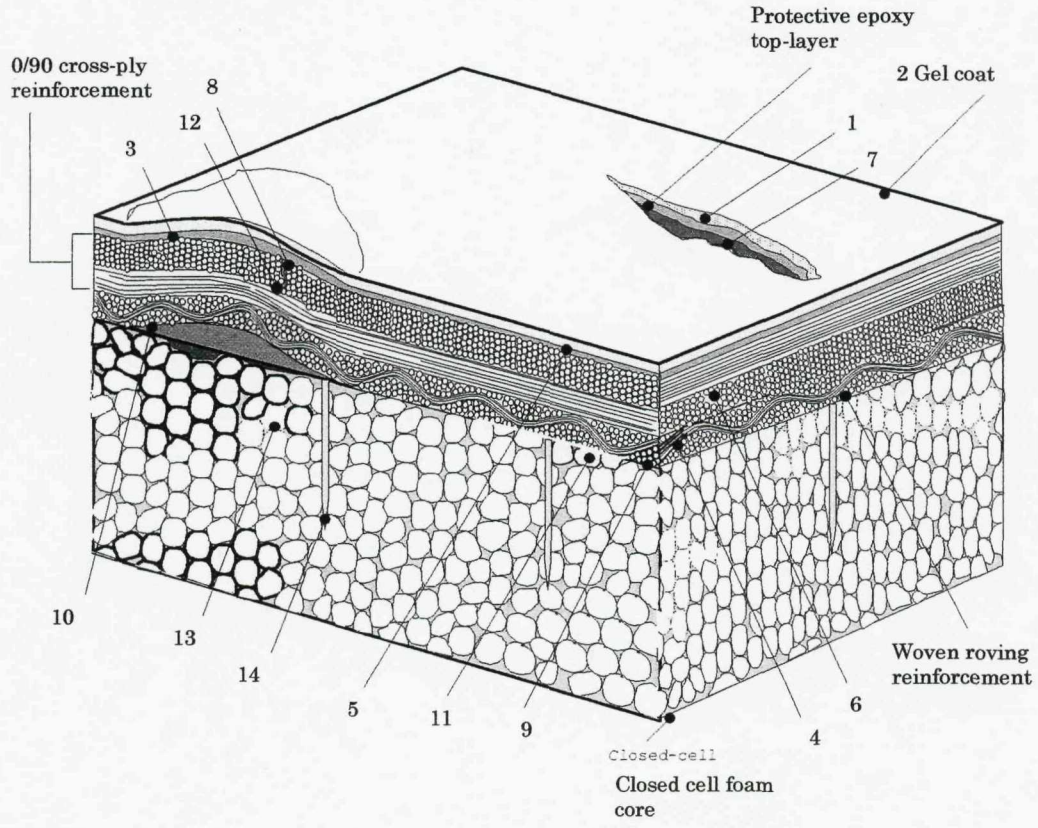

Figure 2- 5 A cross-section schematic to illustrate the damage mechanisms and moisture ingress routes of a marine sandwich composite (Size is not to scale). 1-deep exposure of fibres or core due to accidental damage such as collision or grounding; 2- diffusion through gel-coat;3- residual stress and swelling;4- capillary action along fibres; 5- un-wet fibres; 6-voids; 7- exposed fibres; 8- matrix cracking; 9- fibre sizing and weakened fibre/resin interphase; 10- delamination; 11- exposed open-cells; 12--water frozen in cavities; 13- outgassing of cells;14-manufacturing features e.g. scoring in foam panels or breather holes

The lowering of the epoxy Tg (originally 84°C), can be attributed to the p-phenylene ring, which also impedes chain flexibility, resisting the rate of moisture ingress. Though these polymers are only partly susceptible to chain-cleaving hydrolysis which causes steep loss of physical properties, the hydrophobic nature of the polymers slows the rate, but thermal activity can accelerate it, most notably for PVC[33]. The rate at which this occurs depends in part, upon the affinity that the polymer has for water determined by the number of reactive groups it contains[34,35].

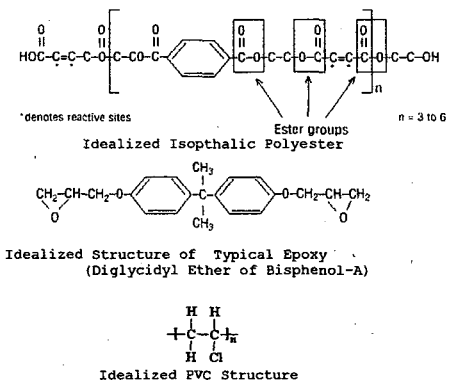

Figure 2- 6 Schematic of the bonds of the three main constituents in a sandwich composite; gel-coat, epoxy matrix skin, and a PVC based foam core.

Cross-linking can improve the strength of the polymer and hinder moisture ingress by the physical constraint of increasingly blocked pathways and molecular chains[36,37], and overrides the effect of additional polar groups formed during cross-linking that attract increased numbers of water molecules[38]. However cross-linking may become highly relevant for materials used for the foam core such as PVC, as exposure testing has shown that moisture effects are increased significantly with the addition of cross-linked plasticisers to PVC[39]. The action of swelling initiates a physical force upon any bonded substrate, or in the case of the skin, the resin /glass interface[40], and may interact further with residual stresses from manufacture(3)[41,42]
Capillary paths(4) may be opened or the presence of incompletely wetted fibres5, microvoids(6) or exposed material(7) due to damage may be capitalized upon to form moisture 'clusters'[14], which may then increase the free volume and mobility of the absorbed moisture[43]. This may lead to micro-cracking(8)[44], and significantly increased moisture absorption[45] along the

fibre-resin interface[46], and further propagation of debonding assisted by any instances of hydrolysis of coupling agents[5](8) and can lead to acidic pockets which can erode and enlarge the void(10)[47].

The chemical reactions involved create molecules that are larger than the moisture which initially diffused in, trapping them within a pocket further attracting moisture through osmosis creating an area of local swelling, while smaller molecules such as plasticizers or additives may be leached out. The process also explains the increased aggression in diffusion rate freshwater compared to saltwater which is of a higher density while smaller-moleculed leachants may migrate within the polymer and act as an electrolyte to enhance osmotic pressure within microcavities.

Diffusion rate is temperature dependent and may double with every 10°C rise or slow upon decrease, which at freezing will lead to expansion of trapped moisture(12) and accentuate internal damage such as delamination. Increasing temperature may also increase vapour pressure within foam closed-cells to cause outgassing(13) and greater susceptibility to moisture ingress. Despite the wealth of work on foams by Ashby[100], it has been proposed by Cerevenka et al[48] that the vapour transport is diffusion controlled, and that upon plasticization of the cell membrane, the surrounding hydrostatic pressure would rupture the cell and allow increased moisture ingress[48]. Cut edges and open cells(11) caused by manufacture or damage readily absorb moisture, accelerating transport of water to the core and core/skin interface, which may take further advantage of any waterways from unwet(5) fibres where the resin was absorbed by the core during manufacture.

The response of the sandwich materials to moisture as described above, may be characterised by gravimetric analysis. Figure 2- 7 presents absorption data taken from open literature to provide an indication of time-scale for the degradation processes described previously. The ordinate is presented as

[5] reinforcements are commonly coated with a binder (commonly silane based) which may remain

logarithmic scale of percentage moisture increase per °C immersion temperature. Moisture uptake determined from gravimetric analysis as maximum percentage weight increase for immersion duration on the other axis. (Specimens normalised per unit surface area if ASTM recommended coupon size of 1450mm^2 is taken as 1 unit). The complexity of polymer chemistry, variations in material composition, dimensions, processing, conditioning, and experimental practice, is beyond the scope of this work, and the test-data cannot be directly related. Instead, Figure 2- 7 is intended to provide a comparative sense of scale for the different response between foams and laminates.

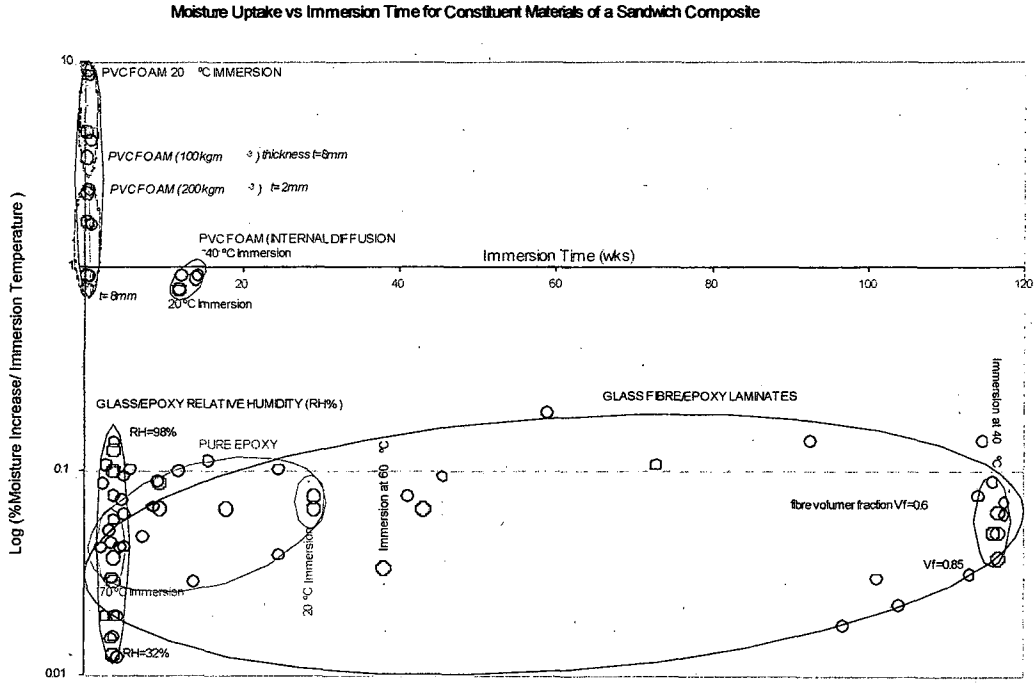

Figure 2- 7 Compilation of moisture absorption data from the references marked in tables of Appendix 2C for PVC sandwich cores and glass fibre laminates.

It is interesting to note the influence of open-cut cells compared to the initial internal diffusion across cell walls almost irrespective of density or global thickness. The minimum immersion time was one day, though due to the 120 week immersion time-scale, the PVC cores are appear as if to start at 0 weeks.

General observations that could be made from this display are :

- Even for a limited exposure time and at room temperature, increasing foam density offers greater protection against moisture ingress than tripling the thickness.

- PVC foam cores even for a 1 day immersion time at room temperature, can be expected to absorb approximately 100 times the moisture of the lowest practicable grade laminate skin at elevated temperatures.

- As an isolated process, internal diffusion for foams is significantly slower than the collective means for moisture ingress in a foam, but appears proportionately responsive to an increase in temperature.

- Relative humidity testing of glass/epoxy laminates may be a more aggressive ageing approach as the full moisture absorption range was traversed within a much more limited time frame than immersion.

- Ageing rate in relative humidity tests is largely controlled by percentage relative humidity, whereas for immersion tests, temperature is the controlling variable.

- In terms of moisture absorption alone without regard for other structural or material properties, the significance of immersion time for glass/epoxy laminates appears limited after 15 weeks irrespective of conditions. Overall, an apparent maximum absorption level is reached quickly as characterised by the pure epoxy data envelope. Prolonged immersion does not to appear achieve proportionately increased absorption of the material itself but may relate to trapped moisture within crevices and voids along fibre pathways as increasing the fibre volume fraction also decreases the percentage moisture intake. Immersion ageing involving laminates may then be considered limited to a maximum of 30weeks for room temperature immersion

rather than 120 weeks (unless examination of other material relationships are required).

2.4 Summary of Foundations of Ageing Modelling

The majority of published composite hygrothermal ageing papers are sponsored by the aeronautics sector and are generally dedicated to carbon fibre epoxy laminates[49]. Tests vary with experimenter, which can lead to anomalous information that is correlated with difficulty as the experimental variables are inconsistent[50]. A table summarizing details from the literature is located in Appendix A2-B, and shows comparisons between the materials used, the exposure conditions and some basic results. The references relating to the table are numbered with a suffix 'T'. Predictive models of moisture absorption have been well documented and generally share a common approach[51,52,53,54,55] based upon Fickian diffusion[56]. Modelling the kinetics of polymer deterioration is difficult and highly complex. There are many variables, many of which are interdependent. Not all occur simultaneously or progress at the same rate and few maintain their rate[57].

Analytical models to accurately describe the ageing of foam, the hygrothermal ageing of foam, the moisture uptake of foam, or the change in any foam property with time and service life do not currently exist[58]. The attempts that have been made, are necessarily built upon simplifications and assumptions. Core foams, as all polymers, may be formed of many functional chemical groups organised in diverse ways and combined with additives such as antioxidants, inorganic fillers, plasticizers, colorants and processing aids which when combined with variations in manufacture and in-service operational conditions, determine the degradation chemistry[59]. The most successful models to date are based upon the mathematics of diffusion[14,17,18,60,61,62,63,64,65 66]. In the engineering forum, the first and second Fickian diffusion laws are cited frequently[23,67,68,69,70] the principals for which have been well explained in a volume by Crank[71] though their full implications are beyond the scope of this current work.

2.4.1 Accelerated ageing

The primary purpose of employing an accelerated ageing technique in this research is to emulate the changes in physical properties experienced by the foam over its service life as a core in a structural sandwich in a marine environment. Despite the complexities of modelling polymer kinetics described above, it is necessary to attempt a broad synchronization of the accelerated ageing time-line with a real in-service time-line in order to establish the feasibility of the approach and provide an initial estimate for experimental immersion times and conditions. Though a significant amount of research has addressed the ageing and degradation of polymers and composites[72,73,74,75,76,77,78], few can be considered applicable to specimens other than those tested as evidenced by the variety of tests in the academic open-literature[79,80] and lack of official standards suitable for marine applications. The standards applicable to core materials are listed in Appendix A2-C.

Commonly, the accelerated ageing conditions are induced by a temperature increase beyond the service-envelope and glass transition temperature (Tg), of the polymer, the resultant microstructural changes are attributed to ageing rather than thermal degradation which may not be a true reflection of a specimen aged to the end of its service life. Analysis of the water used to hygrothermally age specimens by immersion using FTIR[1] to characterize remaining matter and determine the presence of leached substances has not been found to be commonplace[81]. These difficulties have been acknowledged in a review of accelerated ageing methods by Gates and Grayson[79] who promote the understanding of molecular morphology recommend sub-Tg temperatures as the most reliable means to accelerate ageing and concur with McKenna[82], Crissman[83], Janas[84] and Read[85] in the use of time-temperature superposition and time-ageing superposition methods[86,87]. Synchronization of accelerated and real-time lines would be achieved by matching ageing 'symptoms' of test specimens with specimens taken from carefully logged service conditions of the aeronautical structures discussed. An approximation termed the '10-

[1] Fourier Infrared spectroscopy

degree rule'[88] and is used as standard in the medical industry[89,90]. to provide a conservative estimate for the demanding applications of PVC materials. It is based on collision theory-based Arrhenius[91] model, and accelerated ageing is conducted at a single temperature to determine the approximate value that the chemical reaction rate increase by a factor Q_{10} for every 10°C rise in temperature. For PVC the typical value suggested is Q_{10}=2 unless another coefficient has been previously determined experimentally. Protocol guidelines then select the maximum test temperature possible which does not exceed the material glass-transition temperature T_g, or heat distortion temperature less a 10°C buffer[92] and a 60°C maximum limit. This is due to the decline in accuracy of the assumptions on which this method is based, as greater geometric multiplication factors are applied with a greater deviation from the ambient temperature, amplifying the error. It is of interest to note that a large selection of accelerated ageing methodologies presented in the literature apply temperature without reference to the material under examination, and temperatures in excess of 80°C are commonly[93,94,95,96,97,98]. A summary of the Ageing standards is summarised and tabulated in Appendix A2-D

2.5 Deformation and Failure Behaviour in Foam

The failure behaviour of a foam, the propagation of a crack or the path it takes, depends not only upon the loading conditions, but also upon the cell morphology of the foam[99]. The loading conditions and failure mechanisms of interest to this study were described in Chapter One.

One of the most comprehensive accounts available is by Ashby1[100] which describes, with amassed experimental evidence in support, the theoretical relationships between cell geometry and fracture behaviour under various loading conditions. From Ashby, rigid structural foams such as the C70 considered in this research, exhibit linear-elastic behaviour up to the point of fracture when under tensile stress. Under compressive stresses, an initial linear-elastic relationship is soon surpassed by a prolonged plateau of cell-collapse truncated by a regime of densification[101]. Energy absorption from

compressive loads was found by Charkravatry et al[102] to be strongly dependent on both the strain rate and foam density. The foam material exhibited a strain rate limit beyond which densification would occur and the core behaved as a solid. This limit was found to be higher for higher density foam.

On falling-tup tests producing an impacting compressive load as conducted on low density foam by Erickson et al[103] , the energy absorption from a low-velocity impact increased with increasing temperature, but *decreased* by the same amount for a high velocity impact over the same temperature range. However, residual strength of the sandwich panels tested remained unaffected by temperature for both impact velocities. The effect of temperature on impact behaviour was attributed to a combination of the temperature dependence of the constituent materials at 75°C, and a change in damage mechanisms.

In shear, the stress-strain curve displays similarities to both tensile and compressive loading scenarios, though influence of shape anisotropy is more pronounced as the thin cell walls are substantially weaker in compression than tension, the dominating failure mechanism in the initial stages of shear is shown to be buckling, and plastic folding of the cells. The structural performance of the foam increases as the ratio between solid material/cell-volume increases, so that higher density foams are structurally more sound. Shear testing conducted by Kanny et al[6] on PVC HD130 and H130 cores adhered to steel plates, one of which was pulled to effect a shear force, and indicated that failure would be preceded by the formation of micro cracks just below the interface. The cross-linked H core was seen to develop approximately 15 microcracks with a quasi-brittle fracture surface, but the HD would formed more than 20 microcracks and behaved in a more ductile manner. The cracks then coalesced into a dominant crack and propagated parallel to the steel plate before kinking at 45° and propagating toward the moving plate.

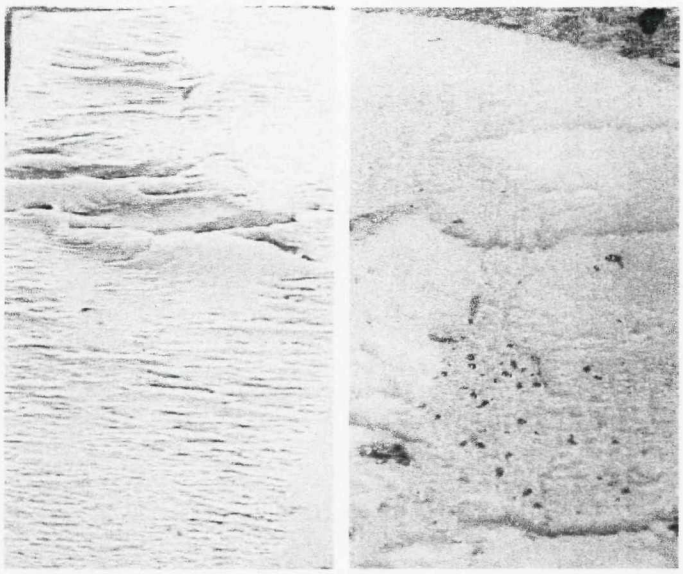

(a) (b)

Figure 2- 8 Shear fracture surface of DIAB cores (a) HD130 (b) H130

The tensile and fracture behaviour of PVC foams was experimentally and systematically studied by Kabir et al[104] using tensile prismatic bar specimens and mode-I fracture tests were performed using single edge notched bend (SENB) specimens under three-point bending. The tensile behaviour of H130 and HD130 foams as illustrated in Figure 2- 9, was found to be very similar which they asserted indicated that cross-linking and cell orientation had a minimal effect on the tensile strength and stiffness especially when compared to the distinctive trend for density in Figure 2- 10. The maximum stress was taken as the tensile strength, and the yield stress is calculated based on the 0.2% offset method.

However cross-linking was reported to have a significant effect on the fracture toughness, with higher cross-linking resulting in lower fracture toughness. This was explained as being due to the 40% smaller cell size lesser of the HD130 foams compared to H130 foam, which yielded a lower length-to-thickness slenderness ratio for this material and made its cells less prone to buckling, thus increases its fracture toughness. Another reason suggested by the authors was the crack path; the greater number of faces, cells and solid edges of the HD130 foam making it an intrinsically tougher material.

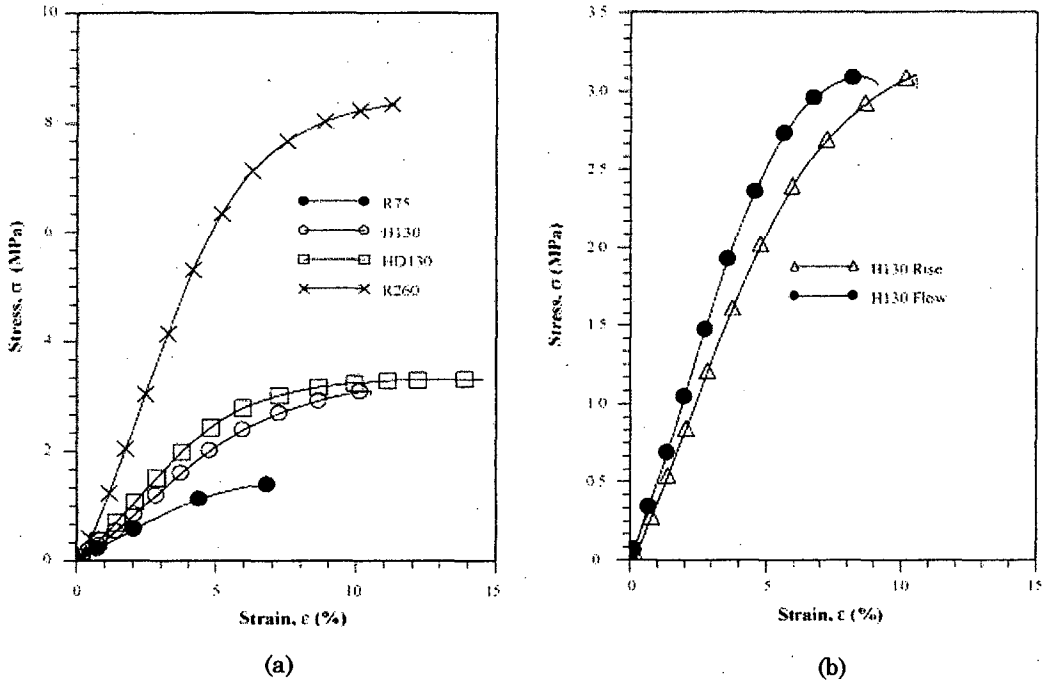

Figure 2- 9 (a) Tensile response of H130 and HD130 in flow direction, (d) Tensile response of H130 in flow and rise directions of cell orientation (Kabir et al)

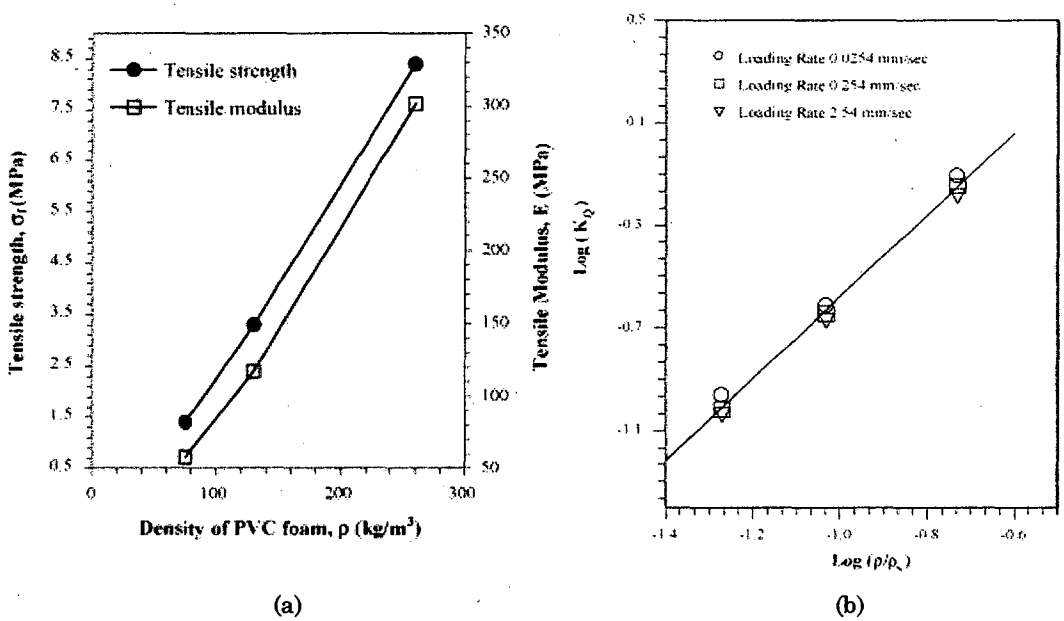

Figure 2- 10 Experimental tensile properties of DIAB H core with respect to increasing density (Kabir et al) (a) Tensile strength and tensile modulus vs density of core (b) fracture toughness vs relative density of PVC core

As there is no ASTM standard for Mode I fracture toughness of foams, Kabir et al relied upon ASTM standard D5045 and conducted a parametric study on single edge notch bend (SENB) specimen dimensions. Their results are

reproduced in Figure 2- 11, and show that fracture toughness for H130 decreased until a stable value achieved at 35mm, though width had no effect.

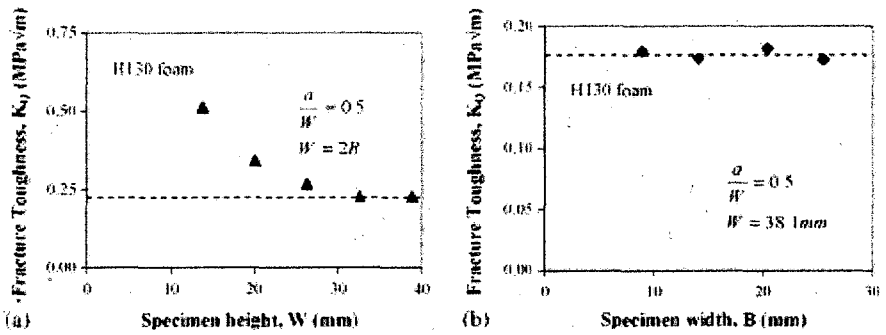

Figure 2- 11 Effect of SENB dimension variation on fracture toughness in mode I (a) specimen height (b) specimen width

The tensile response of a hygrothermally aged foam will differ if it is tested in an in-situ or dry condition. Without encroaching into molecular polymer chemistry, if tested in the wet condition, the presence of water molecules within the polymer chains act as lubricant serving to procure plasticizing behaviour. If a specimen is tested in the aged, but dry condition, the loss of leached plasticizers and stabilisers, may induce brittle behaviour. The differing responses are shown schematically in Figure 2- 12. The linear elasticity seen is caused by cell wall bending and stretching[105].

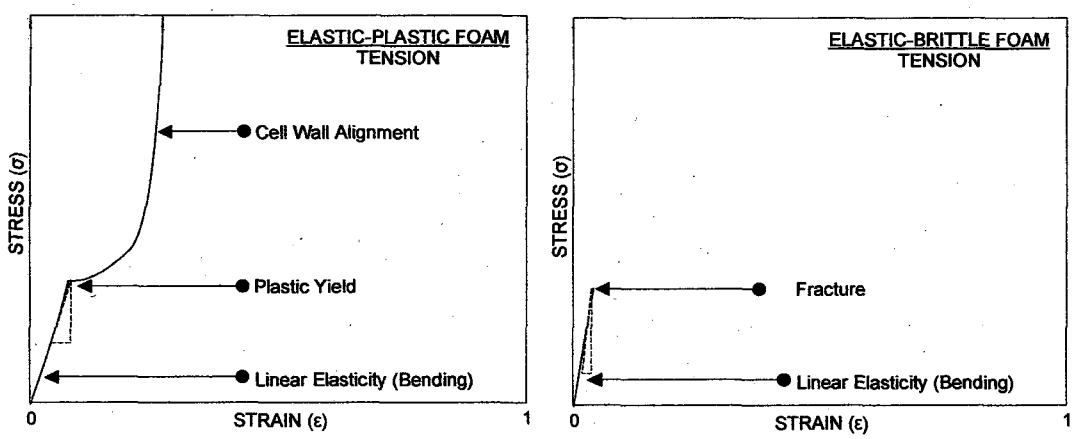

Figure 2- 12 Schematic tensile stress-strain curves for elastic-plastic and elastic-brittle behaviour of foams.

In the plastic foam, the cell walls undergo plastic bending and rotate towards the tensile axis to yield to produce a rising stress-strain curve until

fracture[106]. The brittle foam linear stress-strain curve is quickly truncated by fracture as a crack nucleates at a weak cell or pre-existing flaw causing cell wall failure, which is fast in tension, but more resilient in compression.
Li and Weitsman[107]determined from face/core debonding fracture tests on sandwich beams of H100 and H200, that sea water immersion at room temperature had caused irreversible damage to the microstructure about the crack-tip. It was found that seawater absorption at the crack-tip region had decreased the debond fracture toughness values of the foams by 36% (H100), and 17% (H200). The plasticizing effects of moisture were noted by an increase in toughness by 31%(H100) and 8% (H200).

The properties of the core are also seen to change when it is exposed to variations in temperature of the scale seen in service as described in Chapter One. The effects of temperature on C70 and R63 (presented in Appendix 2E) were obtained by private communication from Airex as details remain unpublished in open literature. It was reported that the effects were dominated by the composition and the processing technique, with the behaviour of R63.140 very similar to that exhibited by R63.80. The shear strength and modulus of the C70.130 drops by 10% for a 10°C increase from room temperature. The R63.80 is twice as sensitive and suffers 20% loss in property for the same temperature increase. These results correspond to changes observed in high strain rate compression tests by Thomas et al for DIAB H130 and HD130 foams at different elevated temperatures[108]. It was found that the amount of recovery the foam underwent could be influenced by cell size. From SEM microscopy, Thomas et al observed that the DIAB HD130 foam was possessed of a smaller cell size and contained a lesser internal gaseous volume than its cross-linked counterpart. It was concluded that this lesser internal volume therefore provided a lesser restoring force and supported findings from a previous study that found the impact response of higher density and smaller celled foams, recovered least at elevated temperatures[109]. It was also observed noted that at a low strain rate, the H130 outperformed the HD130, but the properties were reversed for a high strain rate regime.

The fracture of foams is commonly discretized into steps of one unit cell width[110], progressing when the crack-tip stress is sufficient to cause the nearest cell wall to fracture[111]. Relationships developed by Ashby and supported by experimental data collected by Brezny and Green[112,113,114], treat the cells as a construction of beams and struts and calculate forces using bending moments and is dependent upon the mechanical properties of the cell wall material[115]. A stress intensity factor approach yields fracture toughness values for a global foam structure as a function of density, an approach apparently validated by successful application to four cell geometries of a PUR foam by Folwkes[116]. Other hypothesised approaches to characterise the average cell diameter as an average flaw size for implementation in Linear Elastic Fracture Mechanics (LEFM) has been generally found to be inadequate, where work by McIntyre and Anderson has determined that the inherent flaw size is greater than the average cell diameter[117]. Further investigations conducted most notably by Zenkert reveal that the mode I fracture toughness of the marine grade structural foam will increase linearly with a corresponding increase in average cell size and applications of LEFM were shown to be successful in predicting an apparently higher mode II fracture toughness[118]. In-depth studies conducted by Zenkert have also shown that mixed-mode and mode II crack propagation may be predicted by the strain energy density function as proposed by Sih[119], and found to be comparable to the hoop stress[120] criterion for accuracy. Other experiments on crack wedges have supported the opening stress-criterion supported by Grenesdtedt[121], however, all these tests were conducted using the traditional means of applying a mixed mode or shear force such as four-point bend tests on sandwich beams. It is only work conducted by Noury[122] that has used the same specimen in a rotating test rig to obtain full range mixed-mode conditions. Noury's findings supported the accuracy of the hoop stress criterion as an estimate, second only to a criterion specifically developed to the test-specimen configuration.[123] The principles of the Noury rig and a comparative critical review of alternative methods for obtaining mixed-mode failure in cores is presented in Appendix 2F.

Direct measurement of cell-wall moduli using conventional testing has proved difficult due to the small size of the specimens and the variation in their cross-section along the length[100,124,125]. Commonly slip or local deformation at loading points where the specimen is gripped mechanically or adhesively, can result in underestimation of the true modulus. The most reliable method has been judged to be ultrasound [100,126,127]. Further studies by Brezny and Green[128] calculated fracture strengths from painstaking fractographic analysis of broken cell walls, from which the incipient crack-size was inferred and combined with the known material fracture toughness, and is referred to by Gibson and Ashby as "approximate, but better than nothing"[100]. It becomes evident from the literature, that there is scope for an improvement in the techniques used to obtain stress data about a damage site in a foam core. Introduced in Chapter One, Thermoelastic Stress Analysis (TSA) is a full-field non-contact method which can remotely provide information on the surface stress field of a structure. TSA has provided promising results for composites, able to visualise the stress surrounding a crack-tip. The methodology was first published by Stanley and Chan[129] by examining cracks propagating from a small hole in a large plate (with crack length to plate width ratios from 0.1 to 0.3), to derive a relationship between the stress intensity around a crack-tip, and the detector signal. Full mathematical derivations of their now established findings have been reviewed fully in the literature [130,131,132]. Another a full-field, non-contact technique that has benefited from recent technological advances is Digital Image Correlation (DIC). DIC uses two camera devices to effectively track the movement of the naturally occurring, or applied surface pattern during the test. This is done by analysing the displacement of the patterns within the discretised interrogation windows of the whole image. The maximum correlation in each window corresponds to the displacement, and this gives the vector length and direction for each window[133]. Though unavailable for this work at the time, DIC shows great potential for foam core testing, despite little information on the application found in open literature at the time of writing. A critical comparison of detection techniques applicable is listed in Appendix 2G.

2.6 TSA, Applications and Implications for Foam

The theoretical principles of TSA are based upon the thermoelastic effect first formulated by Lord Kelvin in 1853[134], though experimentally, the full potential of TSA could only be realised through the recent advances in high resolution infrared detectors. The TSA system used in this work is the Cedip Silver system. The principles behind TSA are well documented and need only be summarised briefly here,[135] and additionally many of the algorithms concerning the operation of the system are both highly complex and confidential. It is therefore the purpose of this section to provide a brief and functional understanding of the TSA system used in this work in order to interpret results, rather than a dissemination of the operation and the validity of the principles behind it.

2.6.1 The thermoelastic effect

The founding tenet of TSA is that all materials experience a change in temperature if their volume is changed by an applied force. Induced either by a compressive stress (which heats the material), or by a tensile stress (which cools it). Under cyclic stress,(typically sine wave form), the net prevailing load, compressive or tensile, determines whether the stressed object is heated or cooled, the reversible conversion of this mechanical/thermal energy causes the thermoelastic effect. The material must not be stressed beyond its elastic limits with no significant transport of heat between loading and unloading the object or the energy conversion can no longer be considered reversible. The latter is accomplished by ensuring the load is applied rapidly arresting any significant conduction.

The Cedip system comprises of a 320x256 focal plane detector array, (that is essentially a photon counter), with a frame rate possible of up to 380Hz. with associated complex signal processing software. The photonic energy detected emitted by the specimen as it cycles under a load, is essentially *counted* and registered as an electrical voltage which is expressed as a Digital Level (*DL*). Figure 2- 13 illustrates the arrangement of the TSA system for operation.

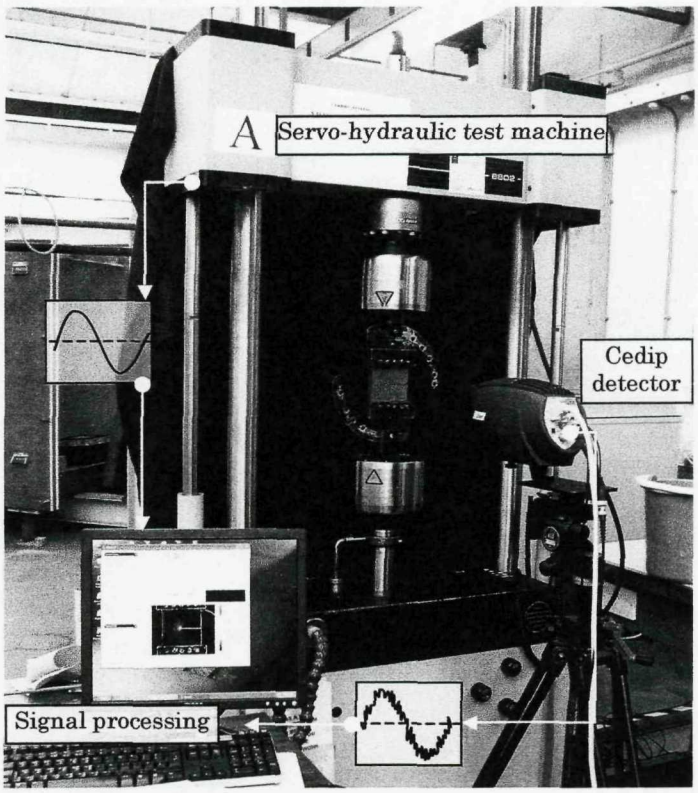

Figure 2- 13 Illustration of Cedip operational arrangement and signal processing software

The associated signal processing software Altair can then correlate the measured signal to that of the *ideal signal*, by relating to a reference signal that is input from the cycle-inducing test-machine. The algorithm used is a relationship similar to the least mean square methods but essentially the signal is mixed with a reference signal that has been cleaned and normalised in signal processing, then and the time-lag difference or phase between the reference and the detected signal may be provided (stored as a *ptp file). Altair is also able to return a change in the peak to peak value of the signal, the conventional TSA result for ΔT. The system works in DL as a *base unit*, before using an algorithm and factory pre-set temperature calibration tables to return data as a calculated temperature in units of °C. The DL signal for each pixel is first converted to T, before the difference between the peaks is calculated (stored as *ptw). The algorithm used by Cedip to calculate temperature is expressed as:

$$Q = \tau_{atm} [\varepsilon * f(T_{object}) + (1-\varepsilon) f(T_{background})] (1-\tau_{atm}) * f(T_{atmosphere}) \qquad \textit{Equation 2- 1}$$

Where Q is the quantity of radiation, ε is the emissivity, T_{object} is temperature of the object (K), $T_{background}$ is the background temperature (K), though is actually measured by a detector behind the lens, and τ_{atm} is the transmission factor in atmosphere %. f is a calibration factor which defines the experimental constant and uses non-linear look-up temperature calibration tables from a calibration file-manager that Cedip have determined to compensate for the system and for any increase in camera body temperature during operation.

The Cedip manual describes the relationship between thermal stress and strain in an isotropic, elastic element as given by the following equation:

$$\Delta\varepsilon = \frac{(1-2\nu)\Delta\sigma}{E} + 3\alpha\Delta T \qquad \textit{Equation 2- 2}$$

where $\Delta\varepsilon$ is the change in the sum of principal strains, $\Delta\sigma$ is the change in the sum of principal stresses (Pa), E is Young's modulus (Pa), ν is Poisson's ratio, α is the coefficient of linear expansion (K^{-1}), ΔT is the change in temperature (K). $\Delta\varepsilon$ and $\Delta\sigma$ are described as invariants that are more scalar than vector. The relationship for the thermodynamic analysis of the reversible, adiabatic behaviour of a stressed, elastic element is provides by Cedip as:

$$\Delta T = \frac{-3T\alpha K\Delta\varepsilon}{\rho C_v} \qquad \textit{Equation 2- 3}$$

where T is the absolute temperature (K), K is the bulk modulus (Pa) ρ is the density ($Kg.m^{-3}$) C_v is the specific heat at constant volume ($J.\ kg^{-1}.K^{-1}$). $\Delta\varepsilon$ is the volume dilatation, so from the relationship in Equation 2-2, if there is no volumetric change in the element (pure shear for example), then there will be no change in temperature under elastic conditions. By using the known relationship between Cv and Cp, the specific heat at constant pressure, Cedip combined equations *1* and *2* to form the following basic equation describing the thermoelastic effect for an isotropic material (foam):

$$\Delta T = -\frac{\alpha T}{\rho C_p}\left(\Delta\sigma_x + \Delta\sigma_y\right) \qquad \textit{Equation 2- 4}$$

This relationship showing that for the small temperature change, ΔT, is directly proportional to the change in the sum of principal stresses in the material, Δ (σ_x+σ_y), is only valid if adiabatic conditions prevail and achieved by cyclic loading, recommended at a frequency greater than 3Hz, to achieve the reversible effect between mechanical and thermal energy. The thermoelastic coefficient K_m is given by:

$$K_m = \frac{\alpha .}{\rho C_p} \qquad \textit{Equation 2- 5}$$

and not to be confused with the relationship between detector signal S, and stress summarised below[132],

$$S = \frac{\Delta\left(\sigma_x + \sigma_y\right)}{A} \qquad \textit{Equation 2- 6}$$

where A is a constant dependent upon the system parameters, the material and the surface condition. S is representative of DL as recorded in the TSA mode of the systems (i.e.ΔDL though still depicted as a DL unit)

For the purpose of these experiments the value of A (inclusive of all variations in system and specimen), is determined experimentally as an initial stress value can be obtained directly from the applied load and the cross-sectional area of a specimen loaded in uniaxial tension. Though in theory, mode II, pure shear cannot be detected using TSA, it is expected that the presence of a crack would create a complex stress field within the foam, which should allow mode II to be detected.

The assumptions of the thermoelastic relationships above, require isotropic and adiabatic conditions to be respected. With regard to the application of TSA to foams, successful TSA and FEA modelling conducted by Earl on a sandwich T-joint[136] assumed the core to be isotropic, and fatigue tests and a comparison of stress intensity factors for closed-cell foams conducted by Noury[122] in both x and y directions of foam rise concluded that the tested

foams of Airex closed cell C70.90,130 and 200 showed only a 5.83% difference between orientations for the highest density in mode I and 2.93% for mode II. Experimental observations made with regard to differences in the cell morphology with respect to direction of rise, treat the foam microscopically, rather than as a bulk material, additionally, from Noury's findings, a higher density foam of 130kgm^{-3} may be approximated homogeneous, as significant changes were observed predominantly in mode II for a core of 90kgm^{-3}.

With regard to the adiabatic requirement, occurrence of non-adiabatic behaviour has been addressed frequently and most notably for metals and well summarised by Dulieu-Barton and Quinn[137] who identify three key influencing factors listed in order of severity:

i. *Geometry dependent factors*- such a geometric feature which creates a temperature gradient and therefore a stress gradient.
ii. *Material dependent factors*- such as material thermal conductivity which relates to thermal diffusivity ($\gamma = k/\rho C_p$).
iii. *Test dependent factors* – Selection of applied loading frequency, or paint coatings.

Heat conduction is theoretically minimised in the examination of a low thermally conductive material[138], but in a practical experimental sense is not expected to be absolutely absent. The size of the affecting heat conduction zone is proportional to the thermal conductivity of the material, extending radially from the plastic region of the crack-tip. Examination of the TSA-signal magnitude and phase data along the straight-line crack-path originating from the crack-tip provides an indication of nonadiabatic severity, which in the case of high thermally conductive materials can differ from theory by up to two orders of magnitude for a sharp crack-tip.
Non-uniform hygrothermal ageing of the foam specimens is expected to have an effect if there is a loss of plasticizers and stabilisers causing an increase in the bulk brittleness of the specimen, it is possible some increase in thermal conductivity may have implications for a possible plastic zone about the

crack-tip. The thermal conductivity of the polymer would still be very low compared to other materials such as epoxies. To put foams within context, if aluminium alloys possess thermal conductivities in excess of 200W/mK, steels are approximately 45 W/mK, low thermally conductive epoxies are 0.5W/mK solid PVC is 0.12 W/mK, while foams exhibit the lowest known values of thermal conductivity at approximately 0.03W/mK. In a practicable sense, foams may be considered the ideal non-adiabatic material.

Standardisation of surface emissivity commonly achieved by layers of non-reflective spray paint may not be possible for foams with irregular surfaces of open cut cells. Additionally, experimental testing conducted by Dulieu-Barton and Quinn[137] indicated that TSA signal could lose approximately 7.5% of its signal strength with every coating of spray paint, and be further attenuated by the presence of irregularities in the paint surface.

2.6.2 Stress intensity factors from TSA

Much of the work on stress around a crack-tip has been conducted primarily for metals, for which there have been numerous publications[139,140,141].

The method most widely used referred to was initially determined by Stanley and Chan[129] then developed by Stanley and Dulieu-Smith[130,131],a technique based on the fact that isopachic contours in the crack tip region generally take the form of a cardioid which is a known mathematical shape. From geometric calculations stress intensity factors can be derived. Though other methods were developed [142,143,144,,145] with reference to section 2.5, and Noury's work on fracture of PVC foams, can be described with Linear Elastic Fracture Mechanics (LEFM). The basis for which is the Westergaard equations[146] which is given below for completeness where K_1 and K_2 are the mode I and II stress intensity factors respectively and x,y,r, and Θ are co-ordinates (both Cartesian and Polar) as shown in Figure 2- 14.

$$\begin{bmatrix}\sigma_x\\ \sigma_y\\ \tau_{xy}\end{bmatrix} = \frac{K_1}{\sqrt{2\pi r}}\cos(\theta/2)\begin{bmatrix}1-\sin(\theta/2)\sin(3\theta/2)\\ 1+\sin(\theta/2)\sin(3\theta/2)\\ \sin(\theta/2)\sin(3\theta/2)\end{bmatrix} + \frac{K_2}{\sqrt{2\pi r}}\begin{bmatrix}-\sin(\theta/2)(2\cos(\theta/2)\cos(3\theta/2))\\ \sin(\theta/2)(2\cos(\theta/2)\cos(3\theta/2))\\ \cos(\theta/2)(1-\sin(\theta/2)\sin(3\theta/2))\end{bmatrix} + \ldots - \sigma_{0X} \quad \textit{Equation 2- 7}$$

The final term σ_{0X} compensates for differences in the applied-stress field but is commonly treated as extraneous[130,147,148]. It is important to note that the Westergaard equations are only considered valid if there is no interference to the crack-tip stress field by other factors such as edge effects[149]. Combining with the TSA equations and neglecting the higher order terms from the Westergaard equation Stanley and Chan were able to obtain the familiar relationship;

$$\sigma_x + \sigma_y = \frac{2K_1}{\sqrt{2\pi r}}\cos(\theta/2) = \sigma_1 + \sigma_2 = AS \qquad \textit{Equation 2- 8}$$

Graphically plotting $\sigma_x+\sigma_y$ provides what is visually recognisable from TSA images as a cardioid curve. A term first used by de Castillon in Philosophical Transactions of the Royal Society in 1741, the specific geometry of a cardioid curve has been used to provide the location of the crack-tip[150] by using TSA data as software programme input. More sophisticated curve-fitting has been recently developed based on Genetic Algorithms and Differential Evolution[151]. Curve fit programs are commonly employed to smooth the raw TSA data, to compensate for experimental noise and obtain an image closer to the theoretical ideal of the cardioid. Figure 2- 14 depicts a representation of the cardioid geometry present at a crack-tip which can be defined as the trace of a point on a circle that rolls around a fixed circle of the same size. A crack subjected to load produces a cardioid which rotates about the crack-tip in response to mixed-mode loading.

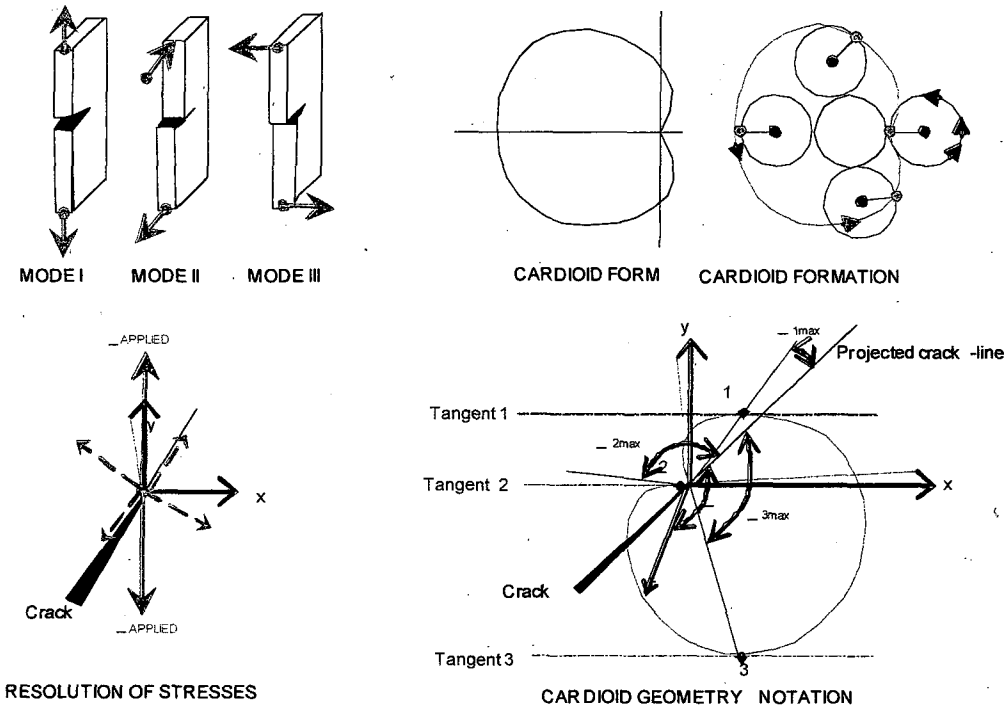

Figure 2- 14 Geometry of a Cardioid and crack-tip exaggerated for clarity.

There are three parallel tangents to the cardioid with any given gradient separated by 120°; the tangents at the ends of any chord through the cusp point of the cardioid are at right angles; and the length of any chord through the cusp is 2a; the curve perimeter is 8a; and the area $3/2\pi a^2$. Derivation of the mixed-mode stress intensity factors from TSA data and cardioid geometry developed by Stanley and Dulieu-Smith[152] (1993), to incorporate K_2 in the form:

$$AS = \frac{2\sqrt{K_1^2 + K_2^2}}{\sqrt{2\pi r}} \cos\left(\phi + \frac{\theta}{2}\right) \quad where \ \phi = \tan^{-1}\frac{K_2}{K_1} \qquad \textit{Equation 2- 9}$$

and when re-arranged for r becomes:

$$r = \frac{K_1^2 + K_2^2}{\pi A^2 S^2}\left[1 + \cos(\theta + 2\phi)\right] \ and \ so \ r_{max} = \frac{2(K_1^2 + K_2^2)}{\pi A^2 S^2} \qquad \textit{Equation 2- 10}$$

From the particulars of cardioid geometry r_{max} is the length of any full chord through the cusp of the curve, and the area enclosed by the curve shown in Figure 2- 14 is denoted Σ, and is related to r_{max} by

$$\Sigma = \frac{3\pi r_{max}^2}{8} = \frac{3}{2\pi}\left[\left(K_1^2 + K_2^2\right)/A^2S^2\right]^2 \qquad \textit{Equation 2- 11}$$

If the line of the crack is represented by θ=0, then let between the crack and the x-axis be known β' and by substituting r=y/sin(θ+θ) into Equation 2-12 (also Equation 2-8)

$$\sigma_x + \sigma_y = \frac{2K_1}{\sqrt{2\pi r}}\cos(\theta/2) = \sigma_1 + \sigma_2 = AS \qquad \textit{Equation 2- 12}$$

obtaining the partial derivative, solving for when it is equal to zero to obtain solutions of the σ_{max} tangents for a specific S value, Stanley and Dulieu-Smith derived a SIF relationship which they renamed C_1

$$\tan\left[\frac{3\theta_{max}}{2} + \beta\right] = \frac{K_1}{K_2} = C_1 \qquad \textit{Equation 2- 13}$$

Similarly equation 2-11 is rearranged:

$$K_1^2 + K_2^2 = A^2S^2\sqrt{\frac{2\pi\Sigma}{3}} = C_2 \qquad \textit{Equation 2- 14}$$

So the individual SIFs can then be described as

$$K_1 = \left[C_1C_2^2\left(1 + C_2^2\right)\right]^{1/2} \qquad \textit{Equation 2- 15}$$

$$K_2 = \left[C_1\left(1 + C_2^2\right)\right]^{1/2} \qquad \textit{Equation 2- 16}$$

These equations commonly form the basis of cure-fit routines such as Fracture Analysis of Crack-Tips Using SPATE (FACTUS) developed by Dulieu-Barton et al[150] which provided increased accuracy in the location of the crack-tip to allow determination of r and subsequently K_1 and K_2. FACTUS receives each Deltatherm image as a matrix of signal values. The signal magnitude range is divided into eight equal intervals, and the pixel positions where each of the eight divisions occurs is then calculated, allowing

a cardioid of constant signal magnitude to be traced therefore yielding nine cardioids. The data is further refined by interpolating between the raw-data points to smooth it and minimise effects of signal noise. A further option of a two-dimensional Gausssian distribution over a nine-point array is available to further filter data, but is a 'destructive' process as original data is irreversibly replaced with smoothed Gaussian interpolations.

A more sophisticated curve-fit routine developed by Dulieu-Barton and Worden[153], is that based upon a genetic algorithm (GA) incorporating a fitness function which allows the cusp (origin) of the cardioid to be described by Cartesian co-ordinates, and the cardioid itself by polar co-ordinates. The principle of operation of the routine has been described by the authors as Darwinian natural selection. A fitness function is applied to the TSA data, or 'members of the current population'. Points that are 'fit' are selected, the rest chosen by 'roulette-wheel' selection. Points are then taken in pairs known as 'parent' points which are then 'mated' to produce the next generation in the population. To ensure increasing fitness of the population 'parent' points are actively composed of one fit and one less fit parent. If a point is extremely fit (known as 'elite'), it is prevented from mating repeatedly and reducing fitness of the overall population by being carried forward to the next generation unchanged, and to prevent the sequence from stagnating, 'new-blood' is introduced into the population whereby points chosen at random are introduced into the iterations. The sequence is repeated from the start with the application of a fitness function until no further improvements can be made. However, once the cardioid curve has been generated from the GA, where the Stanley-Dulieu-Smith equations are again utilised to determine SIF's. Results have shown near perfect and symmetrical cardioids effectively correcting distorted data which could not be accomplished by the FACTUS method and also revealed the importance of attaining the cardioids as only the nearest cardioid to the crack-tip yielded the anticipated SIF's. Application of the GA method gave only 1% error from the theoretical, while for Mode I SIF's and Mixed-Mode (30°) K_2 was predicted with only a 2% error, and K_1 with 7%. Reasons suggested for this were that for the metal plate tested, the accuracy of the Westergaard equations declines with distance from the crack-tip, and possibly the neglect of the far-field stress term.

The applied stress itself was been calibrated with use of strain gauges on metallic specimens[154], though a comparative review of non-destructive means to analyse the stress field around a crack-tip conducted by Patterson and Olden[155] stated that strain gauges are not preferentially used to determine the strain field around a crack tip primarily because their finite dimensions means the signal output represents the average strain over their length, and was found to underestimate SIF at short crack lengths, and overestimate at long crack lengths[156,157,158,159], while TSA was found to be highly sensitive to interference stresses such as edge effects. Patterson and Oldens's findings seem to preferentially support TSA with special relevance for sensitive specimens such as the PVC foam cells.

2.7 Gap Analysis and Summary

Considerable research has been published regarding hygrothermal effects on laminates, with sandwich and especially foam cores in the minority. An overview of the research published in open literature is graphically presented in Figure 2- 15 based on a coxcomb format. Each sector represents an interest of hygrothermal ageing of marine sandwich composites. The sectors are scaled with respect to the number of papers reviewed (i.e. the larger the sector, the greater the percentage of research addressing that area). Each sector is distinguished by shade indicating volume of research, the darker the shading the lesser the research conducted, visually representing gaps in the knowledge at which new research should be ideally aimed (i.e at the centre bulls-eye of the graph). The review, though extensive is not exhaustive as the focus was placed on materials and methods of primary relevance to the marine sector[‡], though it is believed that the papers included[†] accurately portray the division of research available in open publication.

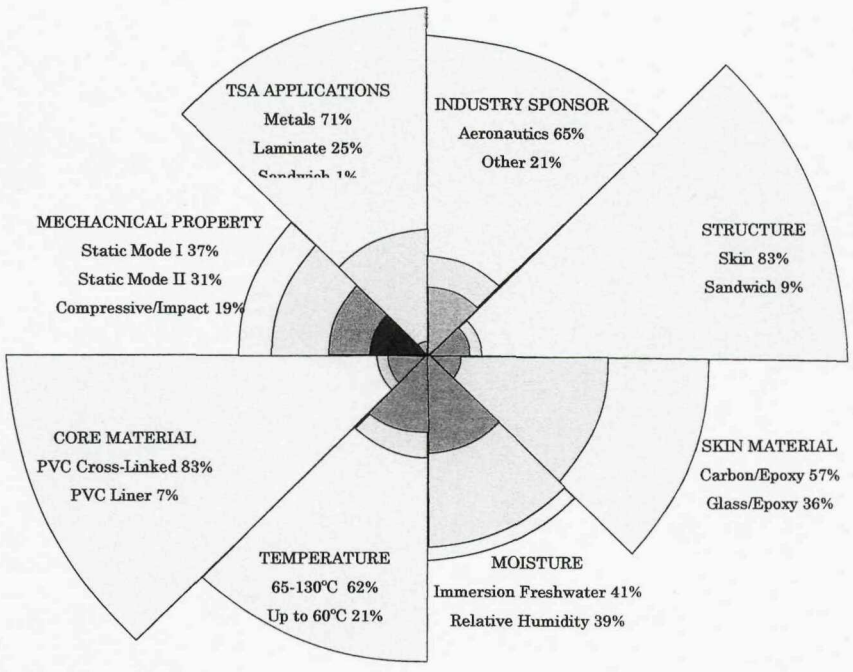

Figure 2- 15 Distribution of research; knowledge gaps represented by darkest shading at centre.

[‡] Preferentially reviewed papers on glass fibre/epoxy resins and PVC closed-cell foams.

[†] primarily from journal publications rather than conference proceedings

Despite encapsulation in laminate skins, the core is still vulnerable to the effects of hygrothermal ageing, and with respect to absorption timescales, has the potential to deteriorate far more rapidly and progressively than the skin.

A large amount of work has been amassed on moisture uptakes of small laminate coupons, largely composed of unidirectional plies in combination, with few publications detailing effects of woven roving reinforcements. Research is balanced between exposure to a relative humidity and immersion, in a continuous rather than cyclic conditions, which are principally restricted to simulation of aircraft service-conditions incorporating oil/fuel immersion with experimental analysis commonly conducted without reference to microstructure or other issues considered interdisciplinary. This experimental approach may extend to the methods used for acceleration of ageing, the condition and exposure time for which, have largely been individually determined and dependent on the application and are rarely expressed with respect to material Tg. From accelerated ageing of PVC in the medical industry, it is estimated that PVC foam should ideally be artificially aged in temperatures not exceeding 60°C, Systematic analysis of data produced by non-standardised means is extremely difficult as many of the variables which critically affect the data are omitted such as specific processing or production route.

Only a small amount of research has been published on hygrothermal exposure of sandwich panels, which then largely focus on the skin or interface rather than the core.

With regards to the core, DIAB and Airex are the two largest competitors in marine structural sandwich materials, and both foam types have been used in large scale marine applications. The Airex linear formulation is considered highly successful and has prompted classification societies to reduce design safety factors in its favour. DIAB planned new production methods and reformulations for 2007. Much of the research in literature on foam materials is conducted on DIAB H and HD materials, a US based company with large production facilities in Sweden. There appears to be a correlation between foam type used and research funding origin.

The static and fatigue failure of foam cores has been dominated by research involving Ashby, while Zenkert is noted for research on sandwich structures though due to the traditional difficulties in obtaining consistent data in mixed-mode loading, experimental research has focused upon mode I and/or mode II. The overwhelming gap in the knowledge appears to be in the response of hygrothermally aged sandwich and/or foam core to a mixed mode loading condition, for which no publications could be located at this time.
The behaviour of the foam is highly dependent upon the microcellular geometry as well as the chemical composition of the polymer used. Of these, relative density is significant. Though wary of the differences between HD130 and R63.140, and H and C70.130, their cell morphology, chemistry and production techniques, and so not directly comparable despite similar cross-linking and bulk density values, similarities in behaviour are expected with multiple microcrack formation in shear and a strong dependence of fracture toughness properties on cell size and morphology.

A hygrothermally aged foam may exhibit increased plasticity and toughness in its wet condition as moisture acts as a lubrication within polymer. In its re-dried state, the core may suffer from plasticiser loss and exhibit increased brittle behaviour and irreversible microstructural damage to the cells. The excellent crack propagation resistance of linear foams may then become compromised. It is unknown if the structural integrity lifetime of a marine sandwich would be adversely affected if the reduced safety factor for linear foams were taken advantage of during design.

A further issue associated with mechanical testing, is the manner by which the property is measured. Most commonly in the reports reviewed herein, strain gauges are attached to specimens to corroborate the load deflection curves obtained directly from the force-applying mechanism. Other non-destructive techniques employed have been acoustic emission and photoelasticity, which endeavour increase experimental accuracy by accommodating the sensitive nature of both foam materials and crack propagation. Thermoelastic Stress Analysis (TSA), is accredited with success

in a diverse range of applications, but the gap analysis highlights the profound absence of TSA data on foam specimens despite its near idealistic nature of low thermal conduction. There is also an apparent imbalance in the current knowledge of fracture and failure mechanisms between sandwich foam cores and laminate skins in response to hygrothermal ageing, and an examination of these issues would provide novel information.

References

[1] Gundberg, T., "History of foam cores", Diab Inc. www.diabgroup.com
[2] Black, S. "Getting to the core of composite laminates" Composites Technology, October 2003
[3] Image from www.marinesurveyorsschool.org
[4] Klempner,D., "Handbook polymeric foams and foam technology", 2nd Edition, Hanser Gardner publishing, 2004
[5] Gibson,L., Ashby,M. "Cellular Solids" 2nd Edition, Cambridge university press, 1997
[6] Kanny,K., Mahfuz,H., Thomas,T., Jeelani,S., "Fatigue of Crosslinked and Linear PVC Foams under Shear Loading" Journal of Reinforced plastics and composites, Vol. 23, No. 6/2004
[7] Zenkert,D."An Introduction to Sandwich Construction" EMAS (1995)
[8] Wickson,E. (ed) Handbook of PVC Formulating" Wiley, (1993)
[9] Simonik, J." The formation of foam by the mechanical foaming of PVC paste" Poly.Plast.Tech.Eng. 41(1), 103–113 (2002)
[10] Klempner, D. "Frisch, K.C. Handbook of Polymeric Foams and Foam Technology"; Hanser: (1991).
[11] SP Systems "Sandwich construction handbook-CD", 2004,
[12] Berggreen,C., Simonsen,B., "Non-uniform Compressive Strength of Debonded Sandwich Panels – II. Fracture Mechanics Investigation" Journal of Sandwich structures and materials, Vol. 7—November 2005 483
[13] Nielsen EL, Landel RF. "Mechanical properties of polymers and composites", 2nd ed. Marcel Dekker, (1994).
[14] Cripps, D., "Guide to Composites", SP Systems Southampton, UK
15 Shirrell, Halpin, "Moisture absorption and Desorption in epoxy Composite Laminates", Composite Materials Testing and Design 4th Conf. ASTM STP 617 1977
[16] Whitney, J., Browning, C. "Some anomalies associated with moisture diffusion in epoxy matrix composite materials" ASTM STP 658 1978, pp43-60
[17] Browning, C. et al. "Moisture effects in epoxy matrix composites", Composite materials testing and design (4th conference), ASTM STP617, 1977
[18] Shen, C., Springer, G., "Environmental effects on the elastic modulus of composite materials", J. composite materials, vol.11, 1977, p250
[19] Loos,A., Springer, G. "Moisture absorption of graphite epoxy composites immersed in liquids and humid air" J. Composite Materials. Vol. 13, 1979, p131
[20] Piggott, M., "Water Absorption in carbon and glass fibre composites, ICCM6, 1987
[21] Cargen, M., Hartshorn, R., Summerscales, J., "Effect of short-term continuous sea water exposure on the shear properties of a marine laminate", Trans. ImarE (C) vol.97. conf.2. paper21
[22] Anstice, P., Beaumont, P. "Hygrothermal ageing and fracture of glass fibre epoxy composites" , J.Materials Science., Vol.18., p3404-3408
[23] Camino, G., Luda, M., Polishchuk,A., Revellino, M., Blancon, R., Merle, G., Martinez-Vega, J. "Kinetic Aspects of Water Sorption in Polyester-Resin/Glass-Fibre Composites." Composites Science and Technology 57 (1997) 1469-1482
[24] Tong, M. et al. "Penetrant diffusion in PMMA near Tg: dependence on temperature and polymer weight fraction", Polymer 41, 2000, p3659-3670
[25] Browning, C. et al. "Moisture effects in epoxy matrix composites", Composite materials testing and design (4th conference), ASTM STP617, 1977
[26] Callister, W. "Materials Science –an Introduction" 1985, 2nEd. John Wiley
[27] Ishai, O., "Environmental effects on deformation , strength , and degradation of unidirectional glass-fibre reinforced plastics" Polymer engineering and science, vol. 15, 1975, July

[28] Unsworth, J.,"Effects of seawater on the properties of submarine cables and wire sheathing compounds", Polymers in a Marine Environment, Marine management, 1987, paper 15, p121-125
[29] Paravatrddy, H, Wang, J., Dillard, D., Ward, T., "Environmental ageing of high performance polymeric composites effects and durability" Composites Science and Technology, Vol.53, 1995, p399-409
[30] Real. L. P., Rocha,A., Gardette J-L. "Artificial accelerated weathering of poly(vinyl chloride)for outdoor applications: the evolution of the mechanical and molecular properties". Journal of Polymer Degradation and Stability 82 (2003)235 –243.
[31] Mathews, F., Rawlings, R., "Composite Materials: Engineering and Science" Chapman and Hall, 1994
[32] Birger,et al. "The Effect of Thermal and Hygrothermal Ageing on the Failure Mechanism of Graphite/Epoxy Composites subjected to Flexural Loading" Composites, Vol.20 No.4, 1989, p341-348
[33] McNeill, I., "Fundamental Aspects of Polymer Degradation", Polymers in Conservation, Ed. Allen, N., Edge, M., Horie, C., Royal Society of Chemistry, Cambridge, 1992
[34] Garbassi,F "Polymer Surfaces", 1998, Wiley
[35] Barrie, J. "Diffusion in polymers", Trans. ImarE (c), International Conf. On Polymers in Marine Environments, Vol.97, Conf.2, P12
[36] Aronhime, M., "Effect of Time-Temperature Path of Cure on the Water Absorption of High Tg Epoxy Resins", J. Applied Polymer Science Vol. 32, 1986, p3589-3636
[37] Mikols et al. "Evaluation of structural changes in epoxy systems by moisture sorption-desorption and dynamic mechanical studies", polymer composites vol.3, no.3, 1982
[38] Tang, J., Springer, G. "Effects of Cure and moisture on the properties of Firberite 976 resin" Environmental Effects on Composite materials" Technomic Publishing 1981, p63-74
[39] Orem, J., Sears, J., "Flexible PVC for Long Outdoor Life", Monsanto Chemical Co., St. Louis , Missouri, 2004
[40] Shirrell, Halpin, "Moisture absorption and Desorption in epoxy Composite Laminates", Composite Materials Testing and Design 4th Conf. ASTM STP 617 1977
[41] Garg, A, Ishai, O. " Hygrothermal influence on delamination behaviour of graphite /epoxy laminates", Engineering fracture mechanics, vol.22, no.3, p413-427, 1985
[42] Bouten P, de With G. "Crack nucleation at the surface of stressed Fibers." J Appl Phys 1988;64(8) p3890-900
[43] Marsh, L., Lasky, R., Seraphim, D., Springer,G. "Moisture Solubility and Diffusion in Epoxy and Epoxy-Glass Composites" Environmental Effects on Composite Materials, Vol.3. Technomic Publishing
[44] Karama, T "tests of Accelerated Ageing of Composite Materials in shipbuilding" 9th Int. Conf. Composite Materials.
[45] Weitsman Y. "Moisture in composites: sorption and damage." Fatigue of Composite Materials. Elsevier Science Publishers, p. 385-429. (1990).
[46] Buck, Lischer Nasser, N. "The combined effect of Load, temperature and Moisture on the Durability of E-glass/Vinylester Composite Materials" 42nd Int SAMPE Proc. 1997,Vol 42,no.1,p444-454
[47] Levy,R., Fanter,D., Summers,C., "Spectroscopic evidence for Micromechanical effects of Moisture in Epoxy Resins2, J. applied Polymer Science. Vol.24, 1979, p1643-1664
[48] Cerevenka,A., Batt, A., Grievson, B., " Interaction of Polyurethane Foams with water and its Effect on Material Properties" Trans. ImarE, Int. Conf. Polymers in Marine Environments Vol.97, C2, P15,1989.
[49] RAE, "Environmental effects in the testing of composites structures for aircraft" RAE TR 88063, Report to Composite Research Advisory Group , April, 1987

[50] Earl,J.S., Dulieu-Barton, J.M, Shenoi, R.A "Determination of hygrothermal ageing effects in sandwich construction joints using thermoelastic stress analysis" Composites Science and Technology 63 (2003)211 –223
[51] Tompkins, S., Tenney, D. Unman, J., "Prediction of moisture and temperature changes in composites during atmospheric exposure", Composite materials testing and design (5th conference), ASTM STP 674 , 1979, p368-380
[52] Phillips, M., "Prediction of long term stress rupture life for glass fibre reinforced polyester composites in air and aqueous environments" Composites Vol.14, No.3, 1983, p270-275
[53] Karama, M., Pegoraro, P., Tourtatier, M., "An Analysis of the hygrothermoelastic behaviour of glass fabric composites" Composites, Part A29A, 1997, p551-563
[54] Chamis, C., Lark, R., Sinclair, J., "Integrated Theory for Predicting the Hygrothermomechanical Response of Advance Composite Structural Components" Advanced Composite Materials, ASTM 658, 1978, p160-192
[55] Shirrell, C., "Diffusion of water vapour on graphite/epoxy composites" Advanced composite materials , environmental effects ASTM STP 658 1978
[56] Brown, R. "Predictive Techniques and Models for durability tests"., Polymer Testing 14(1995) 403-414
[57] McKague L. Vinson JR,(Ed.) "Environmental synergism and simulation in resin matrix composites." Advanced Composite Materials Environmental Effects. American Society for Testing and Materials, 1978. pp. 193-204 ASTM STP 658.
[58] Chiang,M., McKenna,G., "Hygrothermal Effects on the Performance of polymers and polymeric Composites" Conf.Report. J. of Res. Of Nat. Inst. Of Standards and Technology, Vol.101, p803, 1996
[59] Hemmerich,K. "General Aging Theory and Simplified Protocol for Accelerated Aging of Medical Devices", Medical Plastics and Biomaterials, July 1998
[60] Lee,M., Peppas,N."Water Transport in Epoxy Resins" Prog.Polym.Sci. Vol.18, (1993), p947-961
[61] Comyn,J." Interaction of Water with epoxy Resins" Polymers in Marine Environment.m 2nd Conf. IMarE,1989
[62] Chateeauminois,A., Vincent,L., Chabert,B., Soulier,J., "Study of the Interfacial Degradation of a Glass-Epoxy Composite During Hygrothermal Ageing Using Water Diffusion Measurements and Dynamic Mechanical Thermal Analysis" Polymer, Vol.35 (1994), No.22, p4766-4774
[63] Valentin,D. Paray,F., Guetta,B.,"The hygrothermal behaviour of glass fibre reinforced PA66 composites:A study of the effect of water absorption on their mechanical properties" J.Mats.Sci Vol.22 (1987) p46-56
[64] Shanker,S., Singh,P., Rao,R. "Hygrothermal effects on chopped fibre/woven fabric reinforced epoxy composites part A Moisture absorption characteristics" J. Reinforced plastics and composites. Vol.10, (1991), p446-456
[65] Smith,C."Design of Marine Structures in Composite materials" Chapman and Hall, 1989, p98
[66] Neumann,S., Gad,M. "Prediction of Moisture Diffusion Parameters in Composite materials under stress" J.Comp.Mats. Vol.21,(1987), p68
[67] Shirrell,D., Halpin, J. "Moisture Absorption and Desorption in Epoxy Composite laminates", Composite Materials 4thConf. ASTM 617,1977
[68] Browing, C. Husman,G., Whitney,J. "Moisture Effects in Epoxy Matrix Composites" Composite Materials 4th Conf. ASTM 617,1977.
[69] Cai,L., Weitsman,Y., "Non-Fickian Mositure Diffusion in polymeric Composites" ICCM 9 , 1992 p509
[70] Barrie,J. "Diffusion in polymers", T.IMarE.Vol.97, Conf2.p79
[71] Crank,J. "The Mathematics of Diffusion (1st ed.) Oxford University Press, (1956).

[72] Bank,L., Gentry.T., Barkatt., "Accelerated Test Methods to determine Long-term behaviour of FRP composite Structures :Environmental effects" J. Reinforced Plastics and Comps. Vol.14, p559-587, (1995).
[73] Struik, L."Physical Ageing in amorphous polymers and other materials", Elasevier Scientific. Pub. (1978)
[74] McKenna,G."On the Physics required for the prediction of long-term performance of polymers and their composites2 J.Res. Nat.Inst.Standards Tech.Vol.99, p169-189,(1994)
[75] David,A., Sims,D."Weathering of polymers" Applied Science Pub., (1983).
[76] Schnabel,W., "Polymer Degradation:principles and practical applications" Hanser Pub. (1981).
[77] White,J., Turnbull,A."Review of weathering polymers:mechanisms of degradation and stabilisation, testing strategies and modelling", J. Mats Sci. (1994), p584-613
[78] Zhou,J."A constitutive model of polymer materiasl including chemical ageing and mechanica damage and its experimental verification" Polymer Vol.34, p4252, (1993)
[79] Gates,T.,Grayson,M., "On the use of accelerated aging methods for screening high temperature polymeric composite materials" American Inst. Aeronautics and Astronautics (AIAA 99-1296) p925-935, V2, 1998
[80] Kessler,S.Gregory,J., et al. "Assessment of durability models for composite materials" Report:Boeing and NAST.
[81] Morii,T., Hamada,H., Maekawa,Z., et al. "Weight changes of the fibre/matrix interface in GRP panels immersed in hot water" Composites Science and Technology 50 (1994), p373-379
[82] McKenna,G. "Ageing of polymeric resins: Implications for composite performance2 Proc. Conf. Amer.Chem.Soc. 1992
[83] Crissman,J., McKenna,G."Physical and Chemical ageing in PMMA and their effects on creep and creep rupture behabiour" J. Poly. Sci. PrtB Poly. Phys. Vol.28, (1990) p1463-1473 ,
[84] Janas,V."McCullough,R., "Effects of Physical ageing on the viscoelastic behaviour of a thermoset polyester" Comp. Sci and Tech. Vol.30 p99-118, (1987).
[85] Read,B., "Analysis of creep and Physical Ageing in Glasssy Polymers" J. Non-Crystalline Solids, Vol.131 p408-419 (1991)
[86] Bradshaw,R., Brinson,L. "Physical Ageing in polymers and polymer composites: An analysis and Method for time-ageing time superposition" Poly.Eng. and Sci Vol.37, p31-44, (1997)
[87] Peng,S., "Consitutive Equations of Aging Polymeric materiasl" J.Mats.Sci., Vol.20,p1920-28, (1985)
[88]ASTM "Standard Guide for Accelerated ageing of sterile medical device packages" ASTM F1980-99
[89] Hemmerich,K."General Ageing Theory and Simplified Protocol for Accelerated Ageing of Medical Devices", Medical Plastics and Biomaterials, July, 1998
[90] Meeker, Hahn., "How to plan an accelerated life test-Practical Guidelines" Vol.10 Amer.Soc. Quality Control., (1985)
[91] Gillen,K., Clough,R., Wise,J."Extrapolating accelerated thermal-aging results: acritical look at the Arrhenius method" Polymer Preprints,American Chem.Soc. Vol.34,(2)p124-129 (1990)
[92] Donohue,J., Apostolou,S., "Predicting Shelf-life from accelerated aging data:the D&A and variable Q_{10} Techniques" Medical Devices and Diagnostic Industry, June 1998
[93]Collings,T.,Copely,S. "On the accelerate ageing of CFRP"Composites,Vol.14,3, p180-188,(1983)
[94] Demuts,E., Shyprykevich,P. "Accelerated environmental testing of composites" Composites Vol.15.No,1. p25-31, (1984)

[95] Cinquin,J., Abjean,P. "Correlation between wet ageing humidity absorption and properties on composite materials based on different resin family" 38th Int SAMPE p1539-1551, (1993)
[96] Delasi,R., Whitside,J." Effect of moisture on epoxy resins" Advanced Composite Mats. ASTM STP 658 p2-20, (1978)
[97] Gillat,O., Broutman, "Effect of an external stress on moisture diffusion and degradation in fraphite reinforced epoxy laminate" Advanced Composite MAteriasl ASTM, STP 658, p61-83 (1978)
[98] Hoa,S., Lin,S., Chen,J., "Hygrothermal effect on mode 2 interlaminar fracture toughness of a carbon/pe laminate" J. Reinforced Plat. And Comps. Vol.11, p3-31 (1992)
[99] Caprino,G."Sandwich Structure Handbook" IL Prato (1989)
[100] Gibson, L. Ashby,M. "Cellular Solids-structure and properties" Cambridge Press, Second Edition, 1997.
[101] Shenoi,R., Wellicome,J. "Composite Materials in Maritime Structures" Ocean Tech. Series., Cambridge University Press (1993)
[102] Chakravarty, U., Mahfuz,H., Saha, M., Jeelani, S., "Strain rate effects on sandwich core materials: An experimental and analytical investigation" Acta Materialia 51 (2003) 1469–1479
[103] Erickson,M., Kallmeyer,A., Kellogg,K.," Effect of Temperature on the Low-velocity Impact Behavior of Composite Sandwich Panels", Journal of Sandwich structures and materiasl, Vol. 7—May 2005
[104] Kabir E, Saha,M., Jeelani,S., "Tensile and fracture behavior of polymer foams" Materials Science and Engineering A 429 (2006) 225–235.
[105] Vaz,., Fortes,M. "Characterisation of deformation bands in the compression of cellular materials" J.Mats.Sci.Lett. Vol.12, p1408-10, (1993)
[106] Suh,K., Webb.D."Cellular Materiasl" Encyclopedia of Polymer Science Vol.3. 2nd Ed. Wiley, (1980)
[107] Li, Weitsman,J., "Sea water effects on foam cored composite sandwich lay-ups", Composites B, 2004vol35, p451-459
[108] Thomas,T., Mahfuz.,H., Kanny,K., Jeelani,S., "High strain rate response of cross-linked and lnear PVC cores"J.Reinforced plastics and composites, Vol23., no.7, 2004.
[109] Thomas, T., Mahfuz, H., Kanny, K. and Jeelani, S. (2002). Temperature and Rate Sensitivity of Polymer
Foams, Developments in Theoretical and Applied Mechanics, 21: 217–226.
[110] Zenkert,D.,Backlund,J. "PVC Sandwich core materiasl :Mode I Fracture Toughness" Composites Sci. and Tech. Vol.34, p247-253, (1989)
[111] McIntyre,A., Anderton,G."Fracture properties of rigid polyurethane foam over a range of densities" Polymer Vol.20, p247253, (1979)
[112] Brezny,R., Green,D., Dam,C. "Evaluation of strut strength in open-cell ceramics" J.Am.Ceram.Sci. Vol.72,p885-9, (1989)
[113] Brezny,R., Green., D., "The effect of cell size on the mechanical behaviour of cellular materials", Acta.Metall.Mater. Vol.38, p2517-26 (1990)
[114] Brezny,R., Green,D., "Factors controlling the fracture resistance of brittle cellular materials" J. Amer. Ceram.Soc. Vol.76, p2185-92
[115] Burman,M."On Crack initiation and growth in cellular foams subjected to fatigue shear loading" Proc.Fatigue p1549-54 (1996)
[116] Fowlkes,C. "Fracture Toughness Tests of rigid polyurethane foam" Int.J. Fract. Vol.10, (1974), p99-108
[117] McIntyre,S., Anderton,G. "Fracture properties of rigid polyurethane foam over a range of densities", Polymer, Vol.20, 1979 p247-253
[118] Zenkert,D. "PVC Sandwich Core materiasl :Fracture behaviour under mode II and mixed mode consitions" Mats.Sci and Eng. P299-240 V.108 (1989)

[119] Sih,G., "Strain energy Density Factor applied to mixed-mode crack problems2 Int. J.Fract. Vol.10, p305, (1974)
[120] Sih,G. Some Basic and new concepts in Fracture Mechanics" Eng.Fract.Mech. Vol.5 p365, (1973)
[121] Grenestedt,J., Hallstrom,S., et al." On cracks emanating from wedges in expanded PVC foam" Eng.Fract.Mech. Vol.54.No.4. p445-6 (1996)
[122] Noury,P." Shear crack initiation and propagation in foam core sandwich structures" PhD Thesis (1998)
[123] Richard,H."Specimen for Investigation of Biaxial Fracture and Fatigue Processes" Proc. 2nd Int.Conf. Biaxial/Multiaxial Fatigue, (1985)
[124] Ryan,S, Williams,J "Tensile testing of rod-like trabeculae excised from bovine femoral bone" J.Biomechanics Vol.22, p351-355, 1989
[125] Choi,K., Kuhn,J.,Ciarelli,M., Goldstein,S. "The elastic Moduli of human subchondral,trabecular and cortical bone tissue and the size dependenency of cortical bone modulus",J.Biomech.Vol23., p1103-13, 1990
[126] Ashman,R.,Rho,J."Elastic Modulus of trabecular bone material"J. Biomech. Vol.21, p177-181 (1988)
[127] Rho,J. Ashman,R., Turner,C. "Youngs modulus of trabecular and cortical bone material:ultrasonic and microtensile measurements"J.Biomech. Vol.26 p111-119, (1993)
[128] Brezny,R., Green,D., "Fracture behaviour of open-cell ceramics", J. American Ceramics Society., Vol.72, 1145-52, (1989)
[129] Stanley,P., Chan,W. "The determination of stress intensity factors and crack-tip velocities from thermoelstic infra-red emissions"Proc.Int.Conf. fatigue Eng. Mats. And Structures. I.Mech.E., 1986, p105-114
[130] Dulieu-Smith, J.Stanley,P., "σ_{0X} and its role in the interpretation of crack-tip isopachics" Proc.BSSM 1995, p28-30
[131] Dulieu-Barton, Stanley,P."Development and applications of thermoelastic stress analysis" Journal of Strain Analysis, 33(2), p93-104, 1998
[132] Dulieu-Barton,J. "Introduction to thermoelastic stress analysis" Strain, 35(2), p35-40, 1999
[133] LA Vision, "Techniques-", http://www.lavision.de/
[134] Thompson,W. "On the Dynamical Theory of Heat" Trans. R. Soc. 20 ,1853, p261-283.
[135] Dulieu-Barton, J.M., Stanley, P. "Development of Thermoelastic Stress Analysis", Journal of Strain Analysis Vol.33, No2, 1998, p93-104
[136]Dulieu-Barton,J, Earl,J, Shenoi,R. "Determination of the stress distribution in foam cored sandwich construction composite tee joints" J.of Strain Analysis p545, (2001)
[137]Quinn,S, Dulieu-Barton,J. "Identification of the sources of non-adiabatic behavior for practical thermoelastic stress analysis" J.Strain Analysis, V37.(1), p57 (2002)
138 Stanley, P. and Dulieu, J. M. "Accuracy and precision in thermoelastic stress analysis." In Proceedings of International Conference on Applied Stress Analysis, pp.627–638. (1990)
[139] Diaz, F., Yates,J., Patterson,E., "Some improvements in the analysis of fatigue cracks using thermoelasticity" International Journal of Fatigue 26 (2004) 365–376
[140]. Huang Y.M,. Rowlands R.E and. Lesniak J.R "Simultaneous Stress Separation, Smoothing of Measured Thermoelastic Isopachic Information and Enhanced Boundary Data" Experimental Mechanics p398 ,, December 1990
[141] Tomlinson R.A, Marsavina L. "Thermoelastic Investigations for Fatigue Life Assessment" Experimental Mechanics (2004) 9 p487
[142] Lesniak JR. Stress intensity measurement via infra-red focal plane array. In: Proceedings of ASTM Non-traditional Methods of Sensing Stress, Strain and Damage

in Materials and Structure, Orlando, USA, 1996. Philadelphia, PA: ASTM; 1996. p. 271–82.

[143] Lin ST. Thermoelastic determination of stress intensity factors in orthotropic composites using the J-integral. Engineering Fracture Mechanics 1997;56:579–92.

[144] Tomlinson RA. On determining stress intensity factor for mixed mode cracks from thermoelastic data. Fatigue and Fracture of Engineering Materials and Structures 1997;20:217–26.

[145] Nurse AD. Determination of predominantly mode II stress intensity factors from isochromatic data. Fatigue and Fracture of Engineering Materials and Structures 1993;16:1339–54.

[146] Westergaard,H."Bearing pressure and cracks" Trans. ASME J.Ap.Mech. Vol6, p49-53, 1939

[147] El-Hajjar, R. F., Haj-Ali, R.,"AQuantitative Thermoelastic Stress Analysis Method for Putruded Composites", Composites Science and Technology, vol. 63, no. 7, p967-978. (2003)

[148] Dulieu-Smith JM, Quinn S, Shenoi RA, Read PJCL, Moy SSJ "Thermoelastic stress analysis of a GRP tee joint." Appl Compos. Mater;V4 p283–303. (1997)

[149] Cunningham PR, Dulieu-Barton JM, Dutton AG, Shenoi RA. "Thermo-elastic characterization of damage around a circular hole in a GRP component". Key Eng.Mater. 204 p453–63. (2001)

[150] Dulieu-Barton,J., Fulton,M., Stanley,P. "The analysis of thermoelastic isopachic data from crack-tip stress fileds" Fatigue and fracture of Eng Mats. And Structures Vol.23 (4), p301, 2000

[151] Worden,K. Spencer,A., Dulieu-Barton,J."The effect of crack-tip interactions on the curve-fitting of isopachics" Applid Mechs. and Mats. Vol1-2 (2004), p121-126

[152] Stanley,P., Dulieu-Smith,J."Progress in the thermoelastic Evaluation of Mixed-Mode Stress Intensity Factors" Proceedings of SEM Spring Conference on Experimental Mechanics, Dearborn, Michigan, 1993, pp. 617–629.p617

[153] Dulieu-Barton,J., Worden,K., "Genetic Identification of Crack-tip Parameters using Thermoelastic Isopachics", Measur. Sci. Technol. Vol.14, (2003), p176-183

[154] Baker,L., Weber,J. "Thermoelastic Stress analysis" OPTICA ACTA, VOL. 29,.(4), p555-563 (1982),

[155] Patterson,E. Olden,E. "Optical analysis of crack-tip stress fields :- a comparative review" Fatigue Fract. Eng. Mater. Struct. 27.p623-635 (2004)

[156] Dally,J.Sanford,R."Strain guage methods for measuring the opening mode stress intensity factor K_I" Exp.Mech. V.27.,p381-388

[157] Parnas,L.,Bilir,O.,Tezcan.,E."Strain gauge methods for measurement of opening mode stress intensity factor"Eng. Fract.Mech. vol.55,p485-492, (1996)

[158] Berger,J., Dally,J."An overdeterministic approach for measuring K1 using strain gauges" Exp.Mech. Vol.28, p142-145 (1988)

[159] Dally,J. Sanford,R. Measuring Stress intensity factor for propagating cracks with strain gauges" J.Testing Eval. Vol.18, p240-249, (1990)

Chapter Three

Experimental Approach

3.1 Introduction

The aim of this work is to provide a novel contribution to the field of marine structure durability and survivability, and the The purpose of this chapter is to establish a route to the main objective, by clarifying the steps that must be accomplished along the way. A general summary, or roadmap, is presented in Figure 3-1. The roadmap has been subdivided into three main sections; problem definition; pre-testing, and testing.

3.2 I-Problem Definition

A review of marine industry concerns, and newly introduced regulations identified environmental degradation and waning confidence in design safety factors of sandwich cores as a key issue to be addressed. An interdisciplinary literature review, identified knowledge gaps where contribution would be novel. The foams found to be most suitable for investigation were the cross-linked C70.130 and the linear R63.140, of densities 130kgm^{-3} and 140kgm^{-3} respectively. The novelty in the investigative approach lies in taking advantage of the opportunity presented by recent advances in infrared detectors for TSA and applying the thermographic technique to the assessment of damage in hygrothermally aged foam cores. It is hoped that TSA methodologies developed for damage detection in metal specimens, may also be successfully applied to foams. The scope of this work is limited to the feasibility of extracting stress intensity information from the crack-tip of aged and unaged foams with TSA data.

3.3 II-Pre-Testing

This section involves the development of an ageing procedure to accelerate the ageing of a foam specimen so that it may be related to an aged state representative of service conditions. The variety of current standardised tests for structural foams were commonly found to be insensitive to the thermal properties of the foams used in this work, with an environmental conditioning procedure that could not be associated with aging damage representative of marine service. It was decided that immersion in temperature controlled distilled water was more appropriate rather than exposure to relative humidity, with a temperature selected to be below the glass transition temperature of the most thermally sensitive foam. Ageing progress was assessed by periodic gravimetric measurement. An estimate of over-ageing limits and relevance to marine service conditions was accomplished by testing the same foam at a range of temperatures to obtain insight into the accelerant effect of temperature on moisture absorption in closed cell foams. The influence of variable in-service profiles was addressed by cyclic exposure tests. The significance of density, material type and cell size was acknowledged by comparing gravimetric results at a single temperature with micrographs of the cells. The severity of the ageing was characterised primarily with fracture toughness testing.

A key vulnerability of the core as determined in *Problem Definition*, is its weakness in shear and mixed-modes. A CTS-type rig that allows the same specimen to be rotated in the plane from pure mode I to pure mode II through five mixed modes was selected. The advantage of using the same specimen configuration for all modes was supplemented by the availability of extensive FEA validation of the geometric factors for the calculation of critical stress intensity factors that are associated specifically with this configuration, and shown to be valid for foams of both high and low densities.

As the linear foam is incorporated in sandwich structures for its excellent impact energy absorption as well as its crack propagation resistance, some additional impact testing was conducted. These tests are specific to the test conditions, and could not provide a material property, but could enhance characterisation of the foam response to ageing. At this point comment may

be made on the implications of these experimental findings to design safety factors, and the potential risks, if any, associated with the special dispensation offered to linear foams, as this has yet to be published and may be considered a contribution to the debate on safety.

3.4 III-Testing

Feasibility testing of the foams for use with TSA were first conducted, but the technique revealed some complex stresses within the specimen that appeared to interact with those about the crack-tip, and which were derived from aspects of the experimental arrangement. As it was the aim of this work to attempt to obtain stress intensity information at the crack-tip using TSA, it was necessary to redesign the CTS-type rig. The proportions of the specimen configuration were retained but upscaled to 150 mm x 100 mm from 60 mm x 40 mm. After several iterations it was determined that it was necessary to adapt the loading pins to more evenly redistribute the small cyclic loads applied during TSA testing at a frequency of 10Hz.

A measure of the stress concentration about the crack-tip is obtained by using a signal reading from the specimen in its un-cracked condition for a known applied load. The proportional relationship between the thermoelastic signal detected and the known stress provides a calibration constant that encompasses the particularities of the detector and test conditions such as environmental temperature and specimen thermal and emissive properties. This 'background' constant can then be used to assess the elevation in stress due to the presence of a crack, if the loading stress applied to the cracked specimen is the same as that of the uncracked sample. The uncracked sample is also used to ensure that the validity requirements for TSA are met. This can be assessed by determining the trends in TSA signal response for increasing amplitude, frequency and mean applied load.

An established, graphically based, TSA method for the extraction of stress intensity factors from a crack-tip can then be applied to the resulting TSA data and the results compared in magnitude to the fracture toughness data collected previously to characterise the severity of the ageing. The method will be initially assessed for mode I. It is a limitation of TSA that data would

theoretically not be available for pure mode II loading as the sum of principal stresses would then be zero and no TSA signal would be expected. Due to the novel nature of the investigation, and the new TSA detection system used, it is in the nature of the work to explore the tools made available and so it is also an aim to identify promising avenues for further research that can provide more information about the crack-tip and the response of the foam to hygrothermal ageing.

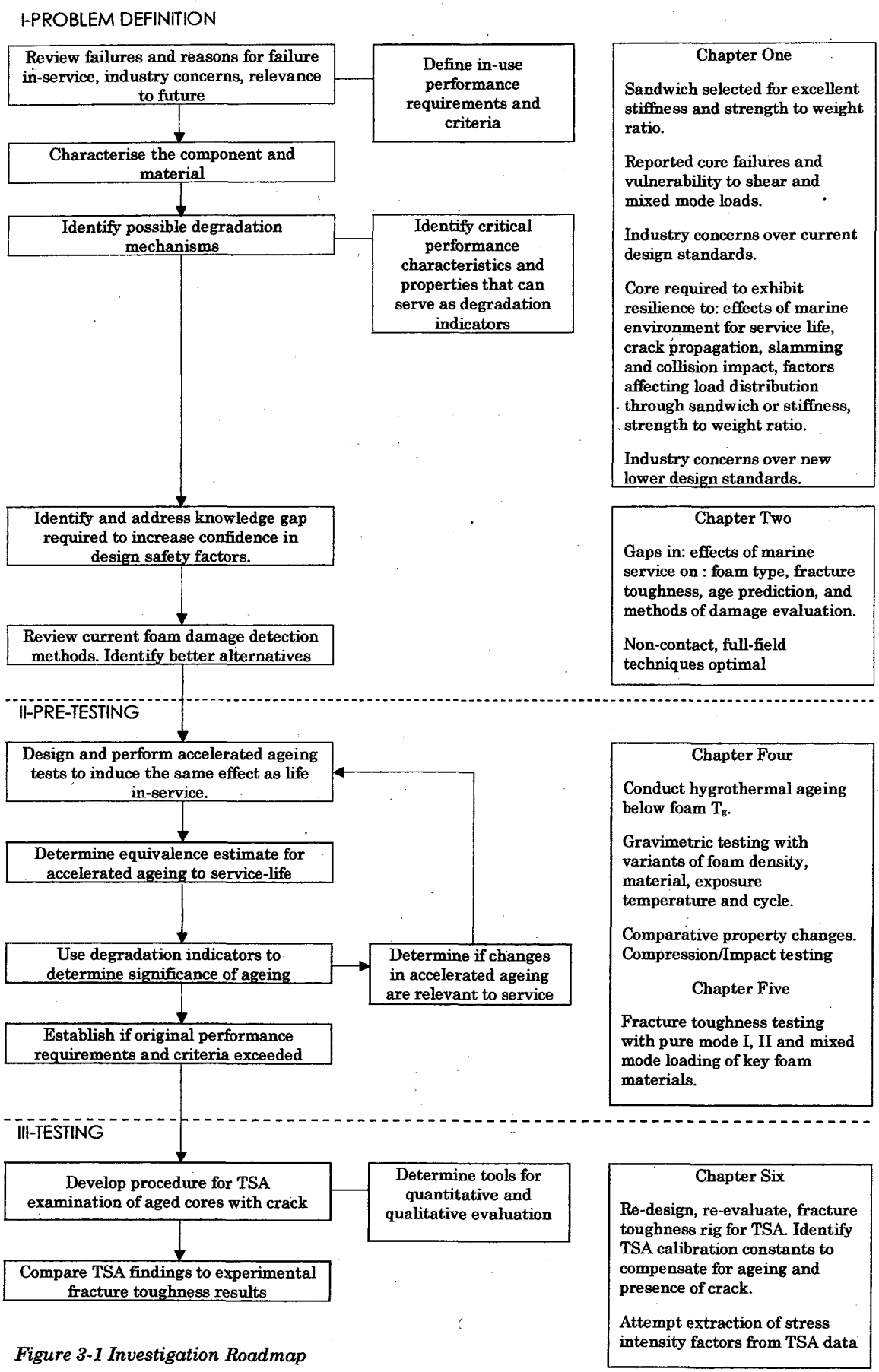

Figure 3-1 Investigation Roadmap

Chapter Four

Hygrothermal Ageing Results

4.1 Introduction

The purpose of this chapter is to establish, perform, and characterise the severity of an ageing procedure that will produce damage of the kind that may be experienced by a marine sandwich in-service. This was first approached with a critical review of the published literature and standardised testing methods, which identified the significance of testing below the glass transition temperature of the foam to maintain relevance to marine service conditions, and the importance of a real-time ageing scale for reference. An estimate of real-time ageing was approached by gravimetric measurement of the same specimen immersed at a range of different temperatures between 20°C and 60°C. Sensitivity to variables such as interrupted exposure and type were considered with cyclic immersion ageing and testing with different foam densities. Ageing was characterised with comparisons of gravimetric changes, mechanical tests (impact), and fracture toughness tests, which are expanded on in Chapter Five.

4.2 Experimental immersion procedure

Specimens were cut to size from a single sheet in the same direction using a band saw, and the edges vacuumed to remove loose particles. The specimen is numbered and weighed using a Mettler AE240 moisture balance with a sensitivity of 0.00001g. Specimens were then immersed in two covered Grant Instrumentation SUB36 water baths, which were set to maintain the distilled-water at a temperature of 60°C. The tanks hold more than 36 litres with working dimensions of 635 mm x 300 mm x 190 mm. The heating mat

and thermostat lay beneath the tank floor, so stainless steel grills were used to raise the specimens and maintain separation to ensure water and temperature freely circulated around them. The stainless steel grills were also used as shelves positioned 30mm apart to promote circulation across the surfaces of all the specimens evenly spaced within the tanks. The top layer of specimens was held beneath the surface by a final grill fixed to the one beneath. Frequent checks were made on the level of the water and the temperature throughout the tank depth. Due to the large number of specimens required for testing, it is acknowledged that the tanks were overcrowded and so specimen positions were regularly rotated within the tank. Specimens designated only for gravimetric measurements were used and positioned in different parts of the tank. The specimens were weighed periodically, by brief removal from the tank, pat drying to removed excess surface moisture from the open cut cells, and weighing using a sensitive moisture balance. Five specimens of each foam type were weighed to obtain an average. Care was taken to minimise the time taken for weighing, which could typically be completed within two minutes. Specimens to be prepared for mechanical testing are removed from the tanks and dried in air at 50°C until no further weight loss is recorded, reweighed, and allowed to rest at room temperature and humidity for two days prior to testing.

4.2.1 Experimental error

During experimentation it was observed that errors could arise from the following:

- Incomplete dislodgement of all the loose or only partially attached particles at the cut edges. Over time particles would dislodge from the specimens within the tank and alter weight change measurements.
- Dislodged particles that coated the tank bottom could affect the thermostat readings taken from beneath them, and could result in erroneous alteration to the temperature of the water bath.
- The number of specimens required for mechanical testing meant the tanks were overcrowded, restricting even temperature distribution within all the shelf levels of the tank affecting moisture uptake rate.

— Pat drying of specimens to remove excess water must be done consistently for all sides and all specimens.
— Each gravimetric data point is an average of five specimens presented as an average percentage change in weight taken from rotating positions within the tank. The variation about the mean was between 3.4-6.7%.

4.2.2 Specimen configuration

The specimen configuration was determined by the requirements of the mechanical and TSA testing that was to follow. Long-term ageing of specimens for fracture toughness tests were 60 mm x 40 mm x 20 mm (sheet thickness). Sizes had to be enlarged for TSA testing and were 150 mm x 100 mm x 20mm.

4.3 Long-term ageing results

Gravimetric results for specimens to be characterised with fracture toughness tests are shown in Figure 4- 1. The ratio of mean cell size between R63.140 and C70.130 shown in micrographs is approximately 2. The ratio of maximum percentage weight change between R63.140 and C70.130 is approximately 1.7. The initial steep incline may be related to the ingress of moisture in the open cut cells, resulting in a similar percentage weight increase for the two foams. The overall trend may be characterised as linear, though the fluctuation about the trend appears to be composed of stages where a plateau proceeds a net drop in weight change drop before a further increase.

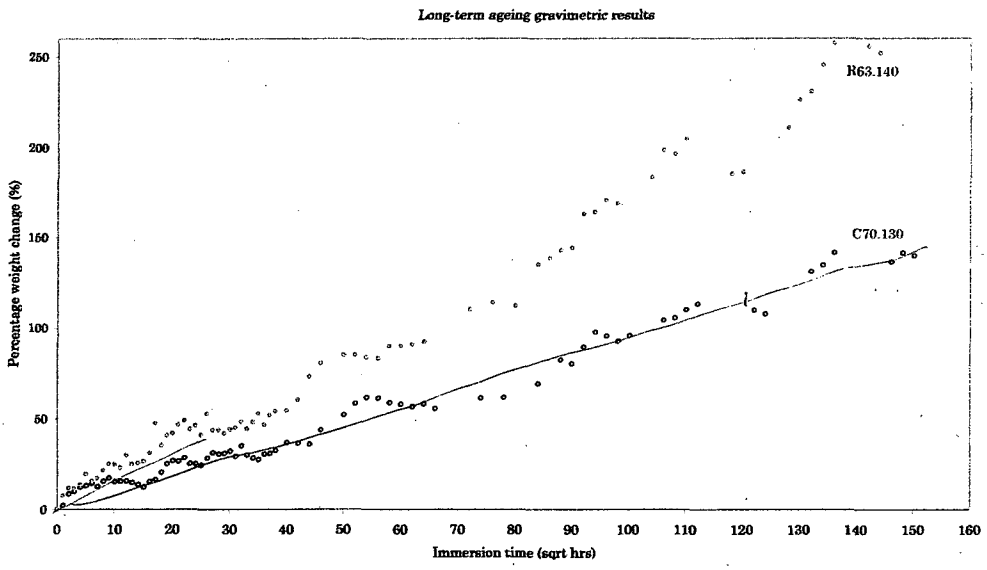

Figure 4- 1 Gravimetric results for long-term ageing of C70.130 and R63.140 at 60°C. (60x40x20mm)

Moisture diffusion characteristics are most frequently quoted in the literature as Fickian or non-Fickian in deference to the Fick laws of diffusion established in 1855.

Fickian behaviour[1] is characterised by an uptake of moisture, which reaches an asymptotic value gradually after a period of time with an initial linear region to 60% of the maximum moisture uptake when percentage weight change is plotted against square root immersion time. For the 20mm thick specimens used in this work, the saturation level required to determine fickian behaviour would not be feasible for this timescale, however, the overall trend in Figure 4- 1 must be considered non-fickian as material loss and additive leaching are not characterised by the Fick laws. The repetitive fluctuations, if taken individually, do display more fickian characteristics prior to the net weight drop. This section of the curve may be representative of diffusion across cell walls prior to material loss from the edges or leaching of additives.

4.3.1 Micrographs of aged specimens

The progressive damage sustained by the foam during ageing can be visualised with micrographs. Accelerated by temperature, moisture may diffuse through the thin cell wall into the cell resulting in swelling of the cells

shown in Figure 4- 2. The undamaged cells of C70.130 and R63.140 are shown for comparison. The larger cell size and thicker struts of the R63.140 are clearly observed. With ageing, polymer additives are leached from the surfaces of the cell walls and struts, as indicated by the pitted appearance in Figure 4- 3, causing irreversible damage and providing a fast access route for moisture ingress.

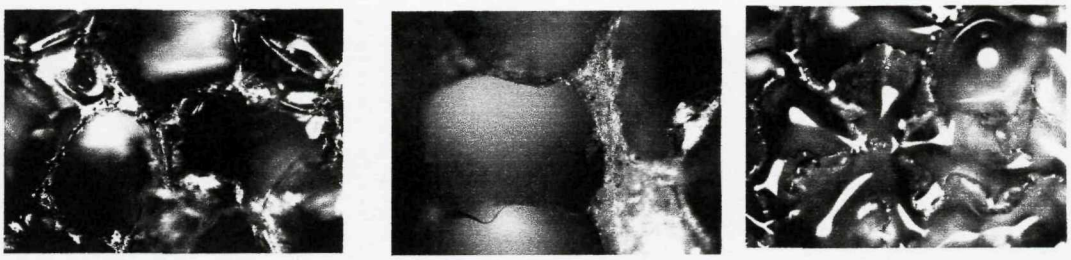

(a) (b) (c)

Figure 4- 2 (a) Unaged C70.130, (b) unaged R63,140, (c) swollen cells R63.140 (mag.x10)

Li and Weitsman[2] in their work on the effects of sea water on foams of a similar type and density as that used here, measured pits that penetrated to a depth of 2.8 mm. in specimens immersed for 10000hrs at room temperature. The same study asserted that the weight gain could be mostly attributed to the filling of the cell volume, with only a very small contribution made from diffusion within the polymer cell walls themselves.

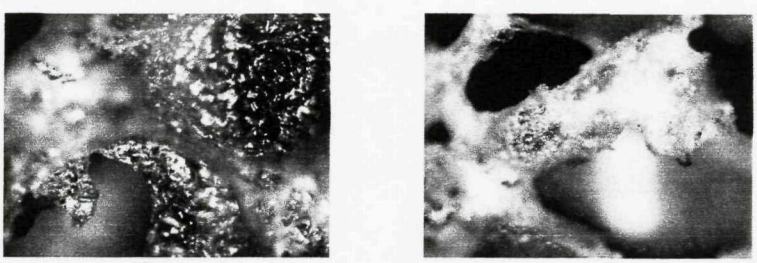

(a) (b)

Figure 4- 3 (a) R63.140 cell-wall aged 15000hrs, (b) R63.140 cell strut aged 15000hrs (mag.x10)

The damage to the R63.140 was noticeable, however, micrographs for C70.130 did not show the same evidence of pitting and damage despite a finer strut and cell matrix. Figure 4- 4 shows high-powered view of aged C70.130 cell walls. It is possible that the polymer additives are more strongly bound within the cross-linked polymer than the linear, increasing the resistance of

the C70.130 to moisture ingress and may explain the less erratic and more linear trends exhibited by C70.130 in the later stages of ageing of the gravimetric data in Figure 4- 1 and Figure 4- 5 when compared to R63.140.

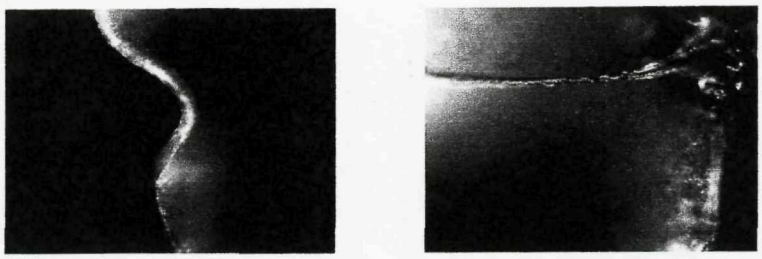

(a) (b)

Figure 4- 4 (a) & (b) C70.130 cell wall aged 15000hrs (mag.x50)

4.3.2 Effect on gravimetric results due to specimen size change

During the course of this work is was found necessary to increase the specimen sizes used for TSA. Larger specimens (150 mm x100 mm x20 mm) were immersed and hygrothermally aged with same procedure used for the smaller fracture toughness specimens (60 mm x 40 mm x 20mm), as described in *experimental procedure.* The consistency of the gravimetric results was found to vary with specimen size. Figure 4- 5 shows recorded percentage change in weight for specimens to be used in TSA tests. When compared to the gravimetric results for the 60 mm x 40 mm specimens seen in Figure 4- 1, a lower mean percentage weight increase was observed for both materials and the data appeared less linear. It is possible that this was due to the ratio between the moulded-surface area and the cut-surface area. The moulded surface of the foam is formed smooth and intact, whereas the edges cut by bandsaw are rough with torn and damaged cells. It is reasonable to suggest that moisture would enter more readily from these areas. Photographs of the two surfaces are shown in Figure 4- 6.

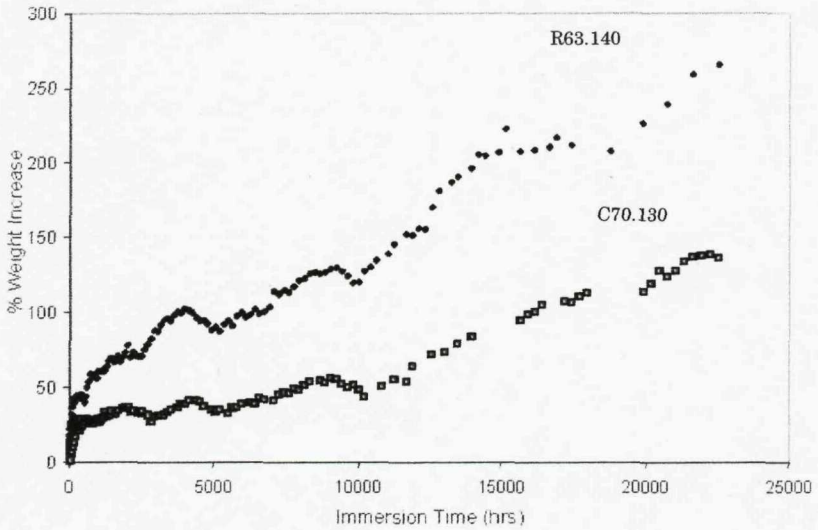

Figure 4- 5 Gravimetric results for long-term ageing of C70.130 and R63.140 at 60°C (150 x 100 x20mm)

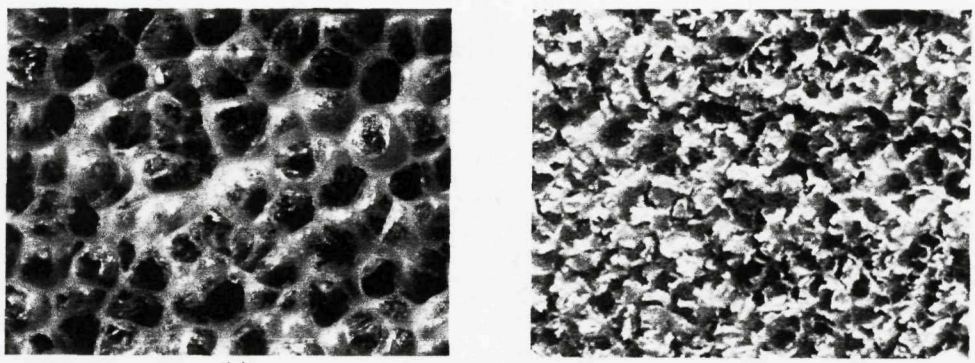

Figure 4- 6 Photographs to compare gross surface roughness and damage between (a) the moulded and (b) the cut surface of a C70.130 specimen

The ratio between moulded surface and cut surface is 1.2 for the 150mm x100 mm x 20 mm specimen and 1.5 for the 60 mm x 40 mm x 20mm specimen. The 20% difference between the cut surfaces relates well to the approximately 20% difference in uptake at 18500hrs seen for both foams. To match the uptake as closely as possible for mechanical test specimens, TSA foams were removed at 15000hrs

4.4 Effect of temperature on ageing

C70.130 and R63.140 were immersed in distilled water at temperatures of 60°C, 40°C, and 18°C (unregulated room temperature). The rates and weight

change levels are shown in Figure 4- 7 and Figure 4- 8 respectively. The similarity in weight change between all the specimens shown as linear in the initial √5hrs of immersion indicates that this part of the curve is dominated by free-volume uptake into the open cut and damaged cells. The net reduction in weight change indicates material loss from the foam, and the specimens immersed at room temperature are shown to suffer the highest loss as a proportion of their total weight change. These weight change fluctuations tend to stabilise within the first √50hrs of immersion for the room temperature specimens, but continue for the elevated 40°C and 60°C temperatures. This may be an indication of two types of material loss, one of which is sensitive to temperature. Discoloration and material loss were evident for all specimens, though it is reasonable to suggest that particulate loss from the cut cell edges of the foam, dominate at low temperatures, while leaching of polymer additives achieves greater significance at elevated temperatures. The extent of the damage that had been reported by Li[2] in the literature for foams at room temperature had not been observed within this work.

The profile of the curves also changed with temperature. The higher the temperature, the more linear the trend. The lower the temperature the more fickian-like behaviour was exhibited.

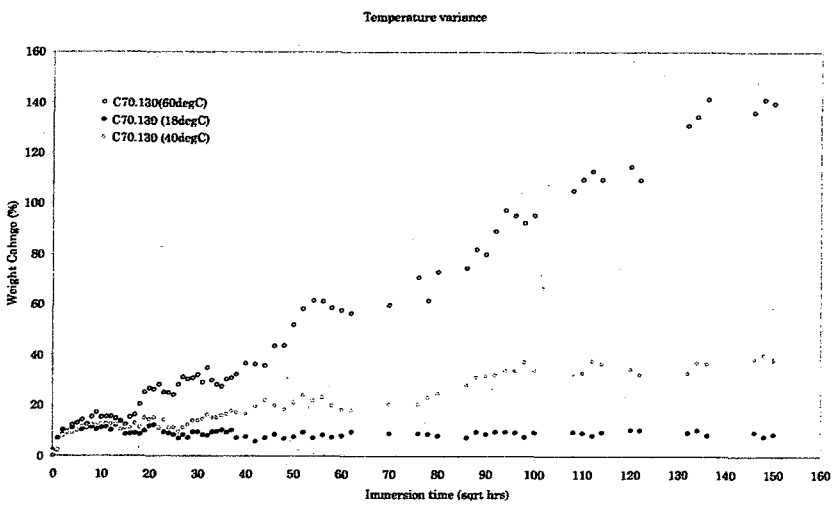

Figure 4- 7 Gravimetric measurements for C70.130 at 18°C (rt), 40°C, and 60°C.

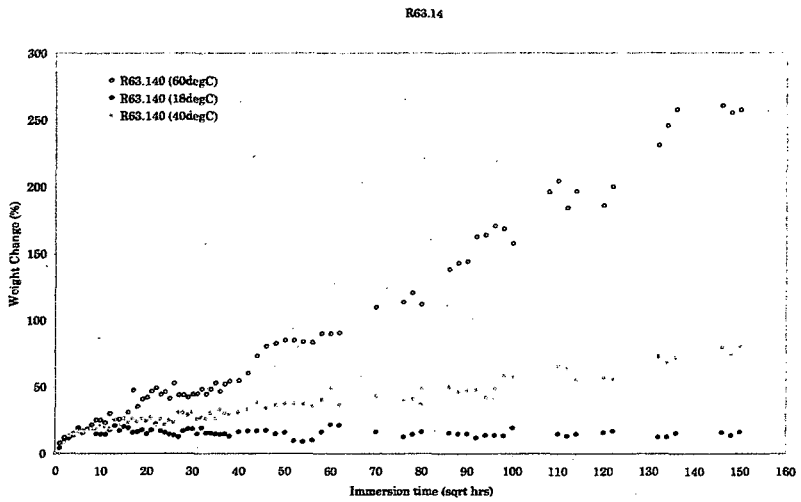

Figure 4- 8 Gravimetric measurements for R63.140 at 18°C (rt), 40°C, and 60°C.

The gravimetric data recorded for the different temperatures could be seen to approximate an Arrhenius type relationship found in the literature, commonly referred to as the *Q_{10} rule*[8]. The relationship is based upon a conservative accelerated ageing factor developed by ASTM standards to provide a performance estimate for the demanding requirements made of sterile medical packaging. The approximation is made that the chemical reaction rate will increase by a factor Q_{10} for every 10°C increase in temperature, and represented as:

$$Time_{immersion} = \frac{Time_{in-service}}{Q_{10}^{(T_{test}-T_n)/10}}$$

Equation 4- 1

The Q10 factor is specific to the material but for a PVC based polymer, Q_{10} is approximately equal to 2, though Q_{10} for C70.130 was found to average as 1.75, and 1.9 for R63.140. Greater emphasis was placed on the data for 40°C to 60°C rather than the room temperature to 40°C ratio to accommodate the effect from moisture entry due to cut and damaged cells rather than a reaction rate. It is possible that the Q_{10} value for the R63.140 is so far from the recommended value of 2, due to the comparatively easier leaching of additives from the polymer. Using the derived Q_{10} values an accelerated

ageing factor can be estimated to relate accelerated ageing to a real-time equivalent. The relationships have been plotted in Figure 4- 9 and Figure 4-10 for 5 and 30 yrs at room temperature respectively.

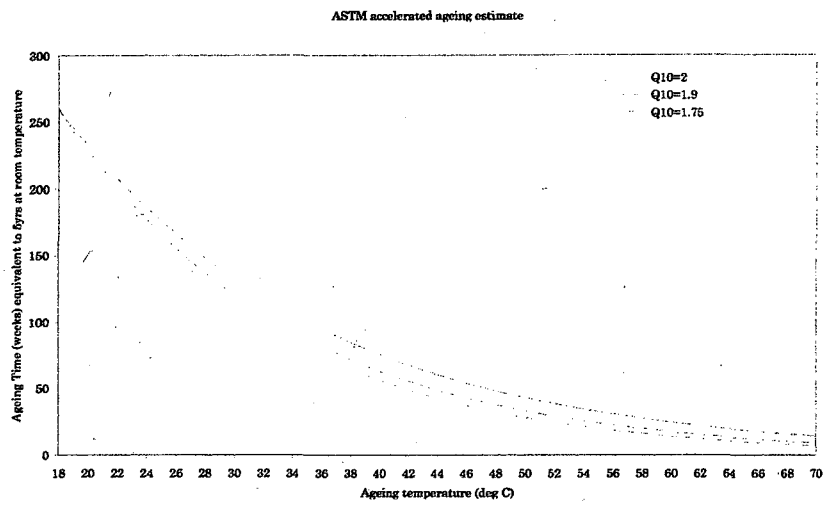

Figure 4- 9 ASTM accelerated ageing estimate for 5yrs at room temperature equivalency

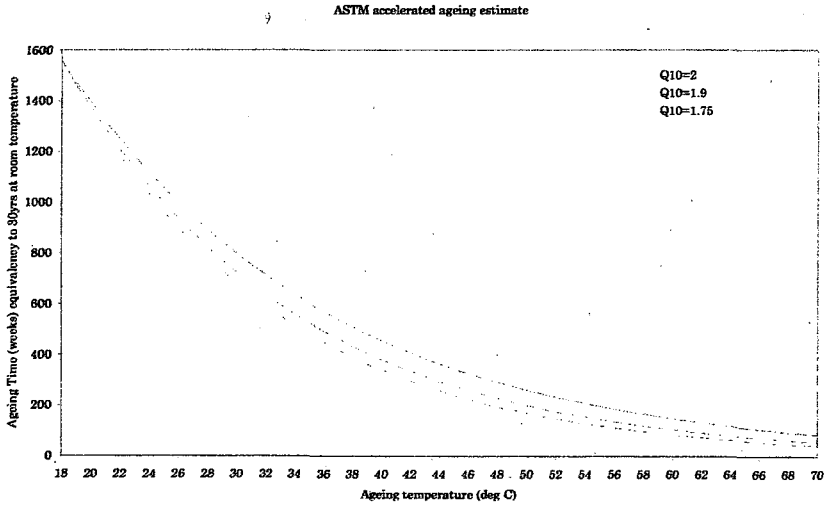

Figure 4- 10 ASTM accelerated ageing estimate for 30yrs at room temperature equivalency

As the estimate is noted by ASTM to be conservative, it can also provide a gross estimate for over-ageing and though seen to be slightly different for the materials, a 185000 hrs limit can be imposed and all subsequent specimens discarded.

4.5 Effect of foam type on ageing

Foam types of C70 and R63 with differing densities were immersed at 60°C and seemed to provide different trends with respect to density. The relationships are shown annotated by a trend line in Figure 4- 11. There were a greater number of C70 types available for testing at the time and so there is inherent error in these extrapolated trends. With the exception of the C70.200 point, the C70 curve could have been a linear relationship. The points for C70.75 and R63.80 are very close, while the C70.55 and the R63.50 diverge considerably. It is possible that this is due to the similarity in cell sizes and cell morphology between the C70.75 and the R63.80 which is less evident in the other foam types. Micrographs of the different types are shown in Figure 4- 13 and Figure 4- 14.

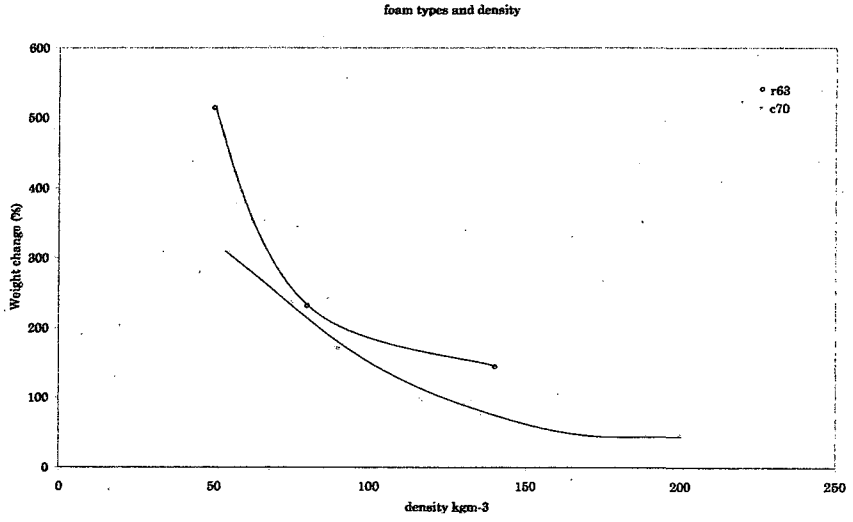

Figure 4- 11 Percentage weight change for C70 and R63 foam types with different densities for 60°C (specimens 60mmx40mmx20mm,√100hrs).

As the foam composition differs between C70 and R63, it is not possible to comment from this if limiting cell size rather than increasing strut thickness is a superior defence to moisture ingress and hygrothermal ageing. However, if the C70.75 and the R63.80 points are so close, and their morphology is the closest to each other at that point, then it may be suggested that resistance to moisture is dominated by smaller cell sizes rather than polymer type.

The foam types tested possessed the properties as seen in Table 4- 1. The relationship between mechanical properties and cell size is also evident, with a thicker strut to reinforce the mechanical strength of the linear polymer while still enabling high shear elongation values.

Material	C70.55	C70.75	C70.90	C70.130	C70.200	R63.50	R63.80	R63.140
Property								
Compressive strength (N/mm^2)	0.9	1.3	1.9	2.6	4.8	0.38	0.9	1.6
Compressive modulus (N/mm^2)	69	97	125	160	280	30	56	110
Tensile strength (N/mm^2)	1.3	2.0	2.7	3.8	6.0	0.9	1.4	2.4
Tensile modulus (N/mm^2)	45	66	84	110	175	30	50	90
Shear strength (N/mm^2)	0.8	1.2	1.6	2.3	3.5	0.5	1	1.85
Shear modulus (N/mm^2)	22	30	38	47	75	11	21	37
Shear elongation at break %	16	23	27	30	30	70	75	80

Table 4- 1 Material properties of Airex foams tested from manufacturer.

Additionally, a further foam type manufactured by a Divinycell, was tested in the same manner as above. The H130 is a direct competitor to the C70.130 and was tested as it is the most frequently referenced make and foam material in the literature. The H130 is listed in the Divinycell data sheets with a tensile strength of 4.2 MPa, a compressive strength of 2.5 MPa, shear strength of 1.8 MPa, and a shear elongation of 30%.

The H130 cell struts appear more fine and refined in the comparative micrographs of Figure 4- 12, with much finer node connections, though the mean cell sizes are comparable. Divinycell have currently withdrawn from manufacture the linear type foam series which could have been compared to the R63 series.

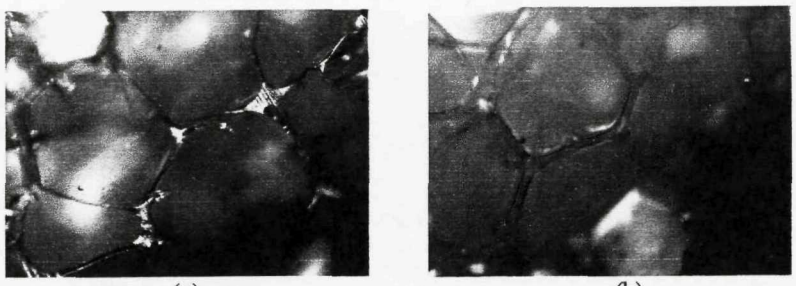

(a) (b)

Figure 4- 12 Cell structure of unaged (a) C70.130 and (b) H130 (mag. x10)

The finalised percentage weight change of the H130 following immersion in 60°C for √100hrs was found to be 23.4% in excess of the C70.130. Upon re-drying from the aged condition, it was observed that the C70 had retained an extra 16.5% of trapped moisture within the cells, while the H130 had more effectively shed the moisture to reach an excess of only 4.6%. It is reasonable to suggest that despite the unknown polymer composition, the difference in moisture uptake behaviour may be accounted for by the fine nature of the struts.

4.5.1 Micrographs of foam types.

The morphology of the two foam types used in this work, the C70 and the R63 are photographed below in Figure 4- 13 and Figure 4- 14, for a range of densities. It can be observed that the C70 type has a decreasing cell size with increasing density, while the R63 mean cell size remains consistent but increases its density by increasing the amount of material between cells.

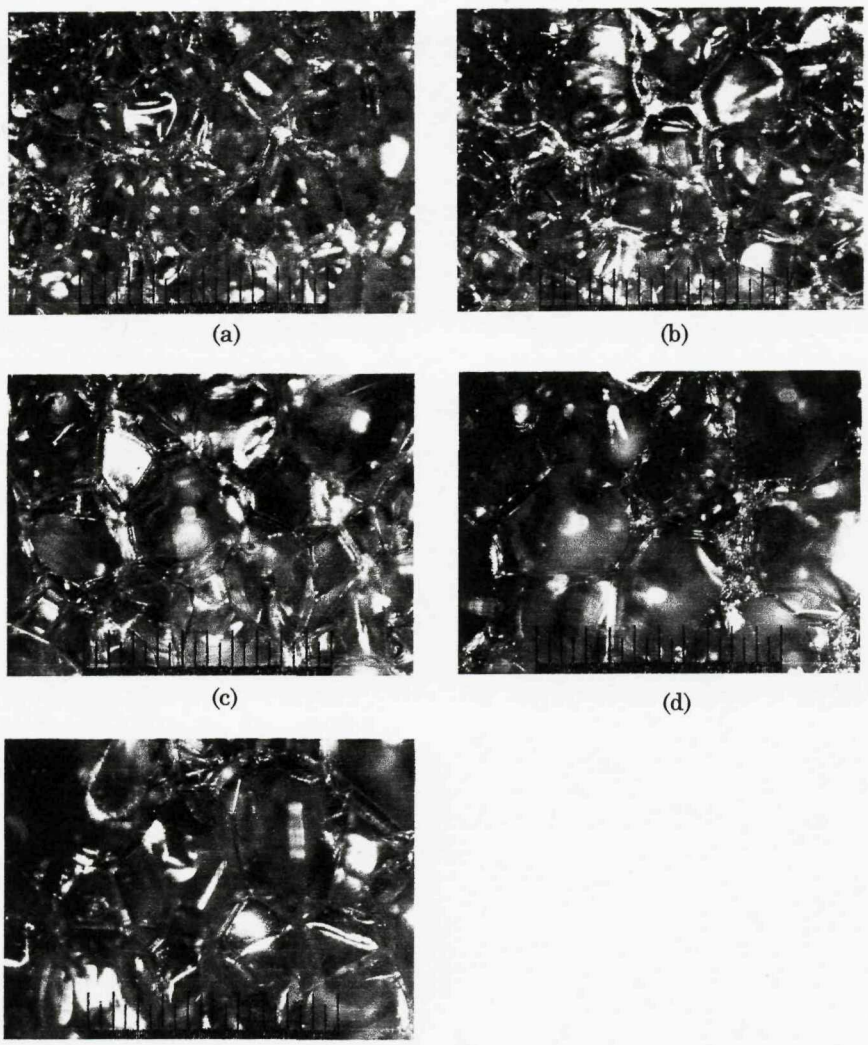

Figure 4- 13 Micrographs of C70 foam type with densities in kgm^{-3} of (a) 200 (b) 130, (c) 90, (d) 75, and (e) 55. (mag.x5 and a 1mm graticule).

It can be seen that the mean cell sizes for R63.140 and may be considered double that of C70.130.

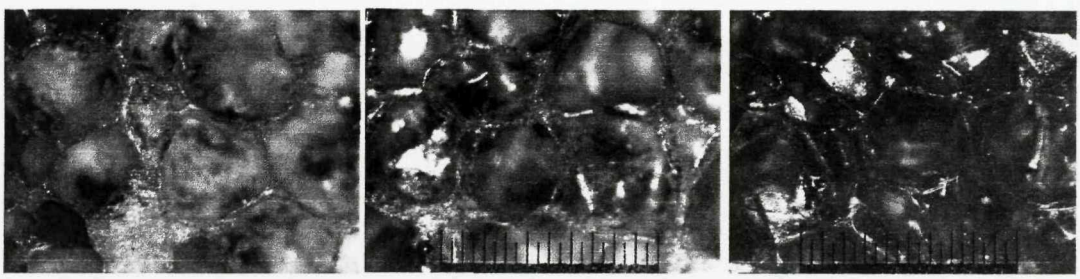

Figure 4- 14 Micrographs of R63 foam type with densities in kgm^{-3} of (a) 140 (b) 80, (c) 50. (mag.x5)

4.6 Effect of cyclic exposure on ageing

The C70 and the R63 60x40mm specimens were exposed to cyclic immersion. Two separate tests were conducted to determine the significance that interruption of the ageing cycle would have on the moisture uptake behaviour of the foams. The first test involved a cycle of 60°C immersion for 500hrs, followed by removal, weighing, drying in air at 50°C for 48hrs, and weighing, before re-immersion. This cycle was repeated 8 times. The second exposure test was a freeze/thaw cycle. A cycle of 500hrs immersion at 60°C, followed by removal, weighing, and freezing in -5°C for 48hrs, before being reweighed, and re-immersed in 60°C to complete the cycle. This was repeated 8 times. The percentage weight change of the specimens could then be compared to a control sample which was held continuously immersed for that period of time. However due to limitations of material and tank space, periodic weight changes were averaged from only two specimens, and the control obtained from only one. The cycles are illustrated in Figure 4- 15. The highest variation in percentage weight gain between two replicant readings was 9.7%, the lowest was 3.1%.

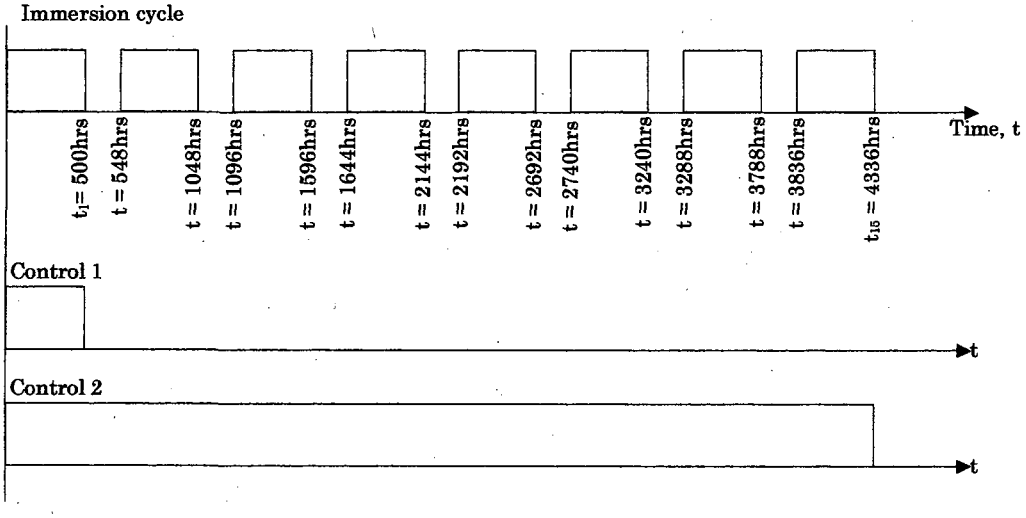

Figure 4- 15 Illustration of immersion cycles

Re-dry weights such as t_2 are shown as a percentage weight change from the specimen initial weight. Immersion weights are listed as a percentage change from the control weight. (The control weight is itself a percentage change

from the initial weight). This is done to clarify the variation caused by interruption to the hygrothermal ageing procedure.

Upon repetitive immersion/dry/immersion cycling, the C70 group suffered from a net weight loss caused by particulate loss, while the R63 group, not only progressively absorbed more moisture than the first cycle, but also retained it upon drying. The greatest effects were observed upon the immersion/freeze/immersion cycles, which could be seen to be apparently far more damaging. The R63 group were almost twice as sensitive to freeze cycling as the C70 group, but in addition retained more than four times as much moisture irrespective of the cell size.

Foam	Control 1 %weight	$\%t_2$	$\%t_{15}$	$\%t_{16}$	Control 2 %weight	$\%t_{15}$	$\%t_{16}$
C70.200	25.8	-1.2	+9.2	-2.2	33.27	+12.2	+4.53
C70.130	27.3	+3.1	+11.7	+4.1	59.63	+12.5	+12.53
C70.90	44.61	-6.7	-4.13	-5.8	172.14	+19.6	+20.4
C70.75	54.94	-1.1	+1.01	-1.0	235.09	+32.1	+67.41
C70.55	66.58	-8.1	-7.1	-8.2	306.72	+37.4	+112.7
R63.140	43.9	+7.4	+11.1	+5.4	107	+26.3	+20.08
R63.80	61.16	+23.1	+140.2	+32.1	275.16	+52.1	+60.00
R63.50	70.81	+101	+276.6	+265	332.1	+73.4	+329.3

Table 4- 2 Cyclic Immersion based on values from Controls 1 and 2

The implications are that;

- the repetitive removal of specimens for weighing would have had little or no effect upon the fluctuations within the results,
- repeated re-drying of the sandwich core may lead to a greater eventual absorption of moisture, though the R63 group are more sensitive than C70.
- Despite re-drying, the R63 foam group would retain moisture locked within, which the C70 would not.
- Exposure of an ageing core to freezing conditions may magnify the ageing once the structure is thawed. All cores are observed to suffer, and though the leaching process appears interrupted in the R63 group, moisture is more readily retained and would increase structural mass. It is not known if the retained moisture would act as replacement for plasticizers lost during ageing as is known to occur during experimental testing on immersed specimens in-situ.

4.7 Effect of Ageing on Impact Response

The purpose of this section is to provide supplementary observations and a fast preliminary characterisation of the aged response of C70.130 and R63.140 prior to mechanical testing, rather than a detailed investigation into the effects of ageing.

One of the key reasons R63.140 is selected by designers is for its excellent behaviour under slam impact loads, so for a preliminary age characterisation, slamming and collision were approximated as distributed compressive and point loads respectively.

Foam response is known to vary with impacting velocity, so to best evaluate the behaviour of the core a high and low velocity test must be administered.

A low velocity point loading, in effect an indentation test, was conducted using the tup (falling weight), method as described in ASTM D3029-84[4], for which a spherical ball-bearing head was found to be the best impactor. Core behaviour from point impacts at higher velocities was compared to failure modes at low-velocity using ballistic projection of a small 4.5mm ball bearing, providing an impact with ten times the energy of that from the low velocity tup, and an indication of the change in relationship between foam cell energy absorption and ageing.

4.7.1 Low Velocity Indentation Test

Relative changes in the impact resistance of foams subjected to accelerated ageing were first characterised by means of a tup (falling weight) detailed in ASTM D3029-84 Method F[5]. A tup-test was selected over the Charpy or Izod tests because it allowed for greater consistency in results as the same specimen could be utilised for impact testing once it had undergone TSA and fracture toughness testing. Additionally, as moisture during the hygrothermal ageing did not penetrate the foam through thickness, a tup-test provided information on the behaviour of a fully aged foam surface, with a test configuration seemingly more applicable to a sandwich panel exposed to service slamming loads as described in Chapter One.

The test arrangement and the three tup configurations recommended by ASTM D3029-84 used are illustrated in Figure 4- 16 with a 0.5kg fixed drop weight from a fixed height of 0.3m. The foam specimen was positioned on supports(2&3) which match the specimen dimensions of 100mmx150mm. The supports are centrally holed with a 60mm diameter to remove a reaction force to the free-falling tup(1). Should a specimen be holed, the tup would be brought to rest by the base(4). The foam specimen was clamped into position by a holed cover plate(7) held in position by four corner screws (which do not penetrate the specimen). The tup support(6) was raised to a height of 0.3m and held in place by a latch attached to a rear support rod(8). The tup impact head (differing stress concentrations) was selected as *C* after initial tests (Figure 4- 16), and the resulting average impact diameter was then measured with Vernier callipers. The test was repeated five times. The 0.3m height selected for the test provided an impacting energy one tenth of the that of from the high velocity indentation test, and information on response to impact without failing the foam through thickness, allowing the same specimen to be tested again in another location to provide a data-set average.

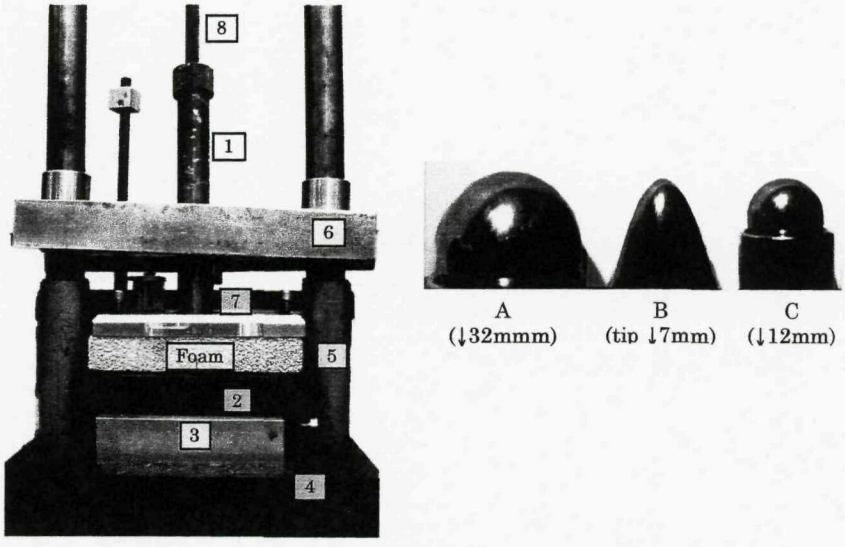

Figure 4- 16 Tup-Test arrangement and tup configurations recommended by ASTM D3029-84. (1)Tup, (2&3)Support with well, (4)Base, (5)Tup supports, (6)Tup supports and release mechanism, (7) specimen clamp (8)Release mechanism support rod.

The tup test is dependent on the geometry of both the falling weight and the support providing only relative rankings of foams unless the geometry of the specimen, test equipment, and test velocity all conform to end-use. Both foam

types showed a change in response to the low strain rate impact of a falling tup. The C70.130 impact showed extensive crushing of the cells to a depth x1.6 times than in its unaged condition. Figure 4- 17 relates impacting measurements to Table 4-3. Observations of increased brittle behaviour were seen for C70 in (b) at the rim of the indentation producing a more defined impact form compared to unaged condition in (a). A smaller indentation radius was seen for C70 than R63, potentially due to the densification of the smaller cells in C70. The image for R63 in (c) was taken within an hour after impact, by which time the foam had seen some recovery producing a shallow indentation with undefined edges. Though (d) also showed a shallow indentation for R63 in its aged condition, it showed a marked change in behaviour by yielding a large area of unrecoverable damage with far less compliance. With ageing, the R63.140 was seen to be penetrated a quarter of its unaged depth, however, it was unable to recover 32% of its impact depth as it was in the unaged condition, indicating further changes in the energy absorption characteristics of the foam. The magnitude of the change in response when related to the proportional amount of moisture uptake, indicates that R63.140 low strain rate impact response is still more sensitive to ageing than C70.130.

	unaged		aged15000hrs	
	C70.130	R63.140	C70.130	R63.140
Impact depth (mm)	1.81	2.75(+1.31)	3.01	0.97

Table 4- 3 mean impact depths from falling tup (low strain rate),on TSA specimens 150x100x20mm

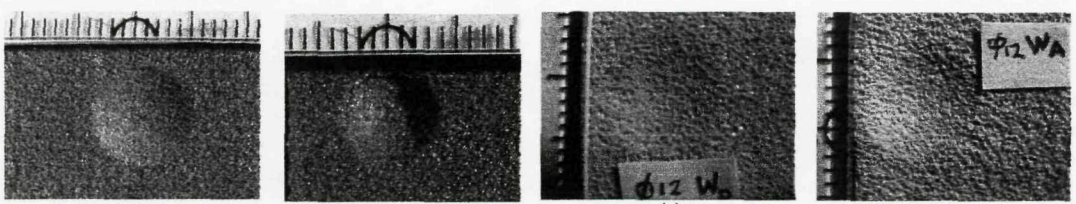

(a) (b) (c) (d)

Figure 4- 17 Falling tup-test indentations for 12mm diameter tup (a) C70.130 unaged, (b) C70.130 aged, (c) R63.140 unaged (recovered), (d) R63.140 aged

4.8 High Velocity Indentation Test

A G10 airgun which delivers a 4.5mm ball bearing at $91ms^{-1}$ was fixed within two supporting clamps at a distance of 0.5m from a specimen clamped in a simply supported position. The specimen was clamped within a standard target box test, which captures rebounding pellets, and testing was conducted at the University rifle range, with full observance of safety regulations. Comparisons of the response of C70.130 and R63.140 to ageing as characterised by a high strain rate are shown in Figure 4- 18 and Table 4- 4. Impact depth for both foams can be seen to be shallower with ageing, and producing a significantly smoother edge profile. R63.140 again shows the greatest change in response to ageing.

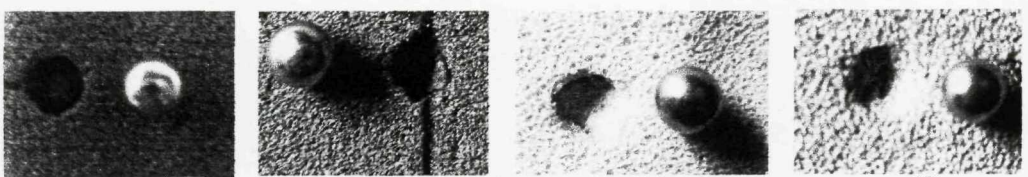

(a) (b) (c) (d)

Figure 4- 18 Photographs of specimens from high-velocity indentation test with impacting 4.5mm ball bearing.

	unaged		aged15000hrs	
	C70.130	R63.140	C70.130	R63.140
Impact depth (mm)	3.16	3.1	3.01	2.41

Table 4- 4 mean indentation depths from high strain rate,on TSA specimens 150x100x20mm

A comparison of the indentation tests conducted has indicated linear foam to be most sensitive to strain rate in both virgin and aged conditions, and also most vulnerable to the effects of hygrothermal ageing for both strain rates.

At a low strain rate, virgin linear cells were observed to effect a recovery in the indentation depth which was absent in the aged specimen. Under visual examination indentation edges appeared smoothed with cells plastically compressed, however, cross-linked cells showed signs of brittle fracture which were emphasized by ageing. While at a high strain rate the change caused by ageing in linear foams was only 10 %, it was six times greater than the change observed for cross-linked cores. At a low strain rate the aged linear cells greatly resisted indentation by 76%, while cross-linked cell resistance decreased by 66%. Damage sustained by the cells during hygrothermal ageing

appears to have affected their energy absorption response considerably, with the implication that a hull cored with a cross-linked foam may be at greater risk to low velocity collision or grounding, while linear cored hulls designed for wave energy impact absorption may risk a reduced fatigue life with increased vulnerability to shear crack development.

References

[1] Vodicka,R., "Acelerated environmental testing of composite materials", Airframes and Engines Division, Aeronautical and Maritime Research Laboratory, Department of Defense, DSTO-TR-0657, 1997
[2] Li, X, Weitsman, J. " Sea-water effects on foam-cored composite sandwich lay-ups" Composites: Part B 35 (2004) 451–459
[3] American Society for Testing of Materials (ASTM), ASTM F1980-99, "Standard guide for accelerated ageing of sterile medical device packages", 1999
[4] American Society for Testing of Materials (ASTM), ASTM D3029-84, "Standard test methods for Impact resistance of rigid plastic sheeting or parts by means of a tup (falling weight)", 1984
[5] American Society for Testing of Materials (ASTM), ASTM D3029-84, "Standard test methods for Impact resistance of rigid plastic sheeting or parts by means of a tup", 1984

Chapter Five

Mechanical Testing Results

5.1 Introduction

Chapter One illustrated the loads and failure modes on a marine sandwich core in Figure 1-5. The core was seen to be vulnerable to shear and mixed-mode loading under slamming and collision loading conditions, for which it must demonstrate continued good performance and resilience for the duration of its service life. The purpose of Chapter Five is to understand the behaviour of aged foams by evaluating changes in the critical performance characteristics identified for a marine sandwich and determine the most relevant properties that can provide an indication of degradation. The main performance indicator used was resistance to crack propagation derived from changes in fracture toughness during pure and mixed-mode loading. Understanding of age-damaged foam behaviour was supplemented with observations made of the response to compressive and impact loads though a detailed analysis is beyond the scope of this work. Marine sandwich design guidelines cite property retention in the development of safety margins, so the experimental tests are only required to produce relative rankings of materials and need not be limited to those that provide absolute property values. This permits greater freedom with the geometry and configuration of the specimen and test equipment.

Shear and mixed-mode loading performance was evaluated through fracture toughness tests using a *Compact Tension* (CTS) type specimen configuration which allowed critical stress of a mixed loading modes (K_{IC} and K_{IIC}), and observations of propagation angle and crack surface, to be compared to provide an indication of shear property retention. Standards for mixed-mode fracture of foam specimens are not currently available, however, ASTM E6-

89[1], E399[2], D5045[3] were referred to as accompaniments to the procedures outlined by Noury[4] who used extensive FEA and experimental testing to validate the loading rig and fracture toughness formulations for use with foams of different densities.

5.2 Effect of Ageing on Crack Propagation

The basic relationship describing fracture toughness can be represented as

$$K_{I,II} = \frac{P\sqrt{\pi a}}{wt} F_{I,II}$$

Equation 5- 1

where $K_{I,II}$ is the fracture toughness for modes I and II respectively, P the applied load, a the crack length, w the specimen width, t the thickness, and $F_{I,II}$ geometrical parameters specific to the configuration. The expressions for $F_{I,II}$ determined by Benitz and Richard[5] for the mixed-mode loading rig used within this work are:

$$F_I = \frac{\cos\alpha}{1-\frac{a}{w}} \sqrt{\frac{0.26 + 2.65\left(\frac{a}{w-a}\right)}{1 + 0.55\left(\frac{a}{w-a}\right) - 0.08\left(\frac{a}{w-a}\right)^2}}$$

Equation 5- 2

$$F_{II} = \frac{\sin\alpha}{1-\frac{a}{w}} \sqrt{\frac{-0.23 + 1.40\left(\frac{a}{w-a}\right)}{1 - 0.67\left(\frac{a}{w-a}\right) + 2.08\left(\frac{a}{w-a}\right)^2}}$$

Equation 5- 3

where α is the angular rotation of the rig.

Though initially developed for metal blocks 60 mm x 40 mm to allow the same specimen to be rotated through 90° from pure mode I to pure mode II, the loading regime has been successfully applied to laminated composites[6,7], and Noury[4] confirmed the accuracy of the method for high density rigid foam specimens.

The test specimen configuration and procedure described by Noury for the determination of toughness values was initially replicated in this work, however, following subsequent TSA testing by Lembessis[8] on both foam types, it became apparent that the weight of the solid steel rig and the small dimensions of the specimens effected interfering stress distributions within the foam specimen which may affect the TSA data quality about the crack-tip. The loading rig was revised in aluminium and rescaled x2.5 to compensate for the sensitivity of the material. Details of the revisions, resolution of forces through the loading pins, and the verification of the Richard geometric factors from equations of 5-2, and 5-3 are summarised in Appendix 6A. Fracture tests were later repeated on specimens sized 150 mm x 100 mm to obtain toughness values from additional loading angles.

5.2.1 Materials and specimen configuration

The materials used were C70.130 (cross-linked) and R63.140 (linear) as manufactured by Airex and described with cell micrographs in Chapter Four *Hygrothermal Ageing*. The typical material properties supplied by the manufacturer are:

Designation	C70.130	R63.140
Description	Cross-linked	Linear
Colour code	Green	Cream
Nominal density kg/m^3	130	140
Compressive strength N/mm^2	2.6	1.6
Compressive modulus N/mm^2	155	110
Tensile strength N/mm^2	3.8	2.4
Tensile modulus N/mm^2	115	90
Shear strength N/mm^2	2.3	1.85
Shear modulus N/mm^2	50	37
Shear elongation to break %	30	80
Thermal conductivity W/mK	0.039	0.039

Table 5- 1 Material properties of unaged test specimens supplied by manufacturer Alcan-Airex[9].

It should be noted that there are variations in composition and material properties both between batches of foam sheets produced, and over time as manufacturing chemical composition and production methods are changed. The materials used for these tests had production dates of 1998.

Test specimens of each foam type, sized 60 mm x 40 mm were cut from a single sheet 20 mm thick, in the same direction with a water-jet cooled fine-toothed bandsaw. Loose particles were dislodged with pressurised air and vacuum suction. Four tapered softwood battens were adhered with slow-setting two-part Araldite epoxy on each loading site of the specimen and is shown in Figure 5- 1. The battens protected the specimen from the clamp used to drill the loading holes and reinforcing the foam at the point of loading contact so as to spread the load and minimise local crushing.

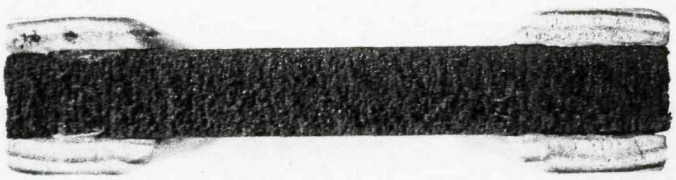

Figure 5- 1 Tapered wooden end tabs shown adhered to an unaged C70.130

The configuration of the CTS specimens used is shown in Figure 5- 2 (a), while the configuration later adopted for TSA and for fracture toughness angles 10° and 80°, is shown to relative scale in (b).

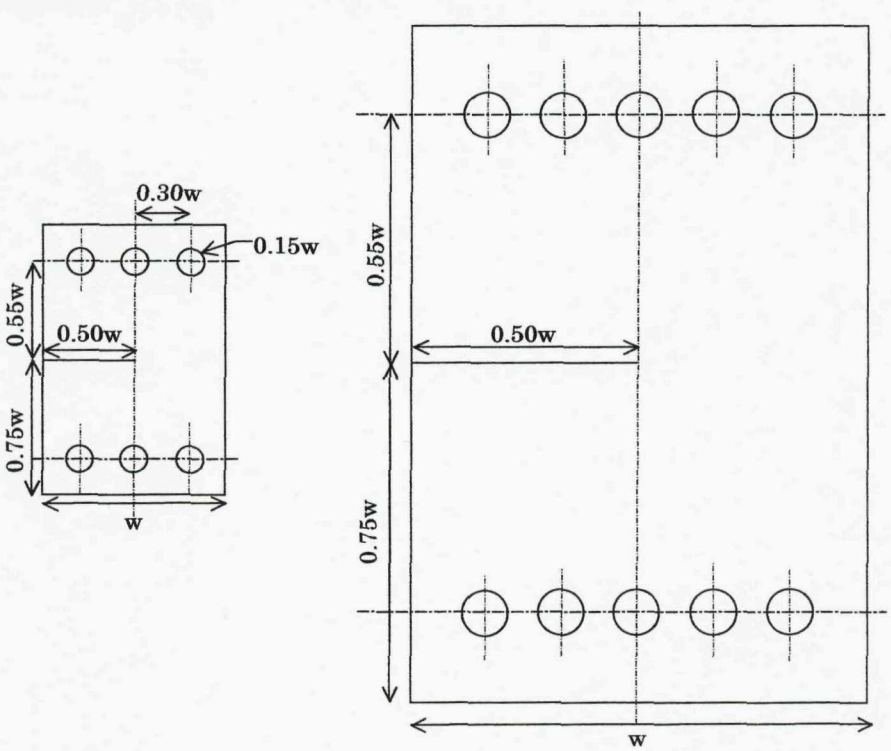

(a) w = 40 mm

(b) w = 100 mm

Figure 5- 2 Fracture toughness specimen configurations shown scaled relative to each other. (thickness t, =20 mm).

The sharp crack-like notched was inserted with a No.11 scalpel which may cut finer than one cell width. The notch was inserted *after* the specimen had been extracted from the water tank, weighed, dried till no further weight loss registered, and reacclimatised for 3 days at room temperature and humidity,

5.2.2 Experimental arrangement

Specimens were positioned within the rig and placed within into a calibrated Instron 8500 universal test machine. A tensile displacement-controlled force was applied as the low loads used for foams are more easily controlled by the test-machine than when in load control. Displacement rate was set at 1mm/min. Load and displacement was automatically recorded on graph paper from the load-cell in addition to a calibrated extensometer gauge clipped into the specimen crack open-mouth with respect to ASTM E399. Extensometers were used with caution as slippage could occur, most notably during testing of the unaged linear foam.

Three replicate specimens were used to obtain an average for each loading angle, for each aged condition. Seven aged conditions were selected, so more than 336 specimens tested in this manner. The loading angle was selected by orientating the rig within the grips of the Instron. Mode I is taken as a rig orientation of 0° and mode II as 90°. Mixed-mode loading is then any angle in between. The rig is pictured in Figure 5- 3 with a sample specimen held in a mixed-mode position at 45°.

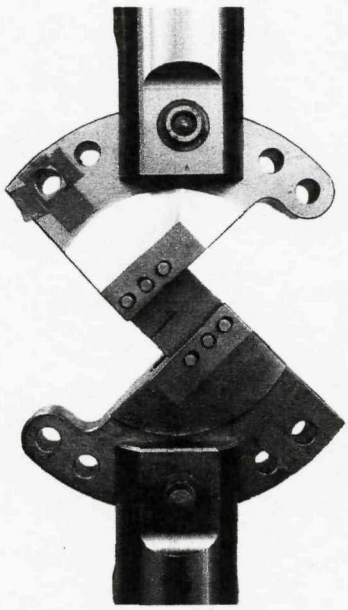

Figure 5- 3 Experimental loading rig with specimen for fracture toughness testing in 45° position.

5.2.3 K_{IC} calculation

In lieu of standards for mixed-mode fracture of cellular materials, the load-displacement curves were used as described by ASTM E399[2]. It is first necessary to establish the validity of the K_{IC} obtained. This is achieved by the calculation of a conditional K_Q based upon a conditional load P_Q as determined from a 5% secant construction from the initial load-displacement gradient. The intersection with the load curve provides P_Q. If the maximum load (P_{max}) applied exceeds P_Q by more than 10%, the test is not considered valid for K_{IC}. If valid, K_Q may then be calculated from the relationship:

$$K_Q = \frac{P_Q\sqrt{\pi a}}{wt} f\left(a/w\right)$$

Equation 5- 4

K_I and K_{II} could then be calculated using the Richard constants F_I and F_{II} in place of the geometric function f(a/w). The geometric constants are obtained from Equation 5-2 and Equation 5-3 and may be graphically represented as in Figure 5- 4.

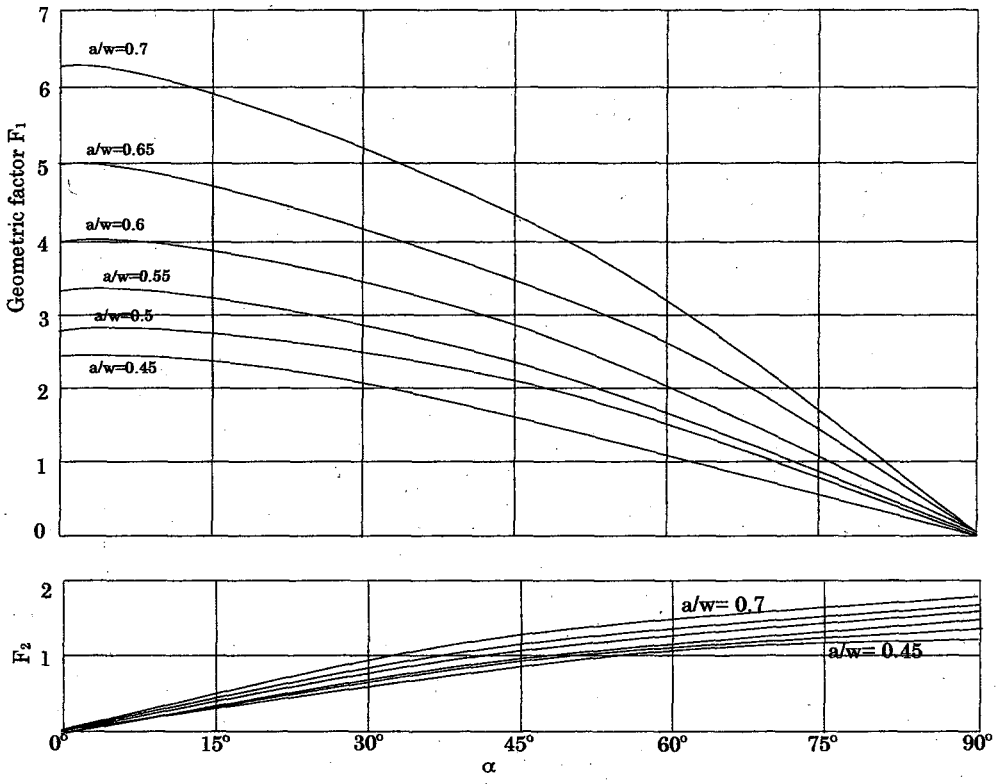

Figure 5- 4 Graphical representation of geometric factors developed by Richard for the experimental rig.

In addition, five assumptions are required for ASTM E399 to be valid. It is assumed that the specimen thickness of 20 mm is sufficient to ensure state of plane strain. It is assumed that the crack inserted by scalpel is sufficiently sharp to ensure that the minimum value of toughness is obtained. It is required that the initial crack be between 45% and 55% of the specimen width. It is assumed that fracture may be classed as 'brittle' to ensure valid application of the method. It is assumed that the specimen thickness t, and crack length a must be greater than $2.5(K_Q/\sigma_Y)^2$ for K_Q to equal K_I.

5.2.4 Sample load-deflection curves

The load-deflection curves for the aged R63.140 and C70.130 in both conditions were seen to exhibit clear linear elastic and brittle behaviour. In its unaged state, the R63.140 material showed some non-linearity indicative

of a tough material with plastic behaviour, and the value of P_{max} was just borderline of the 10% P_Q secant construction limitations imposed by ASTM E399. The representative shapes of the load-displacement curves in mode I are shown below in Figure 5- 5. Given the more linear behaviour of R63.140 in its aged condition, the linear response of the C70.130 material, the absence of fracture standards for foam cores, the previously successful and FEA validated approach by Noury[4], it was decided for reasons of continuity of comparison, to use the same approach in the definition of P_{max} and P_Q. However, it should be noted that the resultant P_{max}, and subsequently K_Q, may then be underestimated.

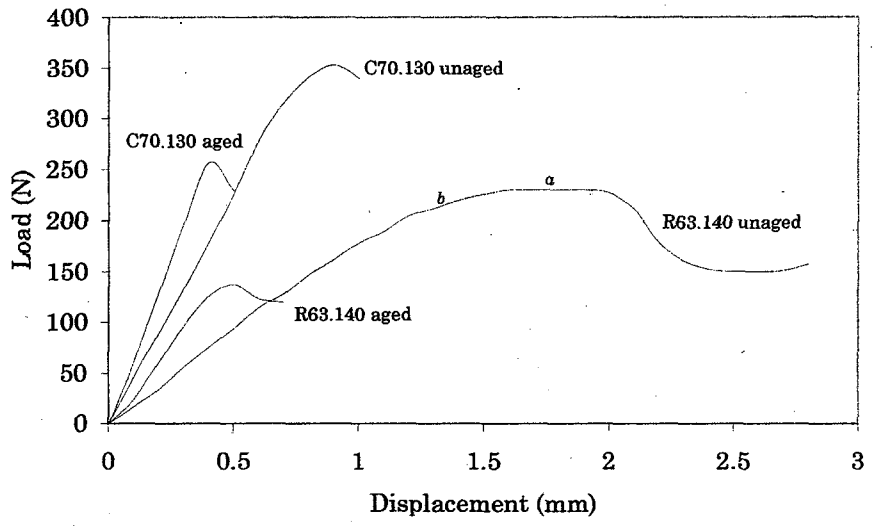

Figure 5- 5 Representative graph to show shape of load-displacement curve for aged and unaged specimens of C70.130 and R63.140 in mode I.

BS 2782 and ISO 527-1[10] describes the P_{max} value to be used for the determination of tensile properties as the point *a* shown in Figure 5- 5, whereas that used by ASTM E399 is represented by the point indicated as *b*. While the ISO 527-1 is the standard used by Airex (the manufacturer of R63.140), to determine its tensile properties, the standard asserts that its methods are applicable to rigid and semi-rigid plastics but are normally unsuitable for cellular materials.

As the R63.140 aged, the load-displacement curve became increasingly linear, and the gradient steeper. The constructed P_Q value was thereby affected,

providing an apparently inflated value for some aged specimens, in contrast to a lower P_{max} value if defined by a in Figure 5- 5. The significance of this error was offset by the apparent rapid change of the load-displacement curve in both shape and magnitude after only minor ageing. This change in material behaviour was most notably displayed in the mode II loading of the R63.140 which initially exhibited excellent resistance to crack propagation in the unaged condition, electing to deform and eventually plastically tear, before suffering a fast brittle fracture in the aged condition. Increased brittle behaviour was further supported by microscopic examination of the crack pathway and the fracture surface.

5.2.5 Effect of ageing on fracture toughness

The average value of three replicated tests used to record K_I and K_{IIC} for C70.130 and R63.140 in the unaged and aged conditions, are presented in Table 5- 2 and Table 5- 3 respectively with the ageing time and corresponding weight change (moisture absorption). These changes are graphically represented for modes I and II in Figure 5- 7 and Figure 5- 8. The ratio of K_{IIc} /K_{Ic} is tabulated in Table 5- 4, and the scatter of the P_Q value used to calculate Table 5- 2 and Table 5- 3 is listed in Table 5- 5.

The greatest changes are seen to occur in R63.140 for both K_I and K_{II} modes with K_{II} seemingly the most sensitive to ageing. In the final aged condition, when the R63.140 had increased approximately twice as much as the C70.130, it also exhibited a change in change in K_{II} that was almost twice that of the C70.130. A comparison between the microstructures of R63.140 and C70.130 shown in Figure 5- 6 suggests that cell-size is a more dominant factor than polymer cross-linking. It also suggests it can be a source of scatter within results for fracture toughness when viewing the errors in Table 5- 5.

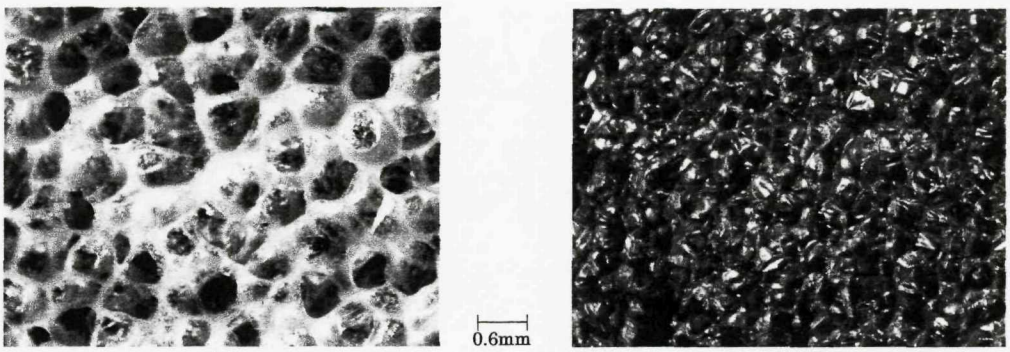

(a)
R63.140

(b)
C70.130

Figure 5- 6 Macrographs depicting unaged, undamaged foam surfaces.

K values in mixed mode followed a similar trend to that of pure K_I and K_{II} but tended to produce more scatter, most noticeably at early stages of ageing and predominantly for the C70.130. This may be related to the shallow penetration depth and through-thickness inhomogeneity of ageing interfering with the propagation of the crack. At later stages of ageing, the mixed-mode trends become more consistent with less scatter.

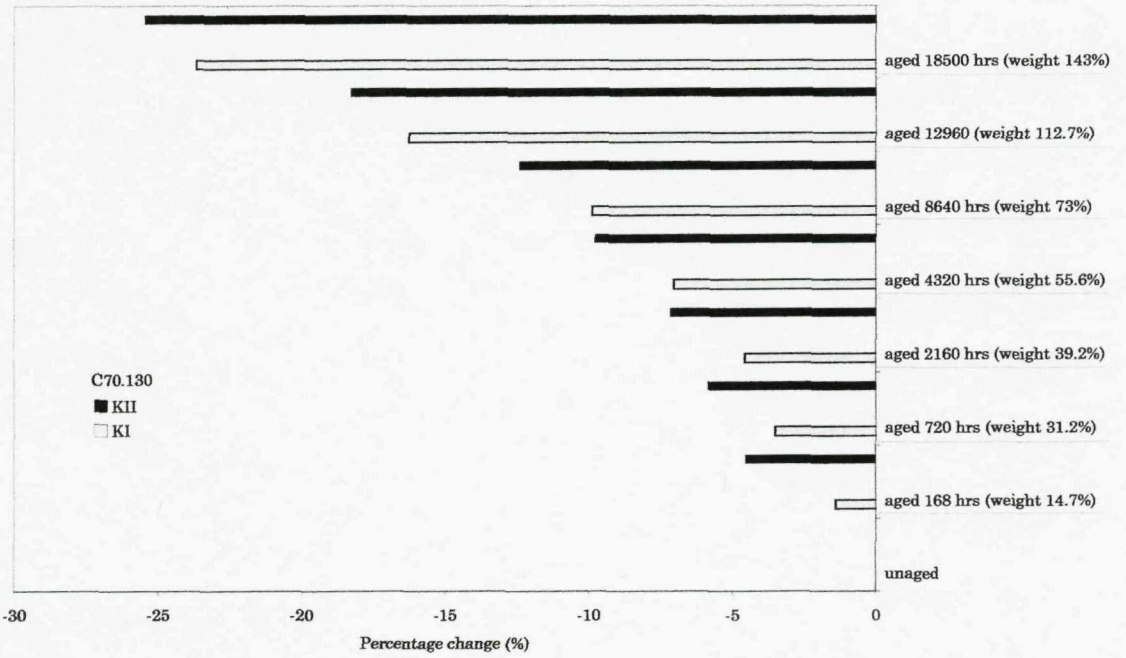

Figure 5- 7 Graphical display of percentage change of modes I and II from the unaged state for C70.130

Angle	unaged		C70.130 aged 168 hrs (Δweight 14.7%)		aged 720 hrs (Δweight 31.2%)		aged 2160 hrs (Δweight 39.2%)		aged 4320 hrs (Δweight 55.6%)	
	K_{IC}	K_{IIC}	K_{IC}	K_{IIC}	K_{IC}	K_{IIC}	K_{IC}	K_{IIC}	K_{IC}	K_{IIC}
0°	0.283	0	0.279	0	0.273	0	0.270	0	0.263	0
15°	0.260	0.051	0.255	0.046	0.248	0.046	0.246	0.045	0.242	0.044
30°	0.237	0.067	0.222	0.065	0.220	0.062	0.220	0.061	0.199	0.060
45°	0.181	0.092	0.176	0.089	0.171	0.085	0.175	0.086	0.157	0.078
60°	0.128	0.106	0.127	0.105	0.124	0.103	0.118	0.103	0.113	0.097
75°	0.066	0.129	0.064	0.128	0.062	0.127	0.059	0.122	0.058	0.113
90°	0	0.153	0	0.146	0	0.144	0	0.142	0	0.138

Angle	C70.130 aged 8640 hrs (Δweight 73%)		aged 12960 (Δweight 112.7%)		aged 18500 hrs (Δweight 143%)	
	K_{IC}	K_{IIC}	K_{IC}	K_{IIC}	K_{IC}	K_{IIC}
0°	0.255	0	0.237	0	0.216	0
15°	0.234	0.042	0.220	0.049	0.199	0.035
30°	0.216	0.059	0.199	0.066	0.177	0.049
45°	0.163	0.080	0.154	0. 078	0.137	0.071
60°	0.124	0.104	0.114	0.099	0.102	0.082
75°	0.061	0.123	0.056	0.114	0.050	0.095
90°	0	0.134	0	0.125	0	0.114

Table 5- 2 Fracture toughness results for C70.130 in stages of aged and unaged conditions. Average taken from three specimens per data point (specimen 60 mm x 40mm)

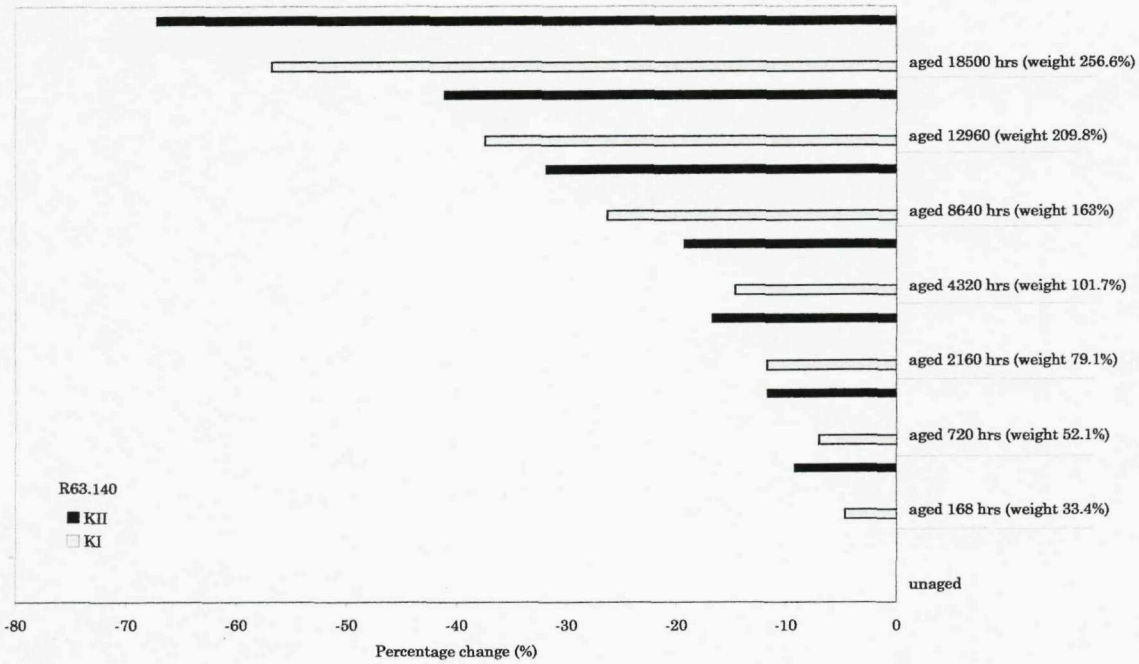

Figure 5- 8 Graphic display of percentage change of modes I and II from the unaged state for R63.140

Angle	R63.140									
	unaged		*aged 168 hrs (Δweight 33.4%)*		*aged 720 hrs (Δweight 52.1%)*		*aged 2160 hrs (Δweight 79.1%)*		*aged 4320 hrs (Δweight 101.7%)*	
	K_{IC}	K_{IIC}	K_{IC}	K_{IIC}	K_{IC}	K_{IIC}	K_{IC}	K_{IIC}	K_{IC}	K_{IIC}
0°	0.171	0	0.163	0	0.159	0	0.151	0	0.146	0
15°	0.163	0.033	0.155	0.029	0.148	0.025	0.139	0.024	0.134	0.015
30°	0.151	0.043	0.150	0.041	0.138	0.038	0.130	0.036	0.123	0.035
45°	0.124	0.062	0.120	0.060	0.114	0.057	0.108	0.056	0.109	0.056
60°	0.096	0.079	0.089	0.076	0.089	0.072	0.083	0.069	0.080	0.067
75°	0.05	0.106	0.048	0.098	0.044	0.095	0.042	0.088	0.041	0.087
90°	0	0.119	0	0.108	0	0.105	0	0.099	0	0.096

Angle	R63.140					
	aged 8640 hrs (Δweight 163%)		*aged 12960 (Δweight 209.8%)*		*aged 18500 hrs (Δweight 256.6%)*	
	K_{IC}	K_{IIC}	K_{IC}	K_{IIC}	K_{IC}	K_{IIC}
0°	0.126	0	0.107	0	0.074	0
15°	0.117	0.020	0.099	0.017	0.067	0.011
30°	0.106	0.030	0.089	0.027	0.064	0.018
45°	0.086	0.043	0.073	0.036	0.047	0.024
60°	0.067	0.056	0.058	0.046	0.035	0.029
75°	0.035	0.073	0.029	0.061	0.017	0.031
90°	0	0.081	0	0.070	0	0.039

Table 5- 3 Fracture toughness results for R63.140 in stages of aged and unaged conditions. Average taken from three specimens per data point. (specimen 60 mm x 40mm)

	unaged	*aged 168 hrs*	*aged 720 hrs*	*aged 2160 hrs*	*aged 4320 hrs*	*aged 8640 hrs*	*aged 12960 hrs*	*aged 18500 hrs*
C70	0.541	0.523	0.527	0.526	0.525	0.525	0.527	0.463
R63	0.696	0.663	0.660	0.656	0.658	0.643	0.654	0.527

Table 5- 4 K_{IIc}/K_{Ic} ratio for C70.130 and R63.140 with progressive ageing

The K_{IIc}/K_{Ic} ratio for R63.140 was greater than C70.130 for all but the final stage of ageing and showed a progressive decreasing trend as it aged, while the C70.130 remained steady.

5.2.6 Results scatter

The scatter between the three repeat tests used to obtain an average P_Q value for use in K_I and K_{II} calculations was presented as a percentage of the average P_Q and compared for loading angles, foam type and aged state in Table 5- 5. The scatter within the results seems to indicate that data in mode I is the most reliable, with accuracy decreasing with respect to higher modes most notably mode II. It also became apparent that 45° also offered good agreement, followed closely by the 30° and 60° angles. However, it should be noted that angles 15° and 30° generally gave high scatter most especially for the linear foam irrespective of ageing stage. This had not been reported previously by Richard[7] when using metal or solid polymer specimens, or in Noury's[4] work on C70.130 foam specimens using the same experimental rig which was conducted on 0°, 30°, 60°, and 90°, but omitted the 15°, 45°and 30° angles available. For the average values of K_I and K_{II} 0°, 30°, 60°, and 90° that Noury recorded for the C70.130, excellent agreement was found within the range of aprox 1.5-9%. There is currently no manufacturers data available for comparison.

Angle	% scatter about $P_{Qaverage}$															
	unaged		*aged 168 hrs*		*aged 720 hrs*		*aged 2160 hrs*		*aged 4320 hrs*		*aged 8640 hrs*		*aged 12960 hrs*		*aged 18500 hrs*	
	C70	R63	C70	R63	C70	R63	C70	R63	C70	R63	C70	R63	C70	R63	C70	R63
0°	4.7	6.1	4.4	5.7	4.5	4.8	4.3	1.7	4.2	2.8	4.3	3.0	2.8	3.1	2.3	2.4
15°	6.9	7.1	6.3	7.6	6.4	8.6	6.2	9.7	5.4	10.3	6.1	7.7	8.7	3.5	7.4	6.8
30°	6.3	5.4	5.4	5.7	8.3	6.2	3.3	5.1	7.7	6.2	4.8	5.3	6.7	4.2	4.1	2.7
45°	5.1	5.4	4.9	5.0	5.2	5.3	5.8	2.7	4.6	2.9	3.4	4.5	5.3	4.8	5.2	4.7
60°	7.2	8.3	4.8	8.6	7.5	8.1	6.0	5.1	5.5	4.7	4.2	5.4	8.2	7.3	7.0	6.2
75°	10.4	11.2	10.3	12.2	7.6	14.1	9.3	9.5	8.7	9.1	9.2	3.2	9.4	7.3	7.9	6.6
90°	8.6	12.7	8.7	13.6	8.1	12.4	8.4	11.2	7.9	9.7	9.1	8.5	8.1	8.9	7.1	7.6

Table 5- 5 Scatter of load P_Q constructed from load-displacement curves of C70.130 and R63.140 in aged and unaged conditions, as a percentage from the mean $P_{Qaverage}$ used in Table 5- 2 and Table 5- 3.

Following FEA analysis, the ASTM E399 requirement for the size of the plastic zone was shown by Noury[4] to be overestimated and unsuitable for foams. For C70.130, a plastic zone of 3.1 mm was calculated for mode I and 6.4 mm for mode II. The size of the plastic zone is proportional to K_I^2, and as K_I for R63.140 was found to be less than that of C70.130, and the K_I value was seen to fall with progressive ageing, the size of the plastic zone was not considered to invalidate the fracture tests.

5.2.7 Effect of ageing on the crack pathway

The crack propagates along a path of least resistance and with respect to the loading angle, representative of the direction of the maximum driving force. Deviation of the crack path from its initial direction is termed the *kinking angle,* ψ. The kinking angle provides information about the stress conditions at the crack tip, the degree of mode-mixity, and an indication of the materials behavioural response to acute stress. The practical implication of this is that the experimental results may be used to inform predictions on whether a crack will penetrate deeper into a structure, if it will arrest, and how long the crack would be at that point[11].

The experimentally obtained kinking angles are shown listed in Table 5- 6 for both materials. The mean kinking angle seemed consistent for both materials for each respective loading angle, though a small trend of decline could be observed during the ageing of the R63.140, and more noticeably during shear loading. This change in kinking angle is perhaps due to a decline in the

rotational mobility of the cell struts from ageing, preventing the material from re-aligning itself.

It should be noted that the kinking angle for unaged R63.140 is unreliable as the specimen distorted significantly without fracture, but tearing at the crack tip. In the unaged condition R63.140 and to a lesser extent C70.130, permit some degree of re-alignment of the cells as the driving force seeks the path of least resistance with respect to the loading angle. Cell walls and struts give way due to excessive plastic deformation though more than one strut in a different direction about the crack-tip may yield. The crack may then change direction towards this path of least resistance, deflecting the crack path away from its original propagation pathway though due to the directionality of the driving force and the loading angle, may effect a meandering pathway as illustrated in (a) Figure 5- 10 when viewed on a microstructural scale. The overall crack path is illustrated in Figure 5- 9 by unaged C70.130. The pathway is shown here for a specimen subject to a static fracture test, and that of a specimen fatigued during TSA to produce a stable crack growth for comparison to service failures.

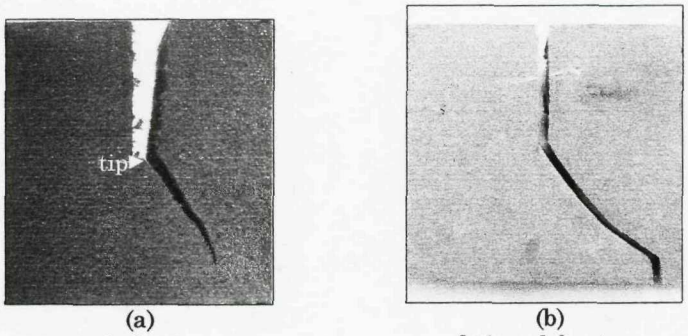

(a)
static fracture

(b)
fatigued fracture

Figure 5- 9 Overall mixed-mode crack pathway for unaged C70.130 at 45°

From the crack pathway the service failure brought on by fatigue appears more susceptible to local stress intensity factors at the crack-tip than a static fracture test indicates, despite the rapid rate of catastrophic failure that was observed once a crack appeared.

Loading angle	0°	15°	30°	45°	60°	75°	90°
C70.130 unaged	0	19	30	41	49	59	61
aged 168 hrs	0	17	28	40	48	61	64
aged 720 hrs	0	18	27	40	46	57	66
aged 2160 hrs	0	17	29	41	44	59	63
aged 4320 hrs	0	17	28	39	46	59	62
aged 8640 hrs	0	16	29	38	44	59	61
aged 12960 hrs	0	18	27	39	46	58	60
aged 18500 hrs	0	16	27	38	44	57	60
R63.140 unaged	0	19	29	42	51	62	*81*
aged 168 hrs	0	17	28	41	50	60	66
aged 720 hrs	0	18	30	40	48	59	65
aged 2160 hrs	0	15	28	40	47	60	66
aged 4320 hrs	0	14	27	38	46	61	66
aged 8640 hrs	0	16	28	38	45	60	65
aged 12960 hrs	0	14	28	38	45	60	65
aged 18500 hrs	0	16	28	39	46	60	65

Table 5- 6 Mean kinking angle for C70.130 and R63.140 in different ageing states

In an unaged condition the crack propagation and pathway appears to be governed by local plastic deformations and local damage accumulation processes as it grows per cell. Extensive fatigue testing conducted on C70.130 beams by Noury[4] concluded that fatigue crack-growth could be considered K_I controlled and accurately modelled with linear elastic fracture mechanics (LEFM) and the Paris law, but warned of K_{II} controlled co-planar crack-growth in mode II loading. The effect is well known in metals and can be described as the magnification of the stress intensity factor due to interaction between two or more cracks on the same plane. Cracks in parallel effectively shield each other, resulting in a decrease of the stress intensity factor when compared to the case of a single crack[12].

(a) C70.130 unaged mode I crack

(b) C70.130 aged mode I crack

(c) R63.140 aged crack-tip

Figure 5- 10 Micrograph slice to illustrate crack-tip and crack pathway before and after ageing 8640hrs (mag. x5)

Loss of plasticity from ageing appeared to restrict mobility providing the more direct crack pathway shown in (b) Figure 5- 10. The direction of the pathway is further complicated by the through-thickness inhomogeneity of the ageing, to mimic a brittle shell that encompasses a ductile centre. An apparent change in failure mode was observed from cell distortion, pathway deflection around cells with thicker cell struts and cell wall tearing, to brittle fracture directly through cells.

Scatter about the mean kinking angle was considerably greater for the unaged R63.140 possibly due to the relationship between the size of the crack-tip and the larger cells around it and seen in (c) Figure 5- 10. Scatter appeared diminished following ageing of the cells for both materials.
The implication of these observations is that any microstructutal or cells-size effects that may affect or deter the propagation of a crack though a foam in its unaged state, are no longer effective when the cells have been subjected to ageing. The effects become more progressively noticeable with ageing and penetration depth. This may have significance for the potential formation of co-planar cracks in the zone beneath the brittle, aged, and crack prone surface as warned by Noury, which if combined with a secondary form of loading such as compression from slamming could lead to failure.

References

[1] American Society for Testing of Materials (ASTM), ASTM E6-89, "Standard terminology relating to methods of mechanical testing", 1989

[2] American Society for Testing of Materials (ASTM), ASTM E399-90, "Standard test methods for Plane Strain Fracture Toughness of Metallic Materials", 1997

[3] American Society for Testing of Materials (ASTM), ASTM D504-95, "Standard test methods for Plane Strain Fracture toughness and strain energy relase rate of plastic materials", 1995

[4] Noury, P., "Shear crack initiation and propagation in foam core sandwich structures", PhD Thesis, University of Southampton,1999

[5] Benitz,K., Richard, H.A, "A loading device for the creation of mixed-mode in fracture mechanics" Int,J.Fracture,vol.22,pR55-58,1983

[6] Pirondi,A., Nicoletto,G. "Mixed mode fracture envelpe of structural adhesive" Conf.Structural adhesives and industrial applications-Alternatives to traditional joining techniques,11-12, Giugno, Italy, 2001

[7] Richard,H. "Some theoretical and experimental aspects of mixed mode fractures" Advances in fracture research.Proc.6th int.Conf.on fracture (ICF6),vol.5, Pergamon Press, p3337-3344, India,4th Dec1984

[8] Lembessis, E. "Evaluation of stress intensity factors for aged sandwich foam using TSA" University of Southampton, 2006.

[9] Airex, "Technical data sheets C70.130, R63.140" CH-5643 Sins/Switzerland

[10] British Standards BS 2782 Part 3: Method 321:1994 /ISO 527-1 "Determination of tensile properties. General principles" 1994

[11]Carlsson, L.A, Matteson R.C, Aviles F., Loup D.C., "Crack path in foam cored DCB sandwich fracture specimens" Composites Science and Technology 65 (2005) 2612–2621.

[12] Anderson.T. "Fracture Mechanics". 3rd edition, Taylor & Francis publishing, 2005

Chapter Six

TSA Results

6.1 Introduction

The purpose of this chapter is to identify the potential of TSA for the assessment hygrothermally aged marine foam core specimens through the evaluation of stress intensity about a crack-tip of an aged and unaged foam. Associated with this chapter is Appendix Six which contains excerpts from previous work done on the re-scaling of the CTS-type rig for use with TSA. This initial work relating to the design and selection of a specimen configuration and subsequent re-scaling of the mixed-mode loading rig was conducted using a DeltaTherm TSA system. The DeltaTherm was withdrawn from service soon after and replaced with a new generation Cedip system but is based upon the same thermodynamic principles and correlations to a reference signal. It wasthe Cedip system which is used to evaluate ageing damage within this work.

6.2 TSA Test Preparation

The original intention was to use the 60 mm x 40 mm x 20 mm specimens from mechanical testing in the TSA investigation, but following a preliminary feasibility study, it was determined that a new configuration was necessary. The reasons for change were based following observations from mechanical and preliminary TSA testing. The mixed-mode rig constructed in solid steel cut from a block an inch thick, was designed for use with metal specimens, and despite load-cell calibration, load arrangement balance within the grips, and previous validation of the technique from work conducted by Noury, the rig weight was felt to be excessive for the sensitive foam material. A larger-

scale rig was designed with a minimum weight requirement and machined from a single block of aluminium. The mechanical testing of fracture toughness properties, was conducted in mixed-modes of 15°, 30°, 45°,60°,75°,with poor results and accuracy recorded for 15° and 75°. The rescaled rig included 10° and 80°. TSA testing used an Instron servo-hydraulic test machine to cycle at 10Hz. The actuator was determined to partially rotate during cycling causing a torsional stress within the specimen. This was counteracted with a supporting rod attached to the actuator to restrict its plane of motion.

In initial fracture toughness testing, strong reinforcements with wooden battens were required to distribute the loading stresses and limit pull-out of the pin loading points. Additionally, initial TSA showed that the resultant stress about these loading points interfered with the stress about a crack-tip if the crack-length were equal to half the specimen width. It was felt that this issue needed to be addressed before the specimen underwent the prolonged and rapid cycling used for TSA testing. After subsequent iterations of the design and testing process, the rig was additionally modified with a larger surface area for load distribution for all five loading points with well-fitting pins. This was deemed acceptable, as the priority of this portion of the testing was to attempt to use TSA to obtain stress intensity factors from the specimens. These factors would differ to the critical stress intensity factors or fracture toughness values that were obtained during mechanical testing, which would act as guidelines providing an indication of the magnitudes involved in foam behaviour when transitioning from unaged to aged states.

6.2.1 Specimen configuration and preparation

The specimen configuration used for TSA is shown in Figure 6- 1. Due to changes in the configuration from the one used in mechanical testing, the TSA specimens were seen to record a different weight change for the same immersion time. As ageing is characterised by the weight change rather than immersion time, it was necessary to extract the TSA specimens as close to these values as practicable. With reference to gravimetric results in Chapter Four, TSA specimens were aged until 15000hrs.

It is common TSA practice, to homogenise the surface emission of a specimen and obtain the most uniform signal reading by spraying two coats of matt black paint across the specimen surface. It is a consequence of the microstructure of the foam that this was not possible. An even coating cannot be applied to the pore-like surface of the foam, and results in an application that is thicker than that of a cell wall. Additionally, the spray cannot be removed and reapplied as it can for metals.

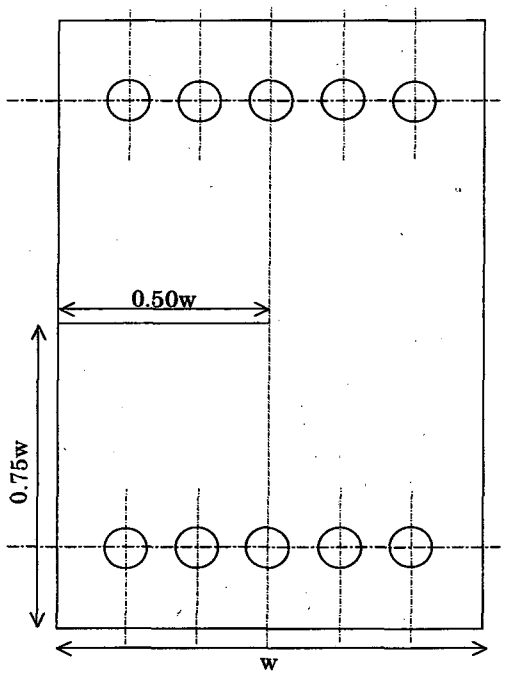

Figure 6- 1 Fracture toughness specimen configuration. Width w = 100 mm, thickness t,=20 mm

The emissivity of the foam surface is expected to alter and increase as the foams are hygrothermally aged and polymer additives are leached from the composition, altering the microstructure and reflectivity of the surface. This is expected to be compensated for by using a calibration constant that encompasses the material property changes also.

6.2.2 Loading arrangement, conditions and testing protocols

The experimental arrangement used is shown in Figure 6- 2. The specimens were prepared using the same procedure as that described for hygrothermal ageing and mechanical testing in previous chapters. Specimens were removed

from the ageing tank, weighed, dried and allowed to acclimatise for 48hrs to the environmental conditions in the lab. The material property changes that are known to occur in aged foams were considered, testing was conducted using displacement control and a calibrated load-cell record of stress for each test run and position. Specimens were typically loaded in a cyclic sine wave form with a frequency of 10Hz. Effort was made to calibrate the servo-hydraulic test machine to confirm load and displacement values, check the cyclic wave form and amplitude stability with an oscilloscope, and maintain the camera position and settings for the duration of testing. From mechanical testing results, it was known to subject the material to only very small amounts of displacement to ensure loading was within elastic limits and plastic deformation would not occur. The specimen was positioned within the rig ensuring the face was perpendicular to the camera lens, with the camera head position adjusted using spirit levels. Distance from the camera lens was measured to the specimen and recorded in the system software. The camera angle and distance were held constant throughout the experiments at 14.50 cm.

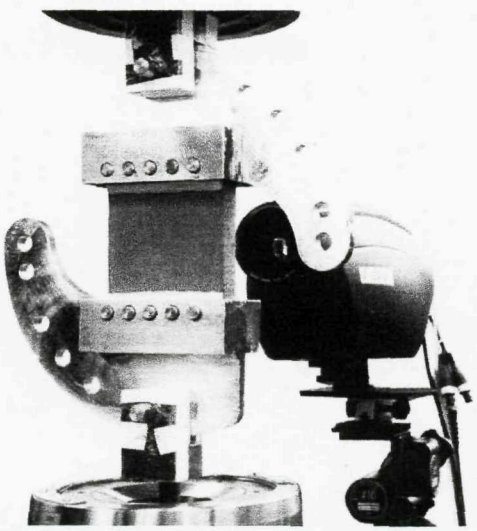

Figure 6- 2 Experimental arrangement of mixed-mode rig and Cedip imaging system

The loading arrangement and procedure was checked using a foam specimen as depicted in Figure 6- 2, loaded under the same conditions, the specimen was rotated from pure tensile to pure shear loading, and the signal data recorded from a $3cm^2$ box average about the centre of the specimen. As the

specimen approached pure mode II, the sum of the principal stresses approached zero, so the signal diminished. Good agreement was found when compared to the theoretical change in stress of the rotated specimen, as calculated from Mohr's circle. shows a sample result of a box signal average taken from a solid unaged R63.140 specimen, in the form of a plot averaged over each frame. The x-axis indicates a value of recorded 300 frames, which is an artefact of the software procedure, which analyses all frames but was set to display every 10 frames. The actual number of frames recorded was then 3000 representing an investment in CPU memory of 490,000KB. Data may be selectively *bracketed* to exclude the initial frames from analysis.

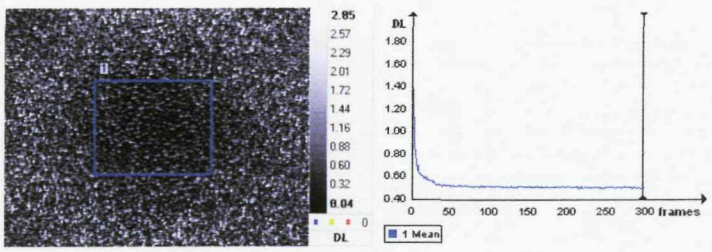

Figure 6- 3 TSA DL Time graph for box-signal average in DL units for solid specimen R63.140 (unaged condition, 10Hz, 0.6mm mean, 0.3mm amplitude)

angle	DL Box average	σ_1	σ_2	$\sum(\sigma_1+\sigma_2)$Theory
0° (mode I)	0.487	0.2	0	0.2
10°	0.465	0.452	-2.58	0.194
30°	0.375	0.189	-0.039	0.15
45°	0.233	0.162	-0.062	0.1
60°	0.224	0.199	-0.113	0.087
80°	0.117	0.212	-0.178	0.034
90° (modeII)	0.062	0.2	-0.2	0

Table 6- 1 Rotation of unaged solid specimen R63.140 TSA, side A (units in DL), 10Hz, 0.6mm±0.3mm

The relationship compared to the expected theoretical values became less accurate when approaching shear modes. Table 6- 1 indicated that the operation of the up-scaled rig design was adequate for TSA testing of foam specimens.

6.2.3 Repeatability and Data Scatter

The same control specimen of unaged R63.140 was tested over a period of 4 months at random intervals, with the same experimental arrangement in

mode I. Table 6- 2 lists the change in the detected signal when compared to the initial value obtained as shown in Table 6- 1. Noticeable scatter was determined for data derived from the same box signal average over the same specimen area. Though a specific trend could not be determined, the greatest scatter occurred following prolonged cycling and was further influenced by the number of accumulated cycles.

cycle duration (hrs)	Accumulated cycles (hrs)	$DL_{Box\ average}$	$\%Change_{0.487}$
0.2	0.2	0.487	0
0.5	0.7	0.471	-3.2
1	1.7	0.466	-4.2
3	4.7	0.466	-4.4
4	8.7	0.510	+4.7
8	16.7	0.522	+7.2
12	28.7	0.526	+8.1
0	28.7	0.456	-6.4
2	30.7	0.516	+5.9
4	34.7	0.520	+6.7
0	34.7	0.459	-5.7
4	38.7	0.530	+9.1
0	38.7	0.503	+3.2
0.1	38.8	0.512	+5.2
2	40.8	0.453	-7.1

Table 6- 2 Results of solid control specimen for unaged R63.140, side A, in mode I (10Hz 0.6mm±0.3mm)

The variations may be influenced by material properties such as creep, or mechanical issues such pulling at the loading points. The loading cycles of the Instron was checked and found to be consistent throughout the test duration.

6.2.4 Calibration constants

From notations during testing relating position control to recorded loads from the Instron, stress values were derived and used to determine the calibration constant A.

Specimen condition	Calibration (A)
R63.140 unaged	0.0225
R63.140 aged	0.0395
C70.130 unaged	0.0313
C70.130 aged	0.0356

Table 6- 3 Calibration constants for material types

6.2.5 Effect of Frequency Variation and Ageing

There appears to be little sensitivity to frequency as shown in Figure 6- 4. In test-runs involving incremental changes in frequency, mean stress, or amplitude, the order was randomised.

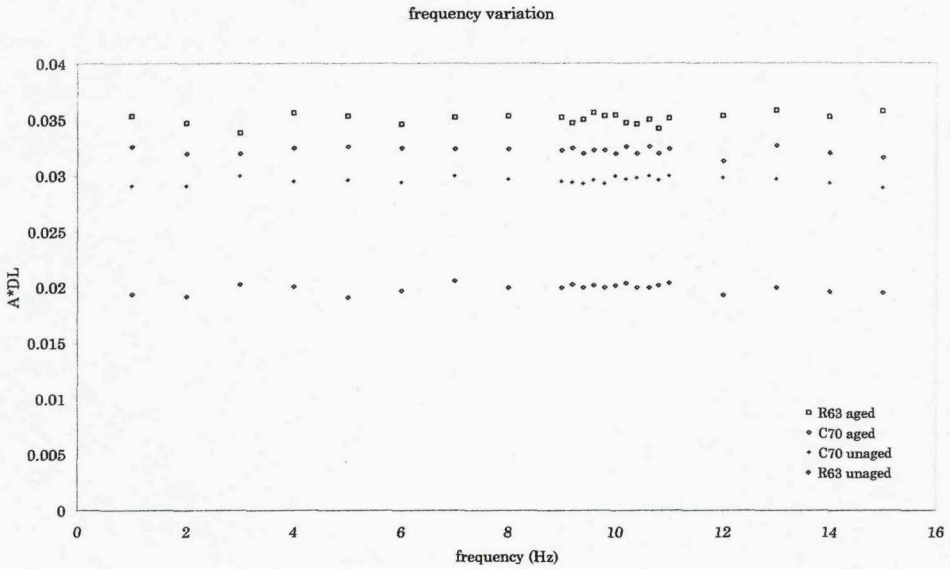

Figure 6- 4 Frequency variation of solid specimen, R63.140, side A, in mode I (10Hz 0.6mm±0.3mm)

6.2.6 Effect of Amplitude Variation and Ageing

All specimens showed a linear trend towards the origin as shown in Figure 6-5.

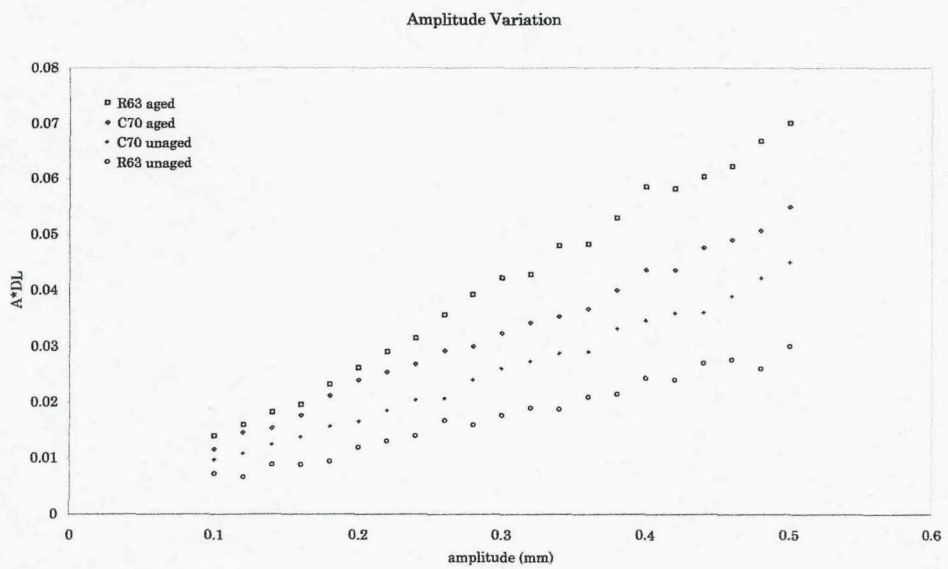

Figure 6- 5 Amplitude variation, frequency 10Hz. Mean 0.6mm

6.2.7 Effect of Mean Variation and Ageing

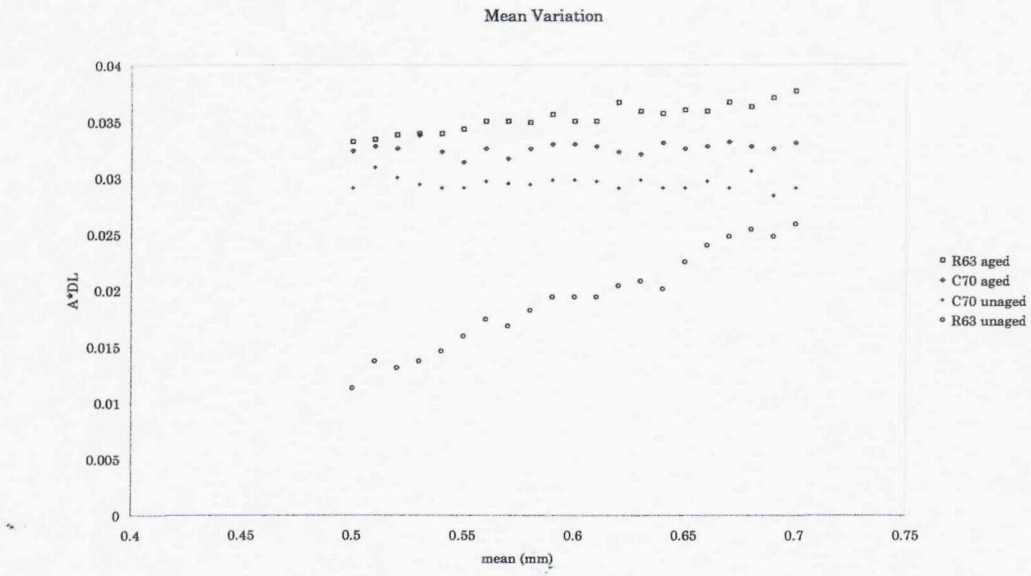

Figure 6- 6 Mean dependency, frequency 10Hz, amplitude 0.3mm

The R63 material is shown to be mean dependent, though upon ageing the influence is less exaggerated. C70 is not seen to be influenced by variation in the mean load, though scatter was observed for both materials and appeared greater for the unaged condition.

6.2.8 Information from the crack-tip

A difference in the behaviour between aged and unaged linear foams in response to a crack was detected and illustrated in Figure 6- 8 and Figure 6- 9. Figure 6- 8 indicates that the stresses around the crack-tip are redistributed by unaged cells, dispersing the crack propagation energy. Phase images showed no significant change indicating adiabatic conditions were maintained, but did provide an indication of damage site location qualitative magnitude as illustrated in Figure 6- 7.

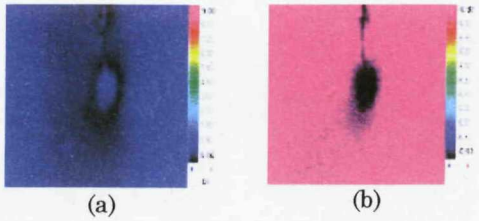

Figure 6- 7 Mode II unaged R63.140 for 10 Hz (a) TSA, and (b) phase data

The cell behaviour in the aged state is seen to differ as the stress is concentration about the crack-tip and depicts apparent increase in brittle behaviour and supporting findings from hygrothermal ageing and mechanical testing. It can also be seen that the area of high stress around the crack tip is composed of clusters of high stress values, as the foam cells in the vicinity have restricted mobility in an aged state. Due to the local cell morphology, it cannot be predicated which cell will fracture as it is not necessarily the one directly in the path of the crack-tip.

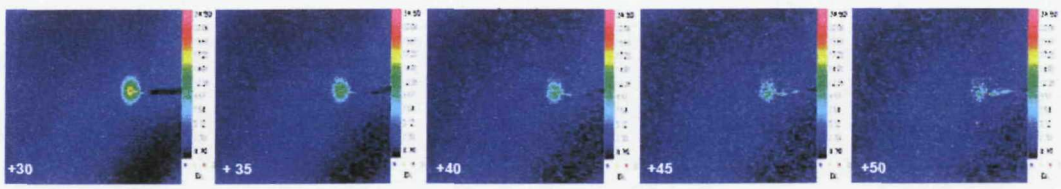

Figure 6- 8 TSA video stills of mode I unaged R63.140 10Hz, 0.6±0.3mm

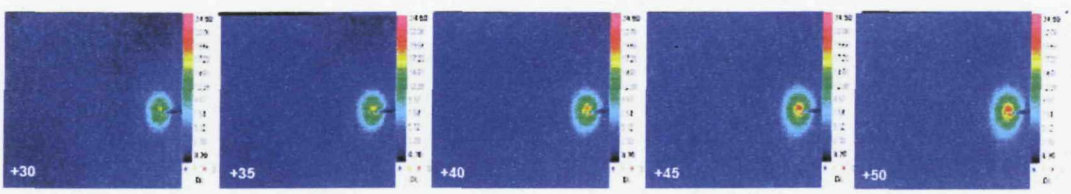

Figure 6- 9 TSA video stills of mode I aged R63.140, 10Hz, 0.6±0.3mm

6.3 Stress Intensity

Using the Stanley[1] method to graphically obtain a stress intensity using a graphical method whereby K_I can be obtained directly from the gradient of a graph of y versus $1/S^2_{max}$ from the expression arranged as :

$$y = \frac{\left(3\sqrt{3}K_I^2\right)}{4\pi A^2}\frac{1}{S_{max}^2}$$

where A is the calibration constant, S the TSA signal, K_I the stress intensity and y, is the line taken parallel to the line of the crack. There was a very high degree of scatter for R63, most notably in the unaged condition, values obtained for C70 in this manner were promising when compared to the critical values obtained in fracture testing with C70 unaged 0.235 $MPa.m^{0.5}$ and 0.179 $MPa.m^{0.5}$ for C70 aged respectively.

For mode I, the sum of the principal stresses with respect to distance from the crack-tip was considered for both linear and cross-linked specimens. There was high scatter in data for the unaged R63 foam, as may be attributed to pockets of high stress values about the tip. Though the general trend of declining stress with increasing crack-length was determined as tests were conducted with constant strain. The effect of ageing on the R63 was to proportionately reduce the magnitude of the peak to approximately a third of the unaged material (which agrees well with mechanical test results), but most noticeably the scatter was greatly reduced, and the peak to base ratio of the aged specimen more than doubled. That is to say, the stress became increasingly concentrated about the crack-tip with less apparent dispersion. The effect of an increasing crack-length on the peak to base ratio was then similar to that observed in both aged and unaged C70 specimens. The peak/base ratio remained consistent at around 1.1 until a/w=0.25, but would then decrease by half for a/w=0.5 at a proportional rate.

Reference

1 Harwood,N Cummings,W "Thermoelastic Stress analysis"IOP publishing, 1991

Chapter Seven

Discussion Summary

7.1 Hygrothermal Ageing Results

The hygrothermal ageing tests indicated that the foam could double its weight in moisture in 5yrs in-service if R63.140 were exposed or 15yrs if C70.130 were exposed. Absorption occurred most easily through damaged cells, and only a relatively small increase in temperature is needed to accelerate the leaching of additives and plasticizers that would lead to increased brittle behaviour. The effects of moisture uptake were affected most damagingly by freeze thaw cycles which may cause the expansion of the absorbed moisture to lead to micro cracking, but also makes the moisture more difficult to extract upon drying. It was found that ageing seemed to be best resisted by foams with smaller cell sizes than thicker struts, and trends of uptake with respect to foam density for both C70 and R63 groups were presented here. R63.140 was consistently seen to be the most vulnerable to ageing, and displayed significant changes in behaviour for both fracture toughness and energy absorption, with apparent increased brittle behaviour. Micrographs also showed pitting like damage to the cell struts and walls with age, which were not advanced on the C70.130 despite evident loss of additives. Local surface indentation testing showed changes in behaviour for both foam types which may have implications for sandwich fatigue life, its response to slamming and collision, and the ability to distribute that energy through the sandwich thickness. If compared to the conservative Q_{10} life-cycle estimates for exposure to service temperatures of 18°C, then it can be said that barring damage, only the R63.140 which may be at risk. However, service temperatures and exposure conditions are known to fluctuate, so it can be seen that ageing could present a significant risk and should be considered in the design safety factor.

The standardised ageing test for medical polymers was found to be the most appropriate and was able to provide a means of relating accelerated ageing time and in-service exposure. Errors in ageing arose from temperature circulation within the tanks, specimen overcrowding and particle breakage from cut edges. Further testing is necessary to improve confidence in accelerated ageing duration to prevent over-ageing and establish a less conservative estimate of in-service time. There is need for a new standardised test aimed at accelerating the ageing and characterisation of foams and materials seen in marine service. The Fick model of diffusion processes was found to have better agreement with the lower experimental temperatures, though material loss such as plasticizers or breakaway particles is considered a violation of the assumptions. An Arrhenius based relationship was found to adequately estimate the relationship between temperature and percentage weight gain. Problems in the accurate prediction of ageing and its properties originated from the variation in composition between foam types, sheets, batches, and manufacturer. Additionally, it was seen difficult to predict the ageing behaviour of a similar foam based on type and mechanical properties without information upon the cell morphology.

7.2 Mechanical Testing Results

The stress intensity factors, K_I and K_{II} were determined for a range of modes from pure tensile to pure shear for both aged and unaged specimens of R63.140 and C70.130. Close agreement was found with comparative tests conducted by Noury on the C70.130 for the x-direction, though testing was characterised with significant data scatter. Subsequently, it could be said that linear elastic fracture mechanics could be applied to the C70 foam, though applicability for R63 may be border-line supporting Noury's conclusion that Richards criterion are the best for prediction of fracture.

A higher error was recorded for shallow mixed modes of 15° and 75° during fracture toughness testing and may have been attributed to the weight of the rig in relation to the sensitivity of the foam. The scale of the testing rig used in mechanical testing was determined to be inadequate and required that the

specimens be scaled-up so as to isolate the stresses at the crack-tip, and it was determined that changes between the response of an aged and an unaged specimen could be observed.

Crack propagation in an ageing foam showed evidence of increasing brittle fracture with a loss energy required to fracture as evidenced from the diminishing area under the load-displacement curves fracture toughness testing. The R63.140 showed the greatest change with the loss of its excellent resistance to a crack in shear. The crack pathway also became increasingly linear with less kinking as the cells mobility was restricted through plasticizer-loss. This altered the behaviour of the cells at the crack-tip which were unable to distort in order to redistribute the local stresses and produced a direct crack pathway as opposed to several additional sites of satellite microcracks about the crack-tip. This provided additional concern for the potential behaviour of R63 core damaged by age.

7.3 TSA Results

TSA successfully detected changes due to ageing for both foam types, though the most significant change was observed in the behaviour of linear foam in the aged and unaged condition in response to a sharp crack. Data supported findings from observations made during hygrothermal ageing and fracture toughness testing that leached plasticizers increased the brittleness of the foam and that the linear material was most vulnerable to the effects of ageing as its mode of diffusing crack propagation energy was compromised. The crack-tip was suffused with pockets of high stress values which complicated extraction of stress intensity factors about the crack-tip.

Chapter Eight

Further Work

8.1 Fatigue Crack Propagation

It is recommended that fatigue and crack propagation conducted by Noury on cross-linked foams using a large-scale CTS-type rig with specimens approximately 0.3mx0.2m, be continued using TSA to monitor crack initiation and its propagation rate. A comparative finite element model of fatigue crack propagation would determine the suitability of the current predictive models. A comparison between core density, morphology and propagation rates would be of benefit. It is recommended that use of the high magnification lenses be used with development of motion compensation techniques to develop micro-fatigue and micro-fracture mechanics models of the propagating crack.

8.2 D-Mode Fatigue Predictions

D-Mode is the name given to the Cedip software that is able to measure the *dissipated* energy rather than the thermoelastic energy from TSA or E-mode, as per software notation. This mode has been used successfully to predict fatigue sites and fatigue limits in metals[1] Dissipated energy is much smaller than the thermoelastic effect and needs a sensitive thermal imaging camera and a dedicated algorithm to function, and subsequently, is a recent development in the field. From the methodology described by Kim[1] D-mode is the intrinsic dissipated energy and the signal (DL) depends on the intensity of stresses or loads, shape of specimens, and periodic frequency and indicates variations in mechanical properties. By maintaining test conditions constant, but increasing amplitude is applied in increments, Kim determined was able to show that the inflection point of the D-mode signal corresponded to the

fatigue limit of the material. When applied to the C70.130 and R63.140 specimens used in TSA, for the aged and unaged conditions, first estimates for a fatigue limit could be attempted and are shown below in Figure 8- 1 Figure 8- 2. The C70.130 was seen to provide little scatter in the data, but the R63.140 showed significant scatter. The C70.130 estimated the fatigue stress limit to have reduced by approximately a third of from its unaged condition to 0.188MPam$^{0.5}$. This first estimate compares favourably in order of magnitude when compared to that of the literature. Noury determined that the Paris law applied to provide da/dN =1.77x10-11 $(\Delta K)^{0.8.026}$, and gave a 0.3MPam$^{0.5}$ estimate for a a/w=0.5 C70.130 specimen. It is believed that these preliminary tests have shown that D-mode has potential for application to fatigue estimates of hygrothermally foam specimens.

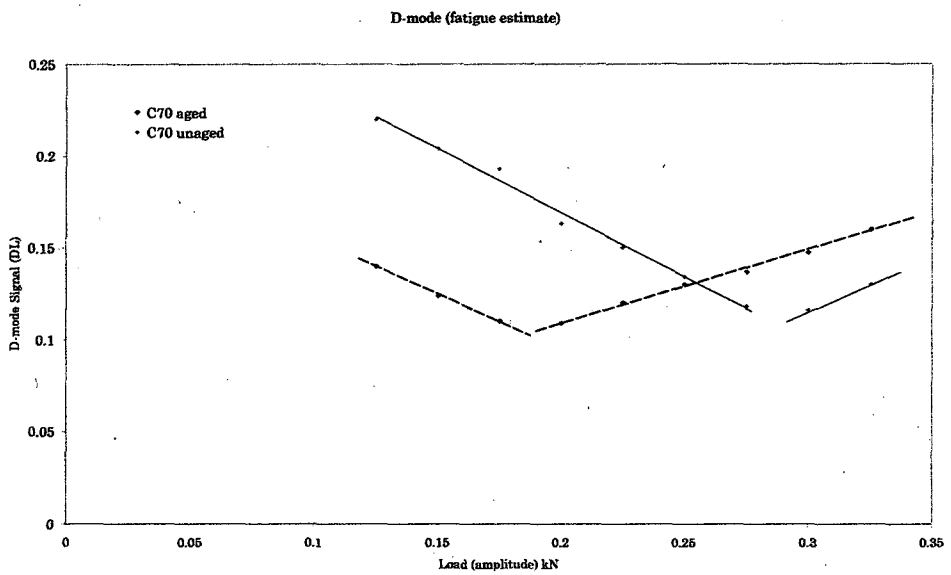

Figure 8- 1 D-mode distribution for load amplitude variation for C70.130

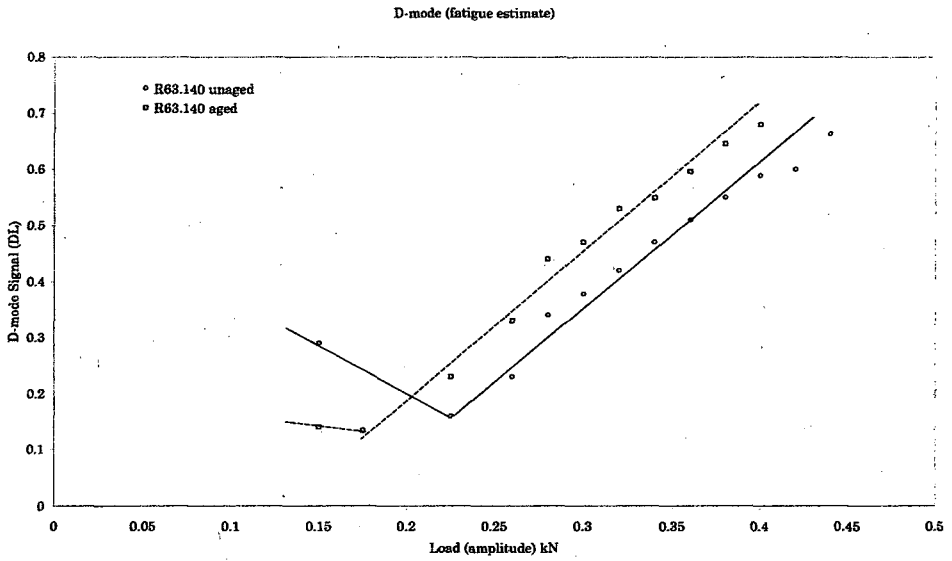

Figure 8- 2 D-mode distribution for increasing load amplitude for R63.140

8.3 Cyclic Creep

It would be of benefit to designers to greater understand the effect of creep and the interactions between creep-fatigue in a sandwich structure and to evaluate the validity of mathematical models.

8.4 Damage Threshold

Non-contact techniques may be further exploited to determine the minimum crack-length or defect size necessary before catastrophic failure is initiated.

8.5 Shear Crack Propagation

One of the most important issues of composites in marine sandwich structures, is their vulnerability to failure in shear. Given the intrinsic problems for shear detection using the TSA technique, it is recommended that the potential of Digital Image Correlation (DIC) be evaluated for the propagation of shear cracks within a sandwich structure such as a T-joint. DIC is another full-field, non-contact technique, but has the advantage of

TSA in being increasingly accurate for materials showing strain, with relevance for flexible polymer foams such as linear foams.

The Figure below shows the experimental arrangement with two cameras and an example of results possible in Mode I for a linear foam.

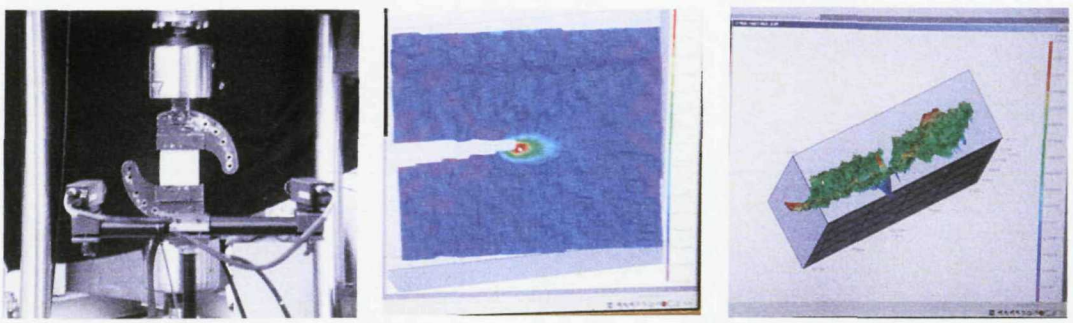

(a) (b) (c)

Figure 8- 3 (a) Arrangement for non-contact Digital Image Correlation (DIC), with linear foam mounted in mode I position of CTS-type rig. (b) screen image of linear foam depicting DIC result (c) screen image of DIC software showing rotated 3-D image of linear specimen.

8.6 TSA Stress Intensity Factor Extraction

The use of linear foams illustrated the difficulty for SIF extraction using TSA. Many of the formulations are based upon the presence of a cardioid shape, and methods determine mathematical curve-fitting techniques to improve accuracy of SIF extraction. However, some results obtained with TSA from the surface of the foams indicated efficient dispersal of the stress from the crack-tip providing R63 with its excellent resistance to crack propagation, and meriting a 15% reduction in design safety factors. A methodology to extract SIFs from a form not immediately identifiable as a definite geometric shape needs to be developed and a numerical method which considers the magnitude, and proximity clustering to each recorded magnitude data point would be helpful in the clarification of data to promote success of the technique for R63.

8.7 Standardised ageing test

From this work it was determined that it would be advantageous for there to be a standardised accelerated ageing test for sandwich materials that are to

be used within marine applications. It would be recommended that the Tg of the material be taken into consideration.

8.8 Predictive ageing

This work has shown that the properties of both cross-linked and linear cores are vulnerable to ageing, with linear foams carrying the greatest potential risk. Experimental tests were conducted to accelerate exposure for the worst-case scenario. It would be beneficial to conduct supporting mechanical tests upon cores from sandwich craft in-service and determine a correlation (if any), between real-time service, exposure conditions from log books, and age. Additionally, it would be of benefit to designers if a formulation were developed to provide a realistic hygrothermal ageing safety factor which considers cell morphology and foam type.

8.9 Structural Component Under Impact

It is recommended that the TSA advantage of a full-field aspect be used to evaluate the response of a complex structural component from a key area of vulnerability within the hull bottom, to fatigue impact loadings. The TSA system is endowed with the ability to evaluate erratic loads, so it would be beneficial to further understand the crack development in a sandwich structure, aged or unaged, when exposed to fatigue conditions of slamming or isolated impact and collision. Additionally, the new TSA system is highly portable, and can be adjusted into any position required, and with the video record function, may be positioned within the curved structure of a yacht hull to monitor the non-contact, full-field, response of a curved sandwich structure to slamming loads in real-time.

Reference

[1]Kim, W., Choi,M., Yong, H., Sung,E. "Measurement of thermal stress and prediction of fatigue for STS using lock-in thermography" 12th A-PCNDT 2006 – Asia-Pacific Conference on NDT, 5th – 10th Nov 2006, Auckland, New Zealand

Chapter Nine

Concluding Remarks

As described in the Introduction, the motivation for this work was based upon lowered design safety guidelines for linear foams in yachts and marine vessels amid concerns over cores weakened by environmental exposure. This work sought to:

- assist marine designers by determining the significance, if any, of ageing upon the properties and behaviour of a foam core,
- consider the implications, if any, of ageing behaviour upon lowered design safety factors for linear materials such as R63.140 compared to the established cross-linked structural cores such as C70.130, and identify if an additional safety margin is necessary,
- assist designers in the optimisation process, by evaluating the potential of the latest developments in TSA systems, as a means of assessment of damage in a hygrothermally aged foam.

This has been accomplished by the evaluation of ageing of foam specimens typical of marine structures and using the established method of fracture toughness testing and a CTS-type experimental arrangement that allows a smooth progression between pure tension and pure shear loading. The change in material and mechanical properties for two foam types, a cross-linked, C70.130, and a linear foam, have been monitored during accelerated hygrothermal ageing and observations related to their cell morphology have been made. It has been determined that the effects of ageing can have a significant contribution towards failure stress and failure mode supporting the recommendation that the issue of lowering of design safety factors for linear materials be investigated further. Confidence in design calculations may be further improved if greater emphasis were placed on relative density of the foam cells to take into consideration cell size and morphology. It has also been expressed that there is need for marine-centric standardised testing and accelerated ageing procedures of foam cores.

Recent developments and system improvements have shown TSA to have potential for damage assessment of hygrothermally aged foams. It was shown that a difference between hygrothermally aged and unaged foams could be detected, and the differences in the behaviour between a linear and cross-linked material in response to a sharp crack-tip in pure and mixed-modes could be determined. It was shown that TSA could be applied to extract stress intensity factors from the C70.130 material, with fair agreement to experimental mechanical testing, though destructive tests are more reliable in this instance. The nature of the foam material encouraged adiabatic conditions, but also introduced uncertainty into the results. Non-uniformity of the surface emissivity, non-uniformity of ageing throughout the specimens, inherent stress alleviating cell distortions, and the need for further information on foam creep under cyclic loads may contribute to data scatter observed in results. These issues would be expected to have greatest significance if fatigue testing of cores were conducted. Additionally, the microcellular behaviour of linear foams with pockets of high local cell stresses, can cause error in the extraction of reproducible stress intensity values and would require development of a numerical method to consider magnitude, and proximity clustering of each recorded data point to clarify the received information. If testing of foam cores within a sandwich lay-up were to be considered, it should be noted that it was the moulded surface of the TSA specimens provided the best surface for data extraction, as cut edges appear frayed with increased noise in the data. With respect to the motivation for this work, the issues noted above, coupled with the Mode II limiting condition, TSA is hindered in its intended practical application in marine design to concerns of lowered design safety factors for linear cores and the consequences of hygrothermal ageing, though TSA can provide a number of advantages over conventional techniques. The greatest strengths being the detailed, real-time, non-contact, full-field, data it can collect with additional promise for use of D-mode for predictive fatigue testing and high resolution lenses to evaluate microcellular models of unit cell behaviour.

Appendix Two

Literature Survey

Appendix Two-A

Sandwich core design

This appendix is referenced to Chapter Two, Literature Survey, section 2.2 The Foam core; Structure and Formation.

ABS rules and guidelines are the most universally referred to as they encompass the most conservative rules for sandwich design of yachts, fast craft and naval fast craft. Excerpts from key guides are included here for reference.

2A.1 Excerpts from ABS Guide for Building and Classing Offshore Racing Yachts (1994)

reinforcement of the laminate and the physical properties of the laminate are such that the laminate meets the definition of a bi-directional laminate it may be considered as such.

The verified minimum mechanical properties of the laminate and lay-up details as indicated in 1.9 are to be indicated on the drawings.

4.7 Wood

4.7.1 General

All wood used is to be of the best quality, properly seasoned, clear, free of defects adversely effecting its strength and with the grain suitable for the purpose intended. It is suggested that all wood members, except cold-molded wood laminates coated with resin, be treated with a preservative.

The strength properties for some such woods are given in Table 4.4. Where other woods are to be used, the strength properties are to be based on the recognized national standards.

SECTION 4 | 3 Materials

4.7.4 Encapsulation

Softwoods encapsulated in FRP are considered effective structural materials where used above the waterline; it is recommended they not be used below the waterline, but where used in this location they are to be considered ineffective, nonstructural, core materials.

With the exception of balsa, hardwoods are not to be used as core materials. Encapsulated balsa or plastic foam are to be considered ineffective in resisting bending or deflection.

4.9 Plywood

Plywood is to be of marine quality and manufactured in accordance with a recognized national standard.

4.11 Core Material

The required core thickness may be based on the following minimum shear strengths, provided they are verified by submitted test data.

	Density		*Minimum Ultimate Shear Strength*		
Material	*kg/m³*	*lb/ft³*	*N/mm²*	*kgf/mm²*	*psi*
Balsa, end-grain	128	8	1.9[1]	0.19[1]	270[1]
Balsa, end-grain	144	9	2.1[1]	0.21[1]	300[1]
Polyvinyl chloride, cross-linked	80	5	1.0 to 1.2	0.10 to 0.12	145 to 171
Polyvinyl chloride, cross-linked	100	6.25	1.4 to 1.5	0.14 to 0.15	200 to 217
Polyvinyl chloride, linear	80–90	5–6	1.2	0.12	169

Note:
1. These values are for Ecuadorian balsa

Where test data is not available for cross-linked polyvinyl chloride, the lower shear strength value of the range is to

4.13 Fastenings

Mechanical fastenings are to be of materials suitable for

2A.2 Excerpts from ABS Rules for High Speed Naval Vessels (2007)

5 Core Materials

Expected shear strengths of core materials are shown in 2-6-1/Table 1. Core materials other than those shown will be subject to special consideration. Polyester fiber or vinylester mat is not considered a lightweight structural core, and use will be subject to special consideration. Shear strength for use in the design is to be verified by test, as required in Section 2-6-5. Construction methods and procedures for core materials are to be in strict accordance with core manufacturer's recommendations.

5.1 PVC Foam Cores

Foam cores are to be of the closed cell types and impervious to water, fuel and oils. Foam cores are to be compatible with the resin system and have good aging ability. Foam cores are to have good strength retention at 60°C (140°F). If the foam core is manufactured into formable sheets of small blocks, the open weave backing material and adhesive are to be compatible and soluble with the laminating resin. Where necessary, foam core materials are to be conditioned in accordance with the manufacturer's recommendations. Conditioning at an elevated temperature in excess of that which may be experienced in service may be necessary to ensure the release of entrapped residual gaseous blowing agents from the cells of the foam core.

5.3 Balsa Wood

Balsa wood is to be end-grained. Balsa wood is to be treated chemically against fungal and insect attack and kiln-dried shortly after felling, and is to be sterilized and homogenized. Balsa wood is to have an average moisture content of 12%. If the balsa wood is manufactured into formable sheets of small blocks, the open weave backing material and adhesive are to be compatible and soluble, respectively, with the laminating resin.

5.5 Core Bonding Materials

Core bonding materials are to be used in accordance with the manufacturer's instructions. The proposed core bonding to be used with the core material is to be indicated on the Material Data Sheet and the construction plans.

TABLE 1
Properties of Core Materials

	Density		*Minimum Shear Strength*		
Material	*kg/m³*	*lb/ft³*	*N/mm²*	*kgf/mm²*	*psi*
Balsa, end-grain	104	6.5	1.6 (1)	0.16 (1)	225 (1)
Balsa, end-grain	144	9	2.5 (1)	0.25 (1)	360 (1)
PVC, crosslinked	80	5	0.9	0.09	122
PVC, crosslinked	100	6.25	1.4	0.14	200
PVC, linear (2)	80–95	5–6	1.2	0.12	170

Notes:

1 These values are for Ecuadorian balsa.

2 Caution is to be taken when linear PVC cores are used in areas that are susceptible to high temperatures because of their low heat distortion temperature.

TABLE 7
Core Shear Design Strength

Core Material	*Design Core Shear Strength*
Balsa Wood	$0.3\tau_k$
PVC*	$0.4\tau_k$

* May be taken as $0.55\tau_k$ where sheer elongation exceeds 40%.

τ_k = minimum core shear strength, in N/mm^2 (kgf/mm^2, psi)

Appendix Two-B

Accelerated Ageing Tables

This section relates to Chapter Two, Literature Survey, section for Accelerated ageing methods.

The references used in the tables are listed in the first column and correspond to the references at the end of the section. The colour coding is used for clarification.

The tables are organised into the following columns;

i. Sponsor; provides the application of the materials or tests and is subdivided into simplistic categories of aeronautics, marine and other. Knowledge the application of the research provides a quick indication of experimental methodology.

ii. Test type; determines if the review paper considers characterisation of hygrothermal effects on the test specimens, and is subdivided into 'Mech&Age' for details of mechanical tests conducted on aged samples; 'MechORAge' for details of experimentation conducted in isolation, or 'Theory' if it is purely a speculative or analytical paper.

iii. Environment, exposure conditions of 'relative humidity' or 'immersion' are noted. As this research is primarily interested in immersion testing, the relative humidity details are not presented in this version of the tables.

iv. Component; determines if the skin, core and/or the sandwich as a whole have been considered.

v. Fibre; distinguishes between the fibre materials used, which is closely related to application. Carbon is most commonly used where the sponsor has been marked as aeronautics.

vi. Orientation; distinguishes between the fibre or ply orientation used in the reviewed paper. Given the complexity of moisture analysis and prediction methodologies it may benefit the reader to be aware of the papers that consider the simplified unidirectional lay-up.

vii. Matrix; Refers to the resin used for the laminate; epoxy, polyester and other. The most recent papers typically focus on epoxy, while the oldest exhibited the broadest experimental range.

viii. Core; if a sandwich or core is experimented consider, the distinction between cross-linked and linear is made.

ix. Strength and Modulus,; share the same colour coding, and relates to a mechanical property obtained by the paper. The basic properties of tensile, shear, flexural compressive and impact modulus and strength are presented separately from fracture toughness and fatigue.

x. Temperature Range is provided both numerically and visually to facilitate comparisons. A blue bar represents a negative temperature, while the yellow and red present the lowest and highest values in the range tested.

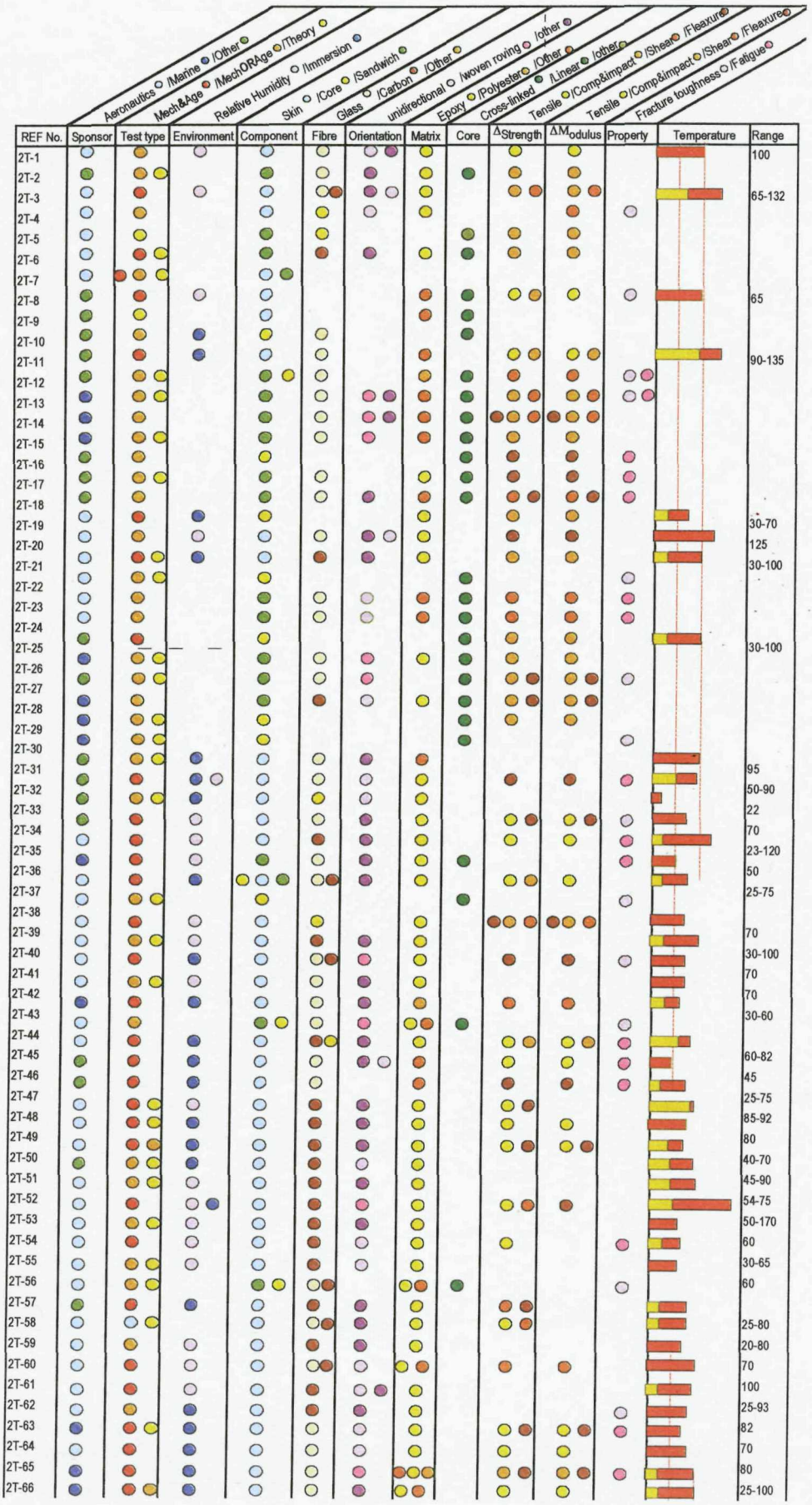
Aeronautics /Marine /Other
Mech&Age /MechORAge /Theory
Relative Humidity /Immersion
Skin /Core /Sandwich
Glass /Carbon /Other
unidirectional /woven roving /other
Epoxy /Polyester /Other
Cross-linked /Linear /other
Tensile /Comp&impact /Shear /Flexure
Tensile /Comp&impact /Shear /Flexure
Fracture toughness /Fatigue
REF No.
Sponsor
Test type
Environment
Component
Fibre
Orientation
Matrix
Core
ΔStrength
ΔModulus
Property
Temperature
Range
2T-1
2T-2
2T-3
2T-4
2T-5
2T-6
2T-7
2T-8
2T-9
2T-10
2T-11
2T-12
2T-13
2T-14
2T-15
2T-16
2T-17
2T-18
2T-19
2T-20
2T-21
2T-22
2T-23
2T-24
2T-25
2T-26
2T-27
2T-28
2T-29
2T-30
2T-31
2T-32
2T-33
2T-34
2T-35
2T-36
2T-37
2T-38
2T-39
2T-40
2T-41
2T-42
2T-43
2T-44
2T-45
2T-46
2T-47
2T-48
2T-49
2T-50
2T-51
2T-52
2T-53
2T-54
2T-55
2T-56
2T-57
2T-58
2T-59
2T-60
2T-61
2T-62
2T-63
2T-64
2T-65
2T-66
100
65-132
65
90-135
30-70
125
30-100
30-100
95
50-90
22
70
23-120
50
25-75
70
30-100
70
70
30-60
60-82
45
25-75
85-92
80
40-70
45-90
54-75
50-170
60
30-65
60
25-80
20-80
70
100
25-93
82
70
80
25-100

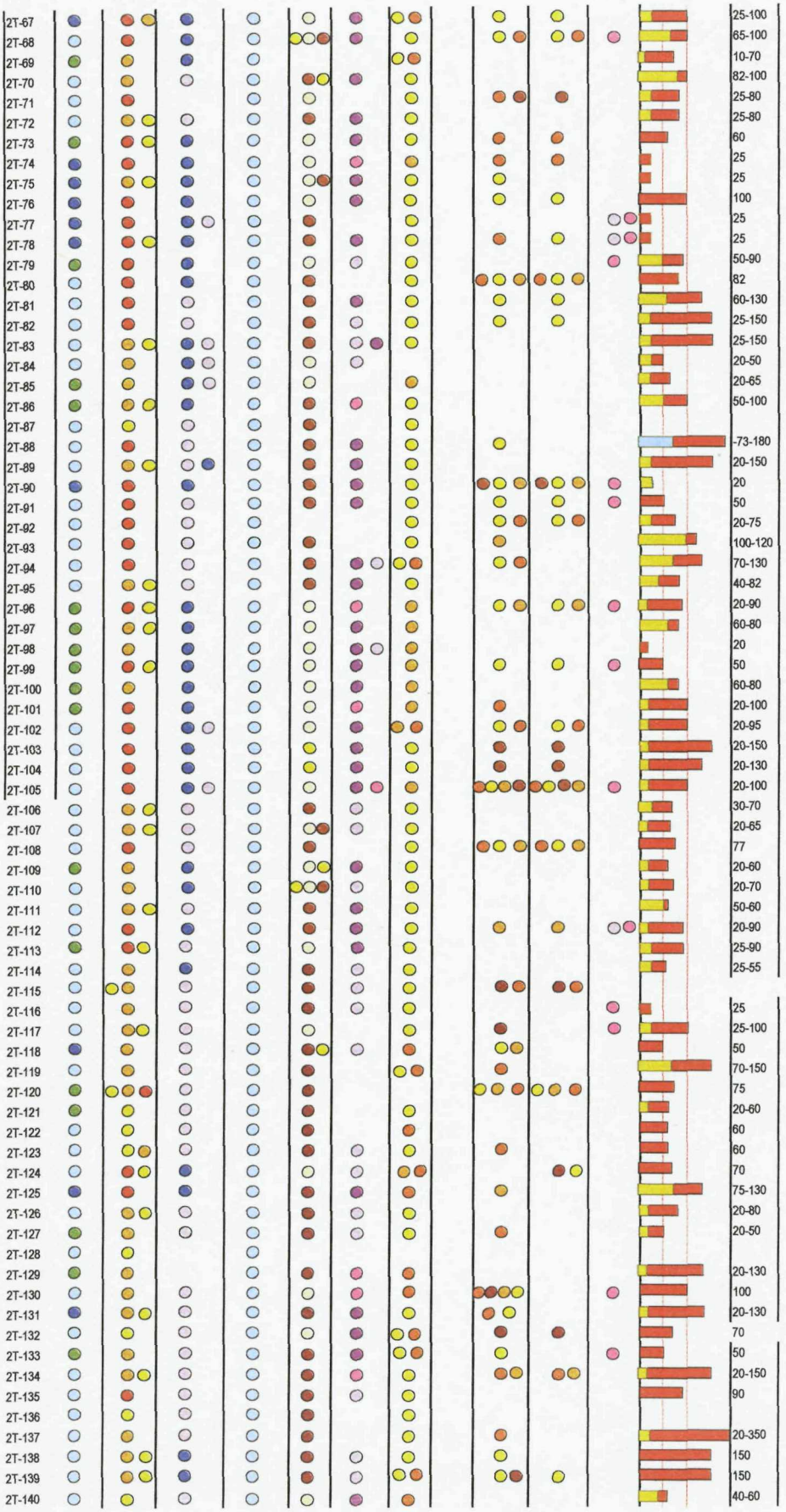
2T-67 25-100
2T-68 65-100
2T-69 10-70
2T-70 82-100
2T-71 25-80
2T-72 25-80
2T-73 60
2T-74 25
2T-75 25
2T-76 100
2T-77 25
2T-78 25
2T-79 50-90
2T-80 82
2T-81 60-130
2T-82 25-150
2T-83 25-150
2T-84 20-50
2T-85 20-65
2T-86 50-100
2T-87
2T-88 73-180
2T-89 20-150
2T-90 20
2T-91 50
2T-92 20-75
2T-93 100-120
2T-94 70-130
2T-95 40-82
2T-96 20-90
2T-97 60-80
2T-98 20
2T-99 50
2T-100 60-80
2T-101 20-100
2T-102 20-95
2T-103 20-150
2T-104 20-130
2T-105 20-100
2T-106 30-70
2T-107 20-65
2T-108 77
2T-109 20-60
2T-110 20-70
2T-111 50-60
2T-112 20-90
2T-113 25-90
2T-114 25-55
2T-115
2T-116 25
2T-117 25-100
2T-118 50
2T-119 70-150
2T-120 75
2T-121 20-60
2T-122 60
2T-123 60
2T-124 70
2T-125 75-130
2T-126 20-80
2T-127 20-50
2T-128
2T-129 20-130
2T-130 100
2T-131 20-130
2T-132 70
2T-133 50
2T-134 20-150
2T-135 90
2T-136
2T-137 20-350
2T-138 150
2T-139 150
2T-140 40-60

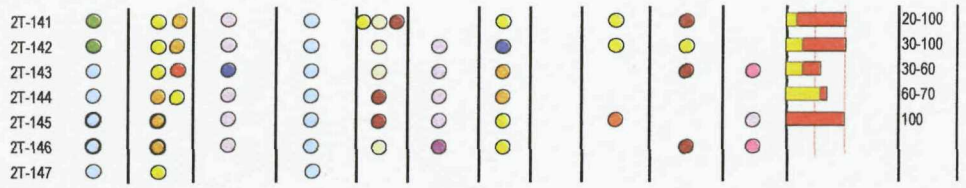

2A.3 References used in Table

2T-1. Anstice, P., Beaumont, P. "Hygrothermal ageing and fracture of glass fibre epoxy composites" , J.Materials Science., Vol.18., p3404-3408

2T-2. Fynbo, J. "Numerical and Experimental Study of Curved Sandwich Panels.", Masters Thesis, 1999, Aalborg University., http://www.ime.auc.dk/people/employees/jfy/MK_10/Start.htm

2T-3. Tomblin, J., Salah, L., Ng, C. "Determination of temperature/moisture sensitive composite properties". Sept. 2001. Office of Aviation Research Report No. DOT/FAA/AR-01/40, Federal Aviation Administration, US Department of Transport

2T-4. Bardis, J., Kedward, K. "Effects of surface preparation on long-term durability of composite adhesive bonds". April 2001. Office of Aviation Research Report No. DOT/FAA/AR-01/8, Federal Aviation Administration, US Department of Transport

2T-5. Sleight, D., Wang, J. "Buckling analysis of debonded sandwich panel under compression" Dec.1995. Technical Report No. L-17476. NASA, Langley Research Centre

2T-6. Lacy, T., Samarah, I., Tomblin, J. "Damage resistance characterisation of sandwich composites using response surfaces" March 2002. Office of Aviation Research Report No. DOT/FAA/AR-01/71, Federal Aviation Administration, US Department of Transport

2T-7. Vodicka, R. "Accelerated environmental testing of composite materials" Department of Defence Report No. DSTO-TR-0657, Airframes and Engines Division, DSTO, Australia.

2T-8. Real. L. P., Rocha,A., Gardette J-L. "Artificial accelerated weathering of poly(vinyl chloride)for outdoor applications: the evolution of the mechanical and molecular properties". Journal of Polymer Degradation and Stability 82 (2003)235 –243.

2T-9. Brown, R. "Predictive Techniques and Models for durability tests"., Polymer Testing 14(1995) 403-414

2T-10. Braun, J., Klein, M.O., Bernarding,J.,. Leitner,M.B,. Mika H.-D "Non-destructive, three-dimensional monitoring of water absorption in polyurethane foams using magnetic resonance imaging" Polymer Testing 22 (2003) 761–767.

2T-11. Bergeret A., Pires, I.. Foulc, M.P. Abadie, B Ferry, L. Crespy A "The hygrothermal behaviour of glass-fibre-reinforced thermoplastic composites: a prediction of the composite lifetime" Polymer Testing 20 (2001) 753–763

2T-12. Burchardt, C. "Fatigue in sandwich structures loaded in transverse shear" Composite Structures Vol 40 (1998), No.1 p73-79

2T-13. Thomson R.S., Shah-Khan, M.Z., Mouritz A.P. "Shear properties of a sandwich composite containing defects" Composite Structures 42 (1998) 107-118.

2T-14. Mouritz, A.P., Thomson R.S, "Compression, flexure and shear properties of a sandwich composite containing defects" Composite Structures 44 (1999) 263-278

2T-15. Boyle, M.P., Roberts, J.C., Weinhold, P.D., BaoG., White G.J "Experimental, Numerical, and analytical results for buckling and post-buckling for orthoropic rectangular sandwich panels" Composite Structures 52(2001) 375-380

2T-16. Kanny, K., Mahfuz, Carlsson,. L, Thomas,T., Jeelani, S. "Dynamic mechanical analyses and flexural fatigue of PVC foams" Composite Structures 58 (2002)175 –183

2T-17. Kulkarni, N., Mahfuz, H., Jeelani, S., Carlsson, L. "Fatigue crack growth and life prediction of foam core sandwich composites under flexural loading" Composite Structures 59 (2003)499 –505

2T-18. Dai J., Hahn H. "Flexural behaviour of sandwich beams fabricated by vacuum-assisted resin transfer molding" Composite Structures 61 (2003)247 –2530

2T-19. Gupta, N., Woldesenbet, E. "Hygrothermal studies on syntactic foams and compressive strength determination" Composite Structures 61 (2003)311 –320

2T-20. Hong,G., Yalizis,A., Frantziskonis,G. "Hygrothermal degradation in glass/epoxy - evaluation via stress wave factors" Composite Structures 30 (1995) 407-417

2T-21. . Qi, B., Herszberg, I.. "An engineering approach for predicting residual strength of carbon/epoxy laminates after impact and hygrothermal cycling" Composite Structures 47 (1999) 483-490
2T-22. Grenestedt, J., Hallstrom, S., Kuttenkeuler, J., "On cracks emanating from wedges in expanded PVC foam" Engineering Fracture Mechanics Vol. 54, No. 4, pp. 445--456, 1996
2T-23. Burman, M., Zenkert,D., "Fatigue of foam core sandwich beams-2:effect of initial damage" Int.J.Fatigue Vol. 19 (1997), No.7., p563-578
2T-24. Burman, M., Zenkert,D., "Fatigue of foam core sandwich beams-1:undamaged specimens" Int.J.Fatigue Vol. 19 (1997), No.7., p551-561
2T-25. Lin, H. "Structure and Property relationships of Commercial foamed plastics" Polymer Testing 16 (1997) 429-443
2T-26. Fleck,N., Sridhar, I., "End Compression of sandwich columns" Composites Part A 33(2002) 353-359
2T-27. Hazizan A., Cantwell, W., "Low velocity impact response of foam-based sandwich structures" Composites Part B 33 (2002) 193-204
2T-28. Gdoutos, E., Daniel, I., Wang ,K.-A., "Compression facing wrinkling of composite sandwich structures" Mechanics of Materials 35 (2003)511 –522
2T-29. Chakravarty, U., Mahfuz, H., Saha, M., Jeelani, S. "Strain rate effects on sandwich core materials: An experimental and analytical investigation" Acta Materialia 51 (2003) 1469–1479
2T-30. Bazant, Z., Zhou,Y., Goangseup, Z., Daniel, "Size effect and asymptotic matching analysis of fracture of closed-cell polymeric foam" International Journal of Solids and Structures (2003) (article in Press)
2T-31. Morii, T., Ikuta,N., Kiyosum, K., Hamada, H. "Weight-change analysis of the interphase in hygrothermally aged FRP: consideration of debonding" Composites Science and Technology 51(1997) 985-990
2T-32. Vauthier,E., Abry,J., Bailliezb, C.T., Chateauminois, A., "Interactions between hygrothermal ageing and fatigue damage in unidirectional glass/epoxy composites" Composites Science and Technology 58 (1998) 687-692
2T-33. Cervenka, A., Bannister, D., Young, R. "Moisture Absorption and interfacial failure ion aramid/epoxy composites" Composites Part A 29A(1998) 1137-1144
2T-34. Scida, D., Aboura, Z. Benzeggagh, M.L. "The effect of ageing on the damage events in woven-fibre composite materials under different loading conditions" Composites Science and Technology 62 (2002)551 –557
2T-35. Patel, S., Case, S. "Durability of hygrothermally aged graphite/epoxy woven composite under combined hygrothermal conditions" International Journal of Fatigue 24 (2002) 1295–1301
2T-36. Earl,J.S., Dulieu-Barton, J.M, Shenoi, R.A "Determination of hygrothermal ageing effects in sandwich construction joints using thermoelastic stress analysis" Composites Science and Technology 63 (2003)211 –223
2T-37. Ishai,O., Hiel, C., Luft, M. "Long-term hygrothermal effects on damage tolerance of hybrid composite sandwich panels" Composites, Volume 26, Issue 1, January 1995, Pages 47-55
2T-38. Noury, P., Shenoi, R., Sinclair, I., " On mixed-mode fracture of PVC foam" International Journal of Fracture 92 (1998) 131-151
2T-39. Akay, M., Kong Ah Mud, S., Stanley, A.,' "Influence of moisture on the thermal and mechanical properties of autoclaved and oven-cured kevlar-49/epoxy laminates" Composites Science and Technology 51 (1997) 565-571
2T-40. Choi, H. S., Ahn, K. J., Nam, J. -D., Chun, H. J. "Hygroscopic aspects of epoxy/carbon fiber composite laminates in aircraft environments", Composites Part A: Applied Science and Manufacturing, Volume 32, Issue 5, 1 May 2001, Pages 709-720
2T-41. Buehler, F. U., Seferis, J. C, "Effect of reinforcement and solvent content on moisture absorption in epoxy composite materials", Composites Part A: Applied Science and Manufacturing, Volume 31, Issue 7, July 2000, Pages 741-748
2T-42. Lundgren, J., Gudmundson, P. "Moisture absorption in glass-fibre/epoxy laminates with transverse matrix cracks", Composites Science and Technology, Volume 59, Issue 13, October 1999, Pages 1983-1991
2T-43. Varelidis, P. C., Kominos, N. P, Papaspyrides, C. D. "Polyamide coated glass fabric in polyester resin: interlaminar shear strength versus moisture absorption studies", Composites Part A: Applied Science and Manufacturing, Volume 29, Issue 12, December 1998, Pages 1489-1499

2T-44. Majumdar, P., Srinivasagupta, D., Mahfuz, H., Joseph, B., Thomas, M., Christensen,S. "Effect of processing conditions and material properties on the debond fracture toughness of foam-core sandwich composites: experimental optimization", Composites Part A: Applied Science and Manufacturing, Volume 34, Issue 11, November 2003, Pages 1097-1104
2T-45. Sala, G. "Composite degradation due to fluid absorption", Composites Part B: Engineering, Volume 31, Issue 5, July 2000, Pages 357-373
2T-46. McBagonluri, F., Garcia, K., Hayes, M., Verghese, K., Lesko,J. "Characterization of fatigue and combined environment on durability performance of glass/vinyl ester composite for infrastructure applications", International Journal of Fatigue, Volume 22, Issue 1, January 2000, Pages 53-64
2T-47. Liao, K., Schultheisz, C., Hunston D. "Long-term environmental fatigue of pultruded glass-fiber-reinforced composites under flexural loading", International Journal of Fatigue, Volume 21, Issue 5, May 1999, Pages 485-495
2T-48. Robson, J., Mathews, F., Kinloch, A. "The bonded repair of fibre composites: effect of composite moisture content" Composite Science Technology 52 (1994)235-246
2T-49. Ogi, K, Kim, H., Maruyama, T., Takao, Y., "The influence of hygrothermal conditions on the damage processes in quasi-isotropic carbon/epoxy laminates" Composite Science Technology 59 (1999)2375-2382
2T-50. Ishai, O., Garg, A., Nelson, H. "Hygrothermal effects on the mechanical behaviour of graphite fibre-reinforced epoxy laminates beyond initial failure" Composites Vol17 no.1 Jan 1986.
2T-51. Zhou, J., Lucas., J. "The effects of a water environment on anomalous absorption behaviour in graphite/epoxy composites" Composites Science and Technology 53 (1995) 57-64
2T-52. Harper, B., Weitsman, Y. on the effects of environmental conditioning on residual stresses in composite laminates", Int. J. Solids Structures, Vol.21. No.8. pp 907-926. 1985
2T-53. Birger, S., Moshonov, A., Kenig, S., "The effects of thermal and hygrothermal ageing on the failure mechanisms of graphite-fabric epoxy composites subjected to flexural loading" Composites Vol.20, No.4, July 1989.
2T-54. Collings,T., Stone, D. "Hygrothermal effects in CFC laminates: damaging effects of temperature, moisture and thermal spiking" Composite structures 3 (1985) 341-378
2T-55. Wang, A., Liu, P. "Humidity Effects on the Creep behaviour of an epoxy-graphite composite" J. Aircraft Vol.14. No.4 April 1977
2T-56. Collings,T., "The effect of observed climatic conditions on the moisture equilibrium level of fibre-reinforced plastics" Composites Vol.17 no.1 Jan 1986
2T-57. Smith, S., Shivakumar, K., "Modified Model cracked sandwich beam (CSB) Fracture test. American Institute of Aeronautics and Astronautics AIAA-2001-1221
2T-58. Gillat,O., Broutman, L. "Effect of an external stress on moisture diffusion and degradation in a graphite-reinforced epoxy laminate" ASTM STP 658, 1978, p61-83
2T-59. Bouadi, H., Sun, C. "Hygrothermal effects on the stress field of laminated composites", Journal of Reinforced Plastics and composites Vol.8 Jan 1989
2T-60. Crossman, F., Mauri, R., Warren, W. "Moisture-altered viscoelastic response of graphite/epoxy composites". ASTM STP 658 1978 p205-220
2T-61. Adams, R., Singh, M., "The dynamic properties of fibre-reinforced polymers exposed to hot , wet conditions" Composites Science and technology 56 (1996) 977-997
2T-62. Rehfield, L., Briley, R., Putter, S." Dynamic tests of graphite epoxy composites in hygrothermal environments" ASTM STP 768, 1982, pp148-160
2T-63. Hahn, H., Kim, R., "Swelling of composite laminates", ASTM STP 658 1978 pp98-120
2T-64. . Karama, M., Pegorarp, P., Touratier, M. "An analysis of the hygrothermoelastic behaviour of glass fabric composites" Composites Part A 29A(1998) 551-563
2T-65. Ishai, O., Arnon, U., "Instantaneous effect of internal moisture conditions on strength of glass-fibre reinforced plastics" ASTM STP 658, 1978, pp267-276
2T-66. Hofer, K., Skaper, G., "Fatigue endurance of glass reinforced plastic laminate material in a marine environment" 40th Annual conference, Reinforced Plastics, The Society of Plastics Industry. 1985
2T-67. Hale, J., Gibson, A., "Strength reduction of GRP Composites exposed to high temperature marine environments" Proc. ICCM-11, 1997
2T-68. Jones, C., Dickson, R., Adam, T., Reiter, H., Harris, B., "The environmental fatigue behavior of reinforced plastics", Proc.R.Soc. Lond. A 396 315-338 (1984)
2T-69. El-Sa'ad, L., Darby, M., Yates, B., "Moisture absorption by epoxy resins: the reverse thermal effect". J. of Materials Science 25n (1990) 3577-3582
2T-70. Delasi, R., Whiteside, J., "Effect of moisture on epoxy resins and composites" ASTM STP 658, 1978, pp2-20

2T-71. Kasturiarachchi, K., Pritchard, G., "Water absorption of glass/epoxy laminates under bending stresses", Composites, Vol.14. No.3., 1983
2T-72. Whitney, J., Browning, C. "Some anomalies associated with moisture diffusion in epoxy matrix composite materials" ASTM STP 658 1978, pp43-60
2T-73. Perreux, D., Suri, C. "A study of the coupling between the phenomena of water absorption and damage in glass/epoxy composite pipes", Composites science and technology 57 (1997) 1403-1413
2T-74. Cargen, M., Hartshorn, R., Summerscales, J., "Effect of short-term continuous sea water exposure on the shear properties of a marine laminate", Trans. ImarE (C) vol.97. conf.2. paper21
2T-75. Wood, C., Bradley, W., "Determination of the effect of the seawater on the interfacial strength of an interlayer e-glass/graphite/epoxy composite by in-situ observation of transverse cracking in an environmental SEM", composites Science Technology 57 (1997) 1033-1043
2T-76. Hale , J., Gibson, A., "Coupon tests of fibre reinforced plastics at elevated temperatures in offshore processing environments" Journal of Composite Materials, Vol.32. No.6 1998
2T-77. Sloan, F., Seymour, R., "the effect of seawater exposure on mode I interlaminar fracture and crack growth in graphite/epoxy" J. cof Composite materials Vol.26, No.18/1992
2T-78. Smith, L., Weitsman, Y. " The immersed fatigue response of polymer composites", International Journal of fracture 82: 31-42, (1996)
2T-79. Vauthier, E., Chateauminois, A., Bailliez, T., "Hygrothermal ageing and durability of unidirectional glass-epoxy composites" ICCM 10 (1997)
2T-80. Verette, R., "Temperature/humidity effects on the strength of graphite/epoxy laminates" J.Aircraft Vol.14. no.1 p90-94
2T-81. Kellas, S., Morton, J., Curtis, P., "The effect of hygrothermal environments upon the tensile and compressive strengths of notched CFRP laminates. Part1: static loading" Composites vol.21, no.1, 1990
2T-82. Shen, C., Springer, G., "Effects of moisture and temperature on the tensile strength of composite materials", J. composite materials, vol.11, 1977, p2-16
2T-83. Shen, C., Springer, G., "Moisture absorption and desorption in composite materials", J. Composite materials, vol.10, 1976, 2-21
2T-84. Loos,A., Springer, G. "Moisture absorption of graphite epoxy composites immersed in liquids and humid air" J. Composite Materials. Vol. 13, 1979, p131
2T-85. Loos, A. C., Springer, G. S., Sanders, B. A., and Tung, R. W. (1980) "Moisture Absorption of Polyester-E-Glass Composites," Journal of Composite Materials, Vol. 14,142-154.
2T-86. Marsh, L., Lasky, D., Seraphim, P., Springer, G., "Moisture solubility and diffusion in epoxy and epoxy-glass composites" Journal of Research and Development, Vol.28, Number 6, Page 655 (1984)
2T-87. Springer, G., "Moisture content of composites under transient conditions". Environmental effects on composite materials, Technomic pub., 1981, vol. p63-78
2T-88. Shen, C., Springer, G. "Effects of moisture and temperature on the tensile strength of composite materials", J. Composite Materials, 1977, vol 11, p2-16
2T-89. Shen, C., Springer, G." Environmental effects in the elastic moduli of composite materials" J. Composite Materials, 1977, vol 11, p250-264
2T-90. Macander, A., Silvergleight, M., Edelstein, H., "Marine Durability of a graphite/epoxy composite subjected to static and fatigue loading" ICM 3, 1979, Vol.2 p333-343
2T-91. Lundemo, C., Thor, S., "Influence of environmental cycling on the mechanical properties of composites materials", J. Composite Materials, Vol.11, 91977), p276-284
2T-92. Nicolais, L., Drioli, E., Apicella, A., Albanese, O., "Effect of applied stress, thermal environmnet and water in epoxy resins", Air Force office of Scientific Research Report no. AFOSR 77-3369 September 1978
2T-93. Maier, G., Kreil, H., Ott, H., Stelter, R., "Testing of wet fibre reinforced plastics at elevated temperatures" Composites Vol.20 No.5. 1989
2T-94. Joshi, O., "The effect of moisture on the shear properties of carbon fibre composites" Composites Vol.14, No.3, 1983
2T-95. Shirrell, C., "Diffusion of water vapour on graphite/epoxy composites" Advanced composite materials , environmental effects ASTM STP 658 1978
2T-96. Watanabe, M., "Effect of water environment on fatigue behaviour of fibreglass reinforced plastics" ASTM STP 674,1979, p345-367
2T-97. Morii, T., Tanimoto, T., Hamada, H.,Maekawa, Z., Hirano, T., Kiyosumi, K., "Weight changes of a randomly orientated GRP panel in hot water" Composites Science and Technology 49 (1993) p209-216

2T-98. Jones, F., Mulheron, M. "The effect of moisture on the expansion behaviour and thermal strains in GRP" Composites, Vol.14, No.3, 1983p281-287
2T-99. Ellis, B. Found, M., "The effects of water absorption on a polyester/chopped strand mat laminate" Composites, Vol.14, No.3., 1983 p237-243
2T-100. Morii, T., Hamada, H., Maekawa, Z., Tanimoto, T., Hirano, T., Kiyosumi, K., Tsujii, T.,"Weight changes of the fibre/matrix interface in GRP panels immersed in hot water" Composites Science and Technology 50 (1994) p373-379
2T-101. Gautier, L., Mortaigne,B. Bellenger,V., "Interface damage study of hydrothermally aged glass fibre reinforced polyester composites" Composites Science and Technology 59 (1999) 2329-2337
2T-102. Springer, G., Sanders, B., Tung, R., "Environmental effects on glass fiber reinforced polyester and vinylester composites", IBID, vol. 14, pp.213-232, 1980
2T-103. Allred, R. "The effect of temperature and moisture content on the flexural response of kevlar/epoxy laminates :part I [0/90] filament orientation" Journal of Composite Materials, Vol. 15, 1981, pp. 100-116.
2T-104. Allred, R. "The effect of temperature and moisture content on the flexural response of kevlar/epoxy laminates :part II [45,0/90] filament orientation" Environmental effects on composite materials, Technomic pub., 1981, vol2, p43-58
2T-105. Springer, g., "Effects of temperature and moisture on sheet molding compounds", Environmental effects on composite materials, Technomic pub., 1981, vol2, p59-78
2T-106. Kondo, K., Taki, T., "Moisture diffusivity of unidirectional composites", Environmental effects on composite materials, Technomic pub., 1981, vol2, p288-299
2T-107. Cairns, D., Adams, D., "Moisture and thermal expansion properties of unidirectional composite materials and the epoxy matrix" Journal of Reinforced Plastics and Composites,vol.2, no.4,p. 239-55
2T-108. Tang, J., Springer, G., "Effects of cure and moisture on the properties of Fiberite 976 resin", Environmental effects on composite materials, Technomic pub., 1981, vol2, p63-74
2T-109. Rao, R. Balasubramanian,N., Chanda, M., "Factors affecting moisture absorption in polymer composites Part1:influence of internal factors", J. Reinforced Plastics & Composites, July 1984, p232-245.
2T-110. Goplan R, Rao, R., Murthy, M., Dattaguru, B., "Diffusion Studies On Advanced Fibre Hybrid Composites", J. Reinforced Plastics & Composites, Vol. 5, January 1986, pp 51-56.
2T-111. Bilkstaad, M., Sjoblom, P., Johansson, T. "Long-term moisture absorption in graphite/epoxy angle ply laminates", Environmental effects on composite materials, Technomic pub., 1981, vol2. p107-121
2T-112. Mohlin, T., "Deterioration in compressive performance of a graphite/epoxy laminate as a consequence of environmental exposure and fatigue loading", Environmental effects on composite materials, Technomic pub., 1981, vol2. P163
2T-113. Bonniau, P., Bunsell, A., " A Comparative Study of Water Absorption Theories Applied to Glass/Epoxy Composites, J.Composite Materials Vo.15, p272-293, 1981
2T-114. Buxton, A., Baille, C., "A Study of the Influence of the Environment on the Measurement of Interfacial Properties of Carbon fibre/Epoxy Resin Composites, Composites Vol.25, No.7, 1994, p604-608
2T-115. Chamis, C., Lark, R., Sinclair, J., "Integrated Theory for Predicting the Hygrothermomechanical Response of Advance Composite Structural Components" Advanced Composite Materials, ASTM 658, 1978, p160-192
2T-116. Chamis, C., Sinclair, J., "Durability /life of fiber Composites in Hygrothermomechanical Environments." Composite Materials; Testing and Deesign 6th Conf. ASTM STP 787, 1982, p498-512
2T-117. Chateauminois, A., Chabert, B., Soulier,J., Vincent, L. "Hygrothermal Ageing Effects on Viscoelastic and fatigue behaviour of glassy/epoxy Composites", Environment Effects on Composites Materials Vol.2, 1991, Technomic Publishing Co. Section 16E
2T-118. Chisholm, J.,Kallas, M., Hahn, T, Williams, J., "The Effect of Seawater Absorption in Pultruded Composite Rods" Environmental Effects on Composite Materials Vol.2, Technomic Publishing Co., Section 16A, 1991
2T-119. Cinquin, J., Abjean, P "Correlation between Wet Ageing, Humidity Absorption and Properties on composite Materials Based on Different Resin Family" Int. SAME Symposium May, p1539-1551, 1993.
2T-120. Ciriscol, P., Woo, L., Peterson, D., "Accelerated Environmental ?Testing of Composites", J. Composites Materials , Vol.21, 1987, p225-242
2T-121. Collings, T., Copley, S., "On the Accelerated Ageing of CFRP Composites" Vol.14, No.3, 1983, p180-188

2T-122. Collings, T., "The us eof Resin hybridss to control moisture absorption in fibre reinforced plastics" Composites Vol.22, No.5, 1991, p369-372
2T-123. Collings, T., "Hygrothermal Effects in CFC laminates damaging effects of temperature, moisture and thermal spiking", Composite Structures Vol.3, 1985, p241-378
2T-124. Davies, P., Lemoine, L., "Nautical Construction with Composite Materials", Int. Conf. IFREMER, Paris, 1992.
2T-125. Demetus, E., Shyprykevich, P., "Accelerated environmental testing of Composites", Composites, Vol.15., no.1, 1984, p25-31
2T-126. Fellows, L., "Moisture Absorption in low level porosity thermoplastic toughened epoxy composites" PhD Thesis, University of Southampton, 1999
2T-127. Garg, A., Ishai, O. ,"Hygrothermal Influence on Delamination Behaviour of Graphite Epoxy Laminates", Engineering Fracture Mechanics Vol.22, No.3, 1985, p413-427
2T-128. Hiel, C., Adamson, M., "New prediction methods for composites hygrothermal behaviour" Composites Structures Vol.6., 1986, p243-260
2T-129. Hoa, S., Lin, S., Chen, J., " Hygrothermal Effects on mode 2 interlaminar fracture toughness of carbon/polyethylene sulphide laminate" J. Reinforced Plastics and Composites., Vol. 11, 1992, p2-31
2T-130. Hofer, K., Skaper, G., "Fatigue endurance of glass reinforced plastic laminate material in marine environment" 40th annual Conf. Reinforced Plastics Inst., Jan., Session 12-B, 1985
2T-131. Joshi, O., "The effect of moisture on the shear properties of carbon fibre reinforced composites" Composites Vol.14., No.3, 1983, p196-200
2T-132. Karama, M., Pegoraro, P., Tourtatier, M., "An Analysis of the hygrothermoelastic behaviour of glass fabric composites" Composites, Part A29A, 1997, p551-563
2T-133. Lundemo, C., Thor, S., "influence of environmental cycling on the mechanical properties of composite materials" J. Composite materials Vol.11, 1977, p276-284
2T-134. Mao-Tang, J., Springer, G., "Effects of Mositure and temperature on the Compressive and short beam shear properties of Fiberite T300/976 Fabric". J.Reinforced Plastics And Composites Vo.7, 1988, p120-135
2T-135. Maymon, G., "Influence of Moisture absorption and elevated temperature on the dynamic behaviour of resin matrix composites" Advanced Composite Materials, ASTM, STP 658, 1978, p221-233
2T-136. McKague, L., "Environmental synergism and simulation in resin matrix composites, Advanced Composite Materials, ASTM STP 658, 1978, p193-204
2T-137. McMahon, P., " Oxidative resistance of carbon fibres and their composites" Advanced Composite Materials, ASTM STP 658, 1978, p254-266
2T-138. Miller, A., Adams, D., "Inelastic micromechanical analysis of graphite/epoxy composites subjected to hygrothermal ageing " Advanced Composite Materials, ASTM STP 658, p121-142
2T-139. Paravatrddy, H, Wang, J., Dillard, D., Ward, T., "Environmental ageing of high performance polymeric composites effects and durability" Composites Science and Technology, Vol.53, 1995, p399-409
2T-140. Phillips, M., "Prediction of long term stress rupture life for glass fibre reinforced polyester composites in air and aqueous environments" Composites Vol.14, No.3, 1983, p270-275
2T-141. Piggott, M., "Water Absorption in carbon and glass fibre composites, ICCM6, 1987
2T-142. Pritchard, G., Speake, S., "The use of water absorption kinetic data to predict laminate property changes" Composites Vol.18, No.3, 1987, p227-232
2T-143. Pritchard, G., Speake, S., "Effects of temperature on stress-rupture times in glass/polyester laminates" Composites Vol.19.No.1, 1988, p29-35
2T-144. RAE, "Environmental effects in the testing of composites structures for aircraft" RAE TR 88063, Report to Composite Research Advisory Group , April, 1987
2T-145. Russell, A., Street. K., "Moisture and temperature effects on the mixed mode delamination fracture of unidirectional graphite epoxy" Delamination and Debonding of materials ASTM STP 876 1985, p349-370
2T-146. Shimodairira, H., Ono, T., Yamashita, S., "Moisture expansion of graphite composites", 1991, Environmental effects on Composite Material Vol.2, Technomic Publishing Section 16H.
2T-147. Tompkins, S., Tenney, D. Unman, J., "Prediction of moisture and temperature changes in composites during atmospheric exposure", Composite materials testing and design (5th conference), ASTM STP 674 , 1979, p368-380

Appendix Two-C

Standards Applicable to Cores

2A.4 ASTM Standards

— D3576-98 Standard Test Method for Cell Size of Rigid Cellular Plastics

— D2856-94 (1998) Standard Test Method for Open-Cell Content of Rigid Cellular Plastics by the Air Pycnometer

— D2126-99 Standard Test Method for Response of Rigid Cellular Plastics to Thermal and Humid Aging

— D1623-78 (1995) Standard Test Method for Tensile and Tensile Adhesion Properties of Rigid Cellular Plastics

— D1622-98 Standard Test Method for Apparent Density of Rigid Cellular Plastics

— D3204-93 (1998) Standard Specification for Preformed Cellular Plastic Joint Fillers for Relieving Pressure

— D6226-98e1 Standard Test Method for Open Cell Content of Rigid Cellular Plastics

— D2842-01 Standard Test Method for Water Absorption of Rigid Cellular Plastics

— D1621-00 Standard Test Method for Compressive Properties of Rigid Cellular Plastics

— D3748-98 Standard Practice for Evaluating High-Density Rigid Cellular Thermoplastics

2A.5 ISO Standards

— ISO 844:2001 Rigid cellular plastics – Determination of compression properties

— ISO 845:1988 Cellular plastics and rubbers – Determination of apparent (bulk) density

— ISO 1183-3:1999 Plastics – Methods for determining the density of non-cellular plastics – Part 3: Gas pycnometer method

— ISO 1209-1:1990 Cellular plastics, rigid – Flexural tests – Part 1: Bending test

— ISO 1209-2:1990 Cellular plastics, rigid – Flexural tests – Part 2: Determination of flexural properties

— ISO 1663:1999 Rigid cellular plastics – Determination of water vapor transmission properties

— ISO 1922:2001 Rigid cellular plastics – Determination of shear strength

— ISO 1923:1981 Cellular plastics and rubbers – Determination of linear dimensions

— ISO 1926:1979 Cellular plastics – Determination of tensile properties of rigid materials

— ISO 2796:1986 Cellular plastics, rigid – Test for dimensional stability

— ISO 2896:2001 Rigid cellular plastics – Determination of water absorption

— ISO 4590:2002 Rigid cellular plastics – Determination of the volume percentage of open cells and of closed cells (available in English only)

— ISO 4651:1988 Cellular rubbers and plastics – Determination of dynamic cushioning performance

— ISO 4897:1985 Cellular plastics – Determination of the coefficient of linear thermal expansion of rigid materials at sub-ambient temperatures

— ISO 4898:1984 Cellular plastics – Specification for rigid cellular materials used in the thermal insulation of buildings

— ISO 4898:1984/Add 1:1988 Phenol-formaldehyde cellular plastics (RC/PF)

— ISO 6187:2001 Rigid cellular plastics – Determination of friability

— ISO 7616:1986 Cellular plastics, rigid – Determination of compressive creep under specified load and temperature conditions
— ISO 7850:1986 Cellular plastics, rigid – Determination of compressive creep
— ISO 8873:1987 Cellular plastics, rigid – Spray-applied polyurethane foam for thermal insulation of buildings – Specification
— ISO 9054:1990 Cellular plastics, rigid – Test methods for self-skinned, high-density materials
— ISO 9772:2001 Cellular plastics – Determination of horizontal burning characteristics of small specimens subjected to a small flame
— ISO 6453:1985 Polymeric materials, cellular flexible – Polyvinylchloride foam sheeting – Specification
— ISO 7203-1:1995 Fire extinguishing media – Foam concentrates – Part 1:
— Specification for low expansion foam concentrates for top application to water immiscible liquids
— ISO 7203-2:1995 Fire extinguishing media – Foam concentrates – Part 2:
— Specification for medium and high expansion foam concentrates for top application to water-immiscible liquids
— ISO 7203-3:1999 Fire extinguishing media – Foam concentrates – Part 3: Specification for low expansion foam concentrates for top application to water-miscible liquids.

Appendix Two-D

Accelerated Ageing Test Summary

2A.6 Introduction

Long service-life requirements of marine sandwich structures, and the limited time available for development, evaluation, and validation of materials makes accelerated ageing characterization necessary. The methods of both accelerated testing and accelerated ageing are employed where a specimen is damaged, to exhibit a progressive accumulation of damage symbolic of realistic end-of –life-service damage which is then artificially aged. For accelerated ageing the calibration of test progression with service exposures is not as important as the confidence that the microstructural features produced using artificial ageing represents those of end-of-life-conditions

The table summarises the artificial acceleration procedures most relevant to this work. The table covers current ASTM,BS and ISO standards and vets the recommended humidity/immersion levels, exposure times temperatures and storage conditions. Each methodology is also briefly described and concludes by rating its applicability for use in this research based upon the requirements. A rating of one is the least applicable and five the most desirable.

Most ASTM standards collaborate closely with the 'MIL-HDBK-17' , a branch of military research aimed at composites, and consequently are generally more considerate of material properties and the effects of morphology than other Standards Bodies. Medical standards (ASTM F series), unrelated to MIL- HDBK-17 corroborate the notion that the maximum test temperatures should be related to the Tg of the material. The maximum test-temperatures

for both aeronautics and medical applications fix a margin of at least 10°C below the Tg , with a rigid maximum limit of 60°C for polymers intended for low temperature applications such as PVC (medical) and 70°C for high temperature polymers such as epoxy laminates (aero).

2A.7 Accelerated Ageing Test Requirements

Despite the numerous approaches to accelerated ageing, published both as standardized testing methods, and tailored by experimenters for specific applications, this section will primarily focus on a comparison of the recommendations by Standards Bodies in order to determine the most applicable method for use within this research. A tabular comparison is presented and rated with respect to five ideal requirements as follows

i. In order for an artificial ageing technique to be considered 'accelerating', it must replicate changes that occur in real in-service conditions. Fracture toughness testing would detect changes of bulk material properties which would be indicative of molecular and morphological changes in the polymer system.

ii. Artificial acceleration relies upon elevated temperatures to increase moisture diffusion rates. Ideally, test temperatures would increase the rate of diffusion without initiating a thermal degradation mechanism. The most reliable predictions of service life are those based upon tests conducted closest to service conditions , while the uppermost limit is set by manufacturers recommendations for maximum processing temperatures as 80-90°C

iii. The test environment would ideally be freshwater immersion not relative humidity as it most closely resembles the service environment and worst-case scenario. The lower density freshwater is more readily absorbed by a material and distilled water further limits the number of complex experimental variables.

iv. Single continuous immersion testing is preferred to staged or cyclic conditions as the complexities involved in understanding the behaviour of a hygrothermally aged core are best initiated with the simplest approach.

v. The specimen geometry is required to be suitable for mechanical testing of bulk material properties. Size is minimized with respect to optimization of moisture absorption and test duration. From the available standard dimensions of sheet thickness supplied by manufacturers (Airex), the maximum size for this work is preferably limited to 20mm (the most popular size sold to marine industry), the minimum thickness may then be determined by optimising for load application.

ASTM F1980-99 is a standard intended for medical polymers, but seemed to fulfill the test requirements more readily than the standards dedicated to sandwich composites or core materials. This was largely due to emphasis on the relationship between immersion temperature and the material. ASTM F1980-99 stipulates that maximum immersion temperature be 10°C below the material transition temperature with a 60°C ceiling though a value of 25°C below the wet Tg is preferred by ASTM D5229-98. Method A of ASTM D5229-98 was the only other clear forerunner as a conditioning technique, but was discounted for its restrictions on specimen geometry in favour of ASTM F1980-99. With reference to foam manufacturers and suppliers Airex, the foams may be used at continuous operating temperatures of 70°C or with a maximum external temperature of 85°C. In this case, ASTM F1980-99 would limit the immersion temperature to 60°C, and correspondingly ASTM D5229-98A also allows a 60°C immersion when the worst-case 85°C service exposure condition is taken. Therefore, the conditioning temperature selected for this research was 60°C.

Furthermore, ASTM F1980-99 was preferred for its environment of freshwater as opposed to relative humidity. As most standards were developed for a particular industrial application such as aeronautics, the conditioning environments were so adapted and lead towards relative

humidity exposure to simulate environmental damage. The industrial application for this work is marine transportation, and thus inclines exposure towards immersion testing to simulate marine environmental damage. The distilled water exposure of ASTM F1980-99 is also attractive as the differing density to seawater means moisture absorption is accelerated but the type of effects upon the material remain unaltered, and distilled as opposed to freshwater further limits experimental variables. Therefore the immersion environment is selected as distilled water. Consequently, accelerated ageing for this work will be conducted with reference to ASTM F1980-99 as a basis.

Key to table:

I Liquid immersion
RH Relative humidity %
/95°C Exposure temperature in °C
(3hrs) Exposure time (hrs)
(Ehrs) Equilibrium exposure time (hrs)
D Drying conditioning
S Storage conditioning

Standard	Max Temp °C	Procedure	Notes
ASTM C481-99 Cycle A	100	[I/50°C (3hrs)] + [100%RH/95°C (3hrs)] + [S/-12°C(20hrs)] + [D/100°C(3hrs)]+ [100%RH/95°C (3hrs)] + [D/100°C (18hrs)] Repeat x6 with [50%RH/23°C]	Resistance of sandwich panels to arbitrary sever conditions and cycles. Geometry varied with regard to ASTM mechanical testing.
C481-99 Cycle B	100	[I/50°C (3hrs)] + [D/70°C (3hrs)] + [1005RH/70°C(3hrs)] + [D/70°C(18hrs)]+ [100%RH/95°C (3hrs)] + [D/100°C (18hrs)] Repeat x6 with [50%RH/23°C]	Complex procedure precludes analysis of relationships between conditioning and specimen morphology/degradation
BS 4370 Pt2 1993	30	[90%RH/30°C (Ehrs)] [50%RH/23°C (Ehrs)]	Rigid cellular plastics also permitted in sandwich format as discs sized from 10-70mm in thickness with minimum exposed surface area.
ASTM D570-95	75 75 75 75 100 50	[D/50°C(24hrs)]+ [S/24°C(1hrs)] +one of: [I/75°C (24hrs)] [I/75°C (2hrs)] [I/75°C (2hrs)]+ [I/75°C (24hrs)] [I/75°C (Ehrs)] [I/100°C (1.5hrs)] [I/50°C (48hrs)]	Tests molded plastic disc 50.8mm x 3.2mm or rods 25.4x25.4mm. temperatures unrelated to material or application.
ISO 4611:1987 A B C	23 40 55	[50%RH/23°C (86hrs)] +one of: [100%RH/23°C (12hrs)] +repeat [100%RH/40°C (12hrs)] +repeat [100%RH/55°C (12hrs)] +repeat	Basic cyclic exposure an temperature for plastics such as PVC sized 50x50x25mm and includes a salt mist condition.
ASTM D2842-48 A	50	[D/50°C(24hrs)]+ [S/50°C(4hrs)] + [I/23°C (96hrs)]	Continuous exposure of rigid cellular plastics using weighted underwater and open cell consideration for for cells greater than 3mm . Specimen geometry 15x15x7.5 & 15x15x t cm, and a coupon of single cell thickness.
ISO 62-1983 A B C D	50 50 50 100	[D/50°C(24hrs)] + [I/23°C (24hrs)] [I/23°C (24hrs)] + [D/50°C(24hrs)] [D/50°C(24hrs)] + [I/100°C (0.5hrs)] [I/100°C (0.5hrs)] +[D/50°C(24hrs)]	Simple recommendations for plastics such as PVC, sized 50x50x25mm under continuous immersion. Conditions unrelated to material properties.
ASTM C72-96 A B C	50 75 75	[D/50°C(24hrs)] + [S/24°C (1hrs)] + one of [I/23°C (24hrs)] [85%RH/75°C (720hrs)] [I/75°C (Ehrs)]	Specifically for water absorption of sandwich cores. Speciemn size fixed at 76.2x76.2x12.7mm specifying direction of rise.

ASTM D2126-99:		[50%RH/23°C)] + one of :	Continuous exposure designed for rigid cellular plastics, permits any temperature/humidity level for individual needs or as per material specification.allows a 4hr interruption to continuous exposure as it has determined no significant difference to results. Recommends min100mmx100mm size and testing to incorporating skins, with finely sanded finish.
A	23	[30%RH/-70°C (24hrs) (168hrs) (336hrs)]	
B	40	[30%RH/40°C (24hrs) (168hrs) (336hrs)]	
C	70	[30%RH/70°C (24hrs) (168hrs) (336hrs)]	
D	100	[30%RH/100°C (24hrs) (168hrs) (336hrs)]	
E	150	[30%RH/150°C (24hrs) (168hrs) (336hrs)]	
F	23	[50%RH/23°C (24hrs) (168hrs) (336hrs)]	
G	40	[100%RH/40°C (24hrs) (168hrs) (336hrs)]	
H	70	[100%RH/70°C (24hrs) (168hrs) (336hrs)]	
ISO 175-1981 E			Broad recommendation of liquid effects on plastics, additional duration up to 5yrs.geometry determined by user, and variation from test temperature to reflect service temperature selected from range 0-150°C
	23	[I/23°C (24hrs) (168hrs)] (336hrs)]	
	70	[I/70°C (24hrs) (168hrs)] (336hrs)]	
ASTM D5229-98			Continuous exposure of matrix materials ; user determined with recommended limits of max test-temp. at least 25°C below wet Tg and max 70°C, and geometry of width/thickness ratio greater than 100. Time determined by theoretical approximations to specimen geometry and diffusivity constant or defaults to a measured equilibrium response. Allows a 30mininteruption to exposure.
A&B	-	[I/ or any %RH /any°C (Ehrs)	
C	-	[50%RH/any°C (Ehrs)]	
D	-	[D/any°C (Ehrs)]	
ASTM F1980-99		[I/Any°C (Ehrs)	Developed for medical polymers and PVC. Correlates artificial ageing time to natural exposure using Arrhenius relationship for conservative estimate. Temperature is user defined with emphasis on material thermal properties, molecular structure. Limits set to 10°C below Tg and max of 60°C. geometry and times defined by user.

Appendix Two-E

Temperature Effects on Core

This section relates to Chapter Two, *Deformation and Failure Behaviour in Foam*

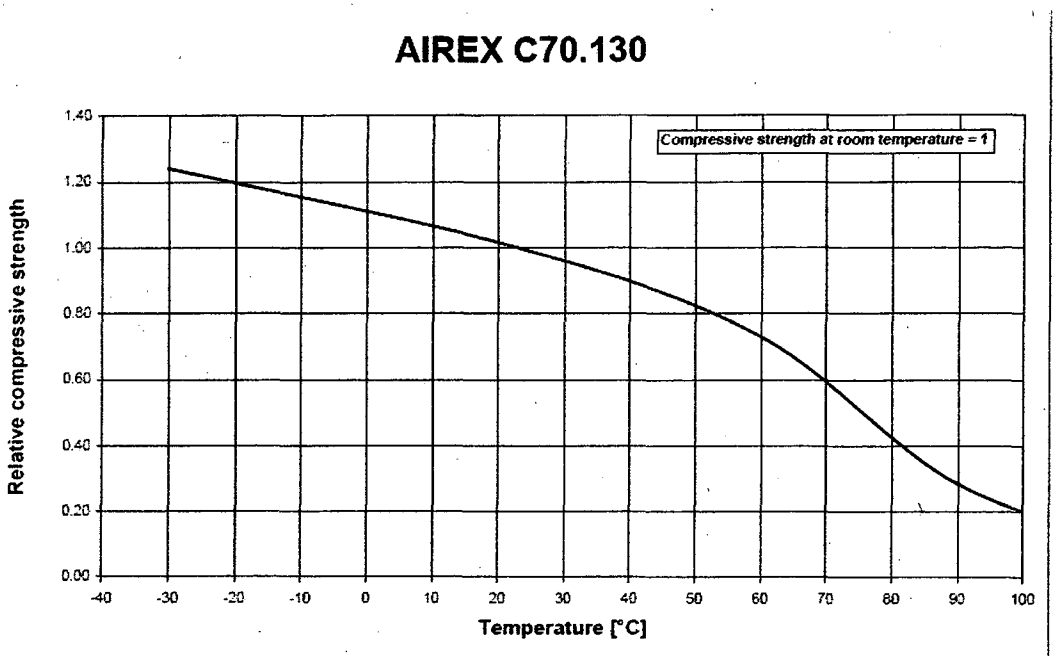

Figure A2- 1 Temperature effects on compressive strength of C70.130

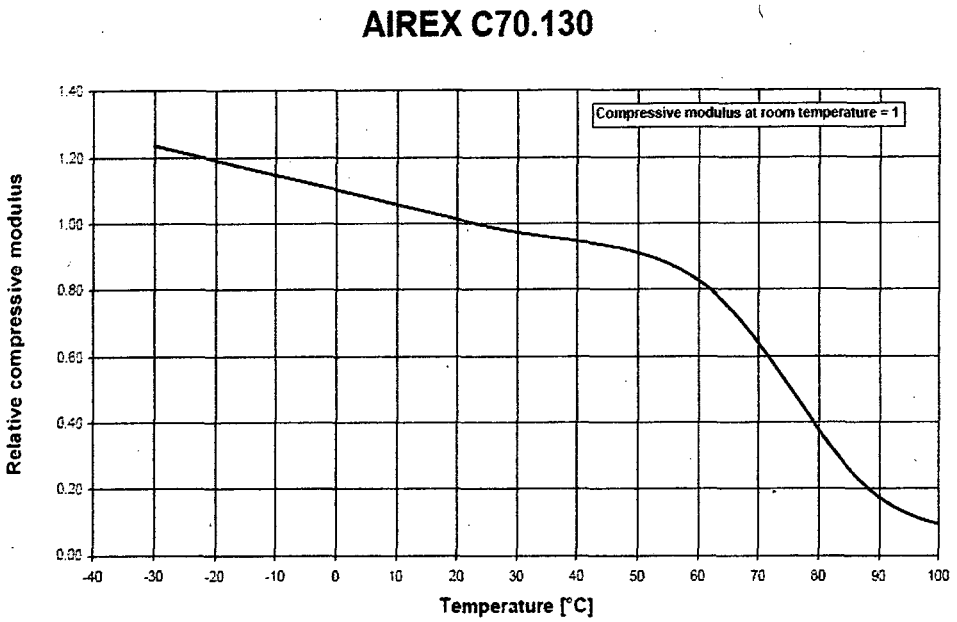

Figure A2- 2 Temperature effects on compressive modulus of C70.130

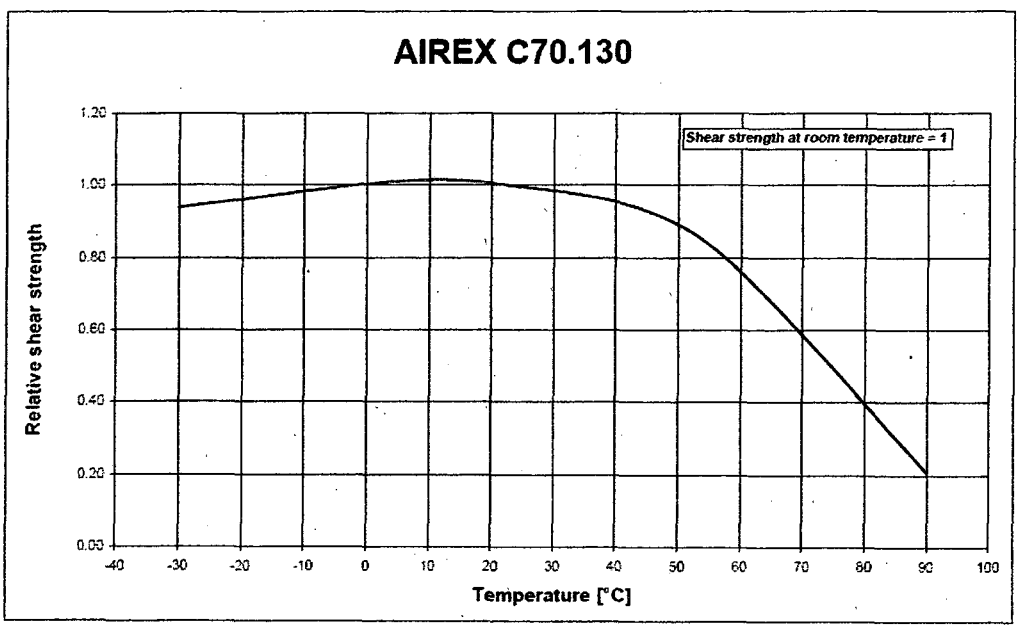

Figure A2- 3 Temperature effects on shear strength of C70.130

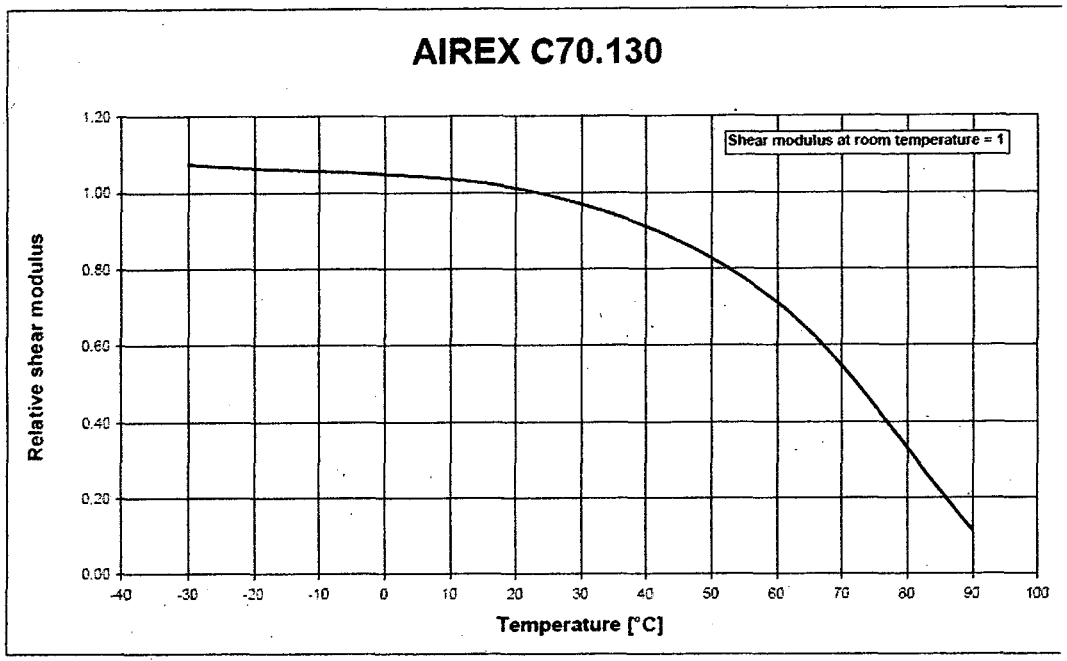

Figure A2- 4 Temperature effects on shear modulus of C70.130

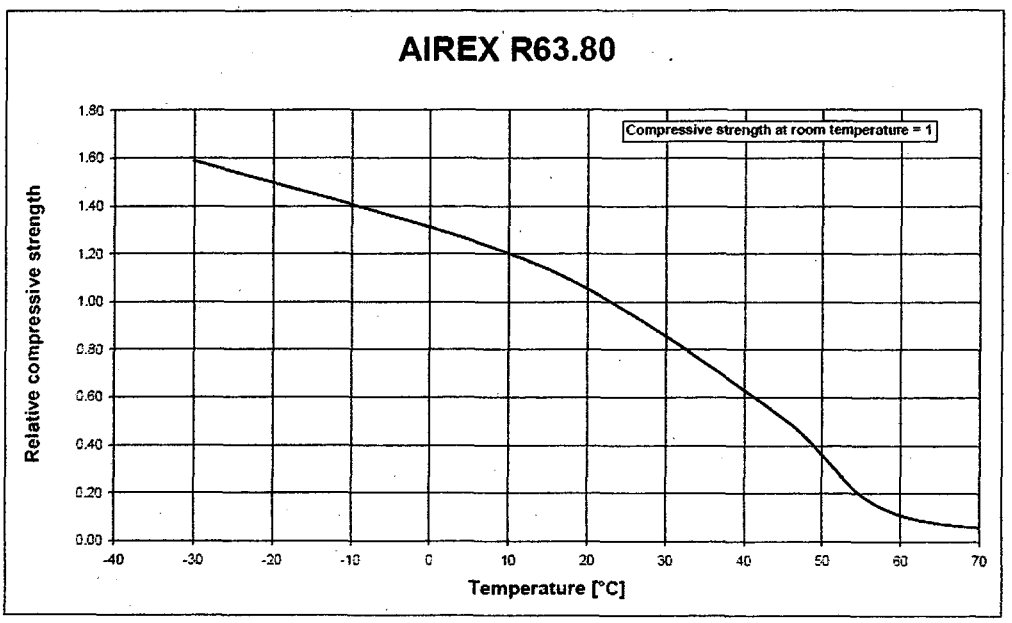

Figure A2- 5 Temperature effects on the compressive strength of R63.80

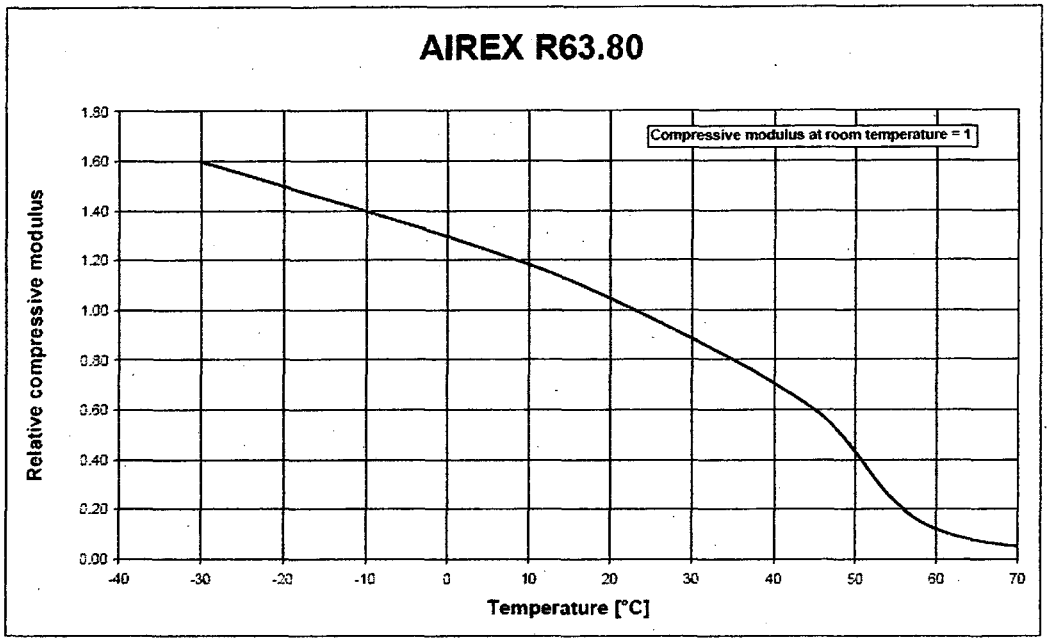

Figure A2- 6 Effect of temperature on compressive modulus of R63.80

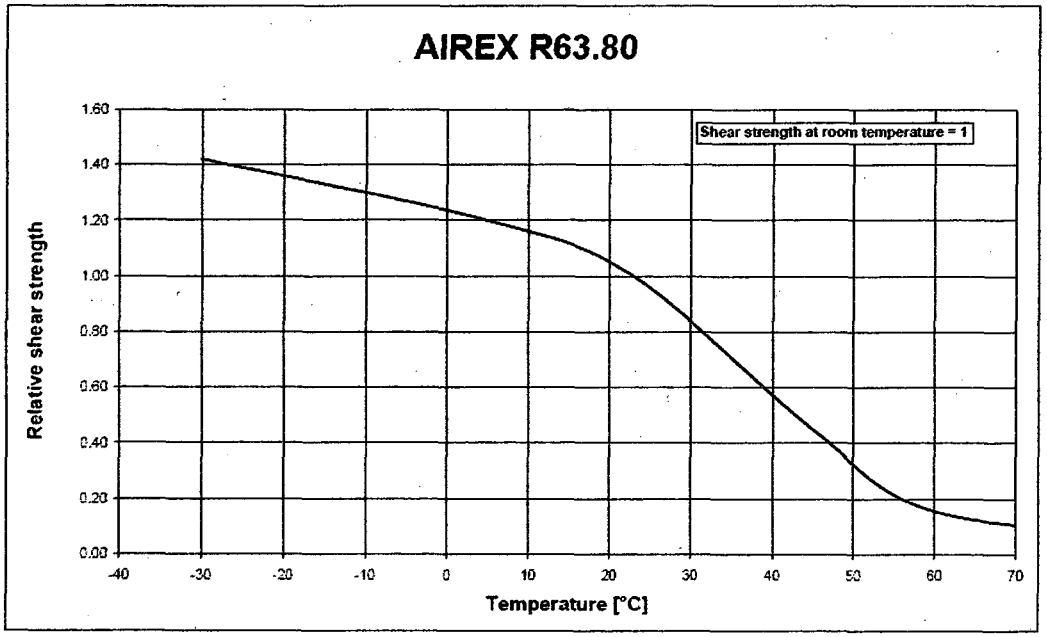

Figure A2- 7 Effect of temperature on shear strength of R63.80

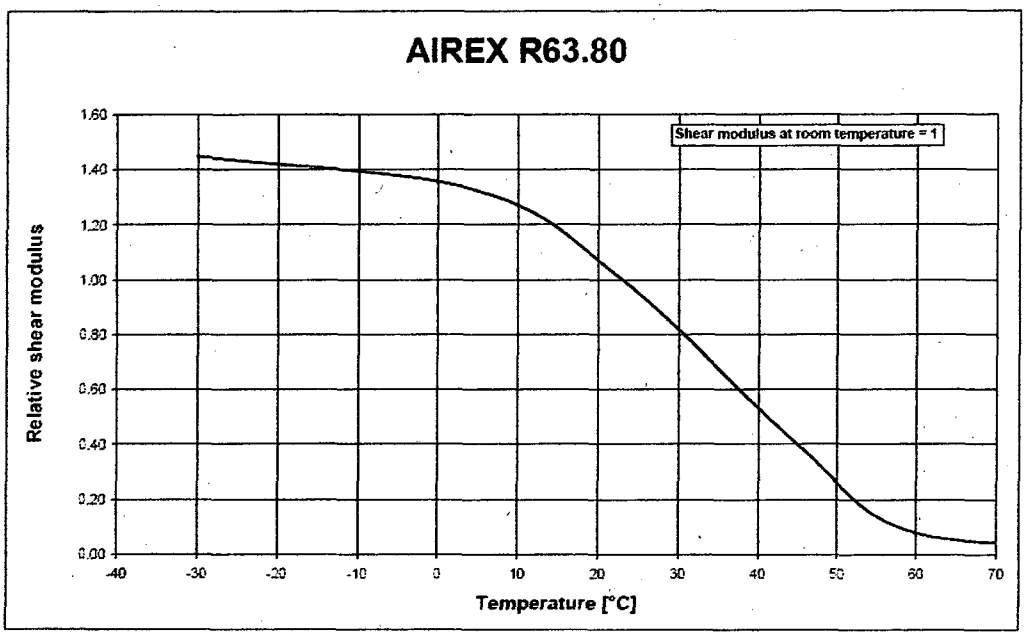

Figure A2- 8 Effect of temperature on shear modulus of R63.80

Appendix Two-F

Mixed-Mode Loading Regime

In order to improve confidence in design safety factors, it is necessary to corroborate theories of foam failure with experimental testing compelling the mixed-mode loading of test specimens.

In the example of an edge crack, Mode I, commonly referred to as the 'opening' mode, is defined as the condition where the crack is perpendicular to the applied stress. In the event of a stress field that is parallel to the crack, the material shears and denoted 'Mode II'. These first two modes or a combination of them are the most commonly experienced by marine structures as discussed in Chapter One. The third, 'Mode III', is out-of-plane shear or tearing and is uncommonly encountered in a hull. Consequently mixed-mode loading is focused upon modes I and II.

Since no uniform test specifications or standards have yet been established to guide the mixed-mode testing of foam specimens, numerous specimen forms and loading methods have been used to investigate fracture toughness, crack propagation, mixed-mode threshold and other fracture criteria. Critical comparisons of the various test methods potentially applicable to mixed-mode foam testing as shown in Figure A2- 9 and indicate that that the most accurate mixed-mode data is obtained by either combining the three-point bend and four-point shear tests or, using a compact tension shear specimen (CTS). Requirements imposed by the environmental conditioning of the specimens favour the CTS specimen.

The loading regime is controlled by two main factors; the practical conditions to be simulated, and the material capabilities of the specimen. These factors

effectively impose constraints upon the specimen, which must be catered for by the loading arrangement.

2A.8 Requirements for Mixed-Mode Loading Regime

The main requirements of the loading and specimen arrangement are described as follows:

i. Full range of mode I and mode II combinations. The stresses at the crack-tip should be fully variable from pure tensile mode I stresses, through to the pure shear stress of Mode II. Ideally, a smooth and easily generated transition between the modes is required to investigate the influence and sensitivity of mode mixity for a hygrothermally aged foam core. Controlled stable crack growth should be achieved from a fine crack starting point as specimens which require wider slots can produce inaccurate results which would be inadmissible for providing threshold values.

ii. Single test specimen. Ideally, a single configuration should be used so that results from samples that are hygrothermally aged, and examined with TSA are directly comparable.

iii. Simple clamping and loading conditions. As a structural foam cannot bear great pressure without significant damage over a large surface, when load is concentrated, the foam cells are easily crushed, and testing is that of the local cells not of the global foam. This further constrains the fixing of the specimen into the loading rig, as it cannot be held in a clamp directly without significant consideration. Sensitivity to localised crushing implies that loading should preferably be tensile rather than compressive, to avoid damaging fracture surfaces unduly. It is preferred that loading be applied in a simple manner as two-axis-stresses cannot be easily accommodated on standard test machines.

iv. Limited Specimen size: The loading method, must allow for small specimen sizes to maximise hygrothermal ageing rates, placement in conditioning chambers, savings in material and cost, while being representative of samples that are possible for removal from a hull during structural survey. Specimens are also required to be larger than coupon-size so as to be relevant of a hull core and allow the crack propagation to be followed by TSA, free from edge stress interference. The thickness of the specimen should still be sufficient to realise a state of plane strain so as to provide material-limit values from fracture testing which can be checked by TSA prior to testing.

v. Simple production. Test specimens are required to be simply manufactured, and the notch and specimen contours easily and quickly formed to ensure accurate replication.

The specific loading configurations have been well documented and beyond a summary of the most pertinent issues affecting this study, need not be considered in greater detail here. .

The logic in selecting the final listed CTS-type specimen shown in Figure A2-9 was not only based upon the unique advantages specific to this specimen, but also upon the elimination of the other specimens with respect to the above requirements. The most obvious and attractive quality of the selected CTS-type specimen, is that the same foam sample can be used to examine with ease a full range of mixed-modes from pure Mode I to pure Mode II, and do not require duplicate specimens for each mode-mixity offering a clear advantage over the first two plate specimens and the beam configuration which otherwise rated highly. Additionally, the CTS-type was preferred as only relatively low forces would be required to yield significant stress intensity field which is a requirement heavily weighted for foam specimens where concern for cell-crushing and tearing is high. Two issues which in association to the complexity of testing and geometry exclude the remaining specimen configurations tabulated in Figure A2- 9.

SPECIMEN	EVALUATION SUMMARY
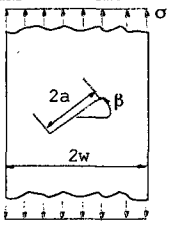	A plate with an oblique central crack subjected to tensile stress produces mixed-mode stresses at the two crack-tips. Mode mixity is altered by varying the crack inclination angle. No transition to pure mode II is possible with this specimen. Problems of cardioid interaction from the two crack-tips may also occur, especially if crack propagation does not begin simultaneously from both tips. Relatively small stress intensity factors produced by small central crack can lead to larger specimen sizes and larger loads required for fracture, with increased risk of crushing at load points.
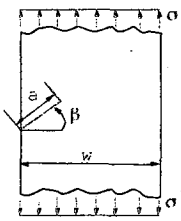	As a variation of the specimen above, the details of crack propagation also apply to a plate with an edge crack. It can also vary the mode mixity by rotating the crack angle, and transition to pure mode II is also impossible. The stress flow from the crack-tip may interact with the edge effects rather than a second crack-tip, which would vary with each new rotation providing an experimental inconsistency. Furthermore, crack growth would be problematic, as the crack direction would be deflected upon application of load. Again, small stress intensity factors may result in larger specimens and fracture loads.
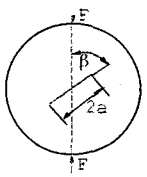	The Brazilian disc specimen is standardised in geology as an indirect tensile test. A disk test uses a very compact specimen and allows smooth transition from pure Mode I to Mode II when the crack is rotated within the range of 0°(mode I) ≤ β ≤25° (mode II). Beyond 25°, compressive stresses at the crack may damage the surface. As the rotation range is so focused, a small angular deflection translates as a significant change in stress intensity. Comparably to the rectangular plate specimen, a central crack incorporates an unfavourable double-crack-tip.
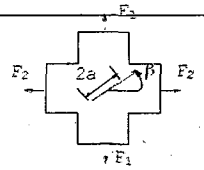	The transition between mode I & II is made by the variation of both the crack angle and the ratio of forces (F_2/F_1) applied to the specimen. Pure mode II can only be obtained when the crack is angled at 45° and the forces F_1 and F_2 are equal and opposite. Load application and testing is complex, requiring special equipment, while Mode II presents buckling problems for thinner specimens.
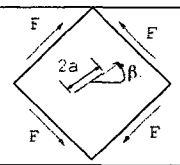	Studs along the edges of a square plate apply a shearing force. As the crack is orientated from the mode I position of 0° to Mode II at 45°, the mode mixity can be smoothly altered. Again a central crack exposes two crack-tips with a weaker stress-intensity field that requires a larger specimen dimensions and testing forces. Further problems of load application and generation of a propagating crack have also been noted.
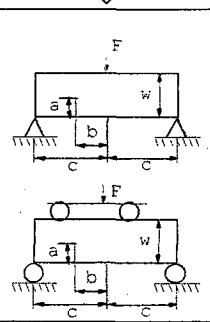	Full range of Mode I and II failures can be obtained by supplementing with a second point load. Essentially a three-point-bend specimen, that is compact and can partially vary the K_2/K_1 ratio up until aprox. 1, by altering the position of the crack along the specimen length (b/c ratio), and its depth (a/w ratio). Pure Mode I will occur when the crack is at mid-length, (b/c =0), while pure Mode II is impossible. By loading the specimen in four-point-bend with the crack offset, predominantly Mode II stresses will dominate and make pure Mode I difficult to achieve. Loading application is simple without specialised equipment, and can achieve a state of plain strain through a thick sample.
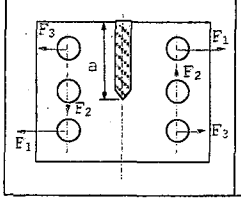	The very compact rectangular specimen is fixed into a rig by the six holes such that it can be rotated with respect to the direction of a tensile force, while producing a state of plane strain. The position of the edge crack and the specimen itself do not change in order to obtain a smooth transition between pure modes I and II. The loading rig allows forces on the loading pins to be statically determined, which are comparatively low for the high stress intensity field obtained, providing a highly desirable ratio to minimise foam crushing potential.

Figure A2- 9 Comparison of mixed-mode loading regimes for MI and MII as applicable to hygrothermal ageing characterisation of foam cores

The vulnerability of the foam cells to localised damage further reinforces selection of the CTS specimen, as it permits high stress intensity values for a comparatively low load. This favourable ratio correlates to when the effective stress intensity factor (K_e), is high. K_e is determined by Richard in the original German publication , from stress intensity factors K_I and K_{II} as shown in, where $\alpha 1$ is a material constant ($= K_{Ic}/K_{IIc}$) .

$$K_e = \frac{K_I}{2} + \frac{1}{2}\sqrt{\left[K_I^2 4(\alpha_1 K_{II})^2\right]} \qquad \textit{Equation A2- 1}$$

Figure A2- 10 depicts a comparison of the three candidate specimens rated in Figure A2- 9and illustrates a significant difference in stress intensity for a given loading configuration (force and loading angle are consistent)

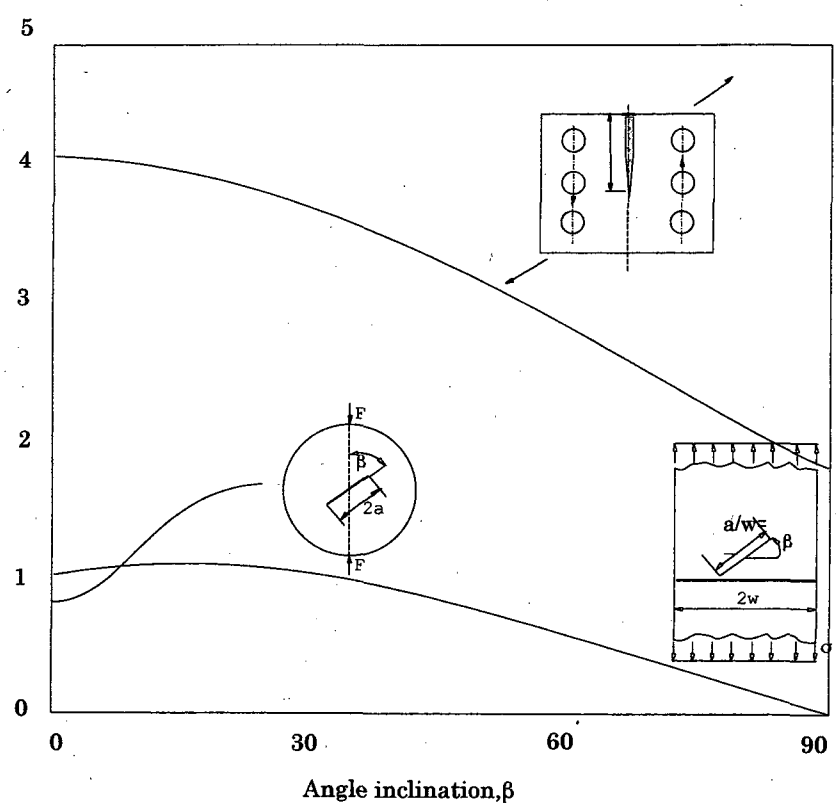

Figure A2- 10 Comparison of the effective stress intensity factors for three specimens for use in mixed mode conditions. The CTS configuration displays the highest stress intensity values

With respect to the fulfilment of the requirements for the foam to be loaded in a mixed mode configuration, the CTS type specimen was selected as the most suitable. The loading rig, originally designed to accommodate metals, has

been validated through successful use since its inauguration in 1986, and for use on structural foams by Noury.

2A.9 CTS-type Theory

Initially designed to overcome the experimental problems associated with mixed-mode loading of traction rods, pressed discs, and torsion tubes, the CTS-type specimen has been adopted for use with composites. Its success lies in the variations from the original CTS specimen.

Figure A2- 11 shows the ASTM standard CTS precursor with its proportionate dimensions and geometrical-factor formulae required for calculations of the fracture toughness for modes I and II.

Figure A2- 12 The new CTS-type specimen (shaded), showing the position of the loading pins (shaded darkly) and their contact points against the loading rig (shaded pale). Slots rather than holes are used so that a statically applied load transfer is ensured. The key to this configuration is that the specimen remains fixed within the test rig which is itself rotated as a whole to alter the angular relationship between crack and applied force as illustrated in Figure A2- 13.

$$F_1 = \frac{2\left(2+\frac{a}{b}\right)}{\left(1-\frac{a}{b}\right)^{3/2}} \cdot \frac{1}{\sqrt{\frac{a}{b}}} \cdot F_2$$

$$F_2\left(\frac{a}{b}\right) = 0.443 + 2.32\left(\frac{a}{b}\right) - 6.66\left(\frac{a}{b}\right)^2 + 7.36\left(\frac{a}{b}\right)^3 - 2.8\left(\frac{a}{b}\right)^4$$

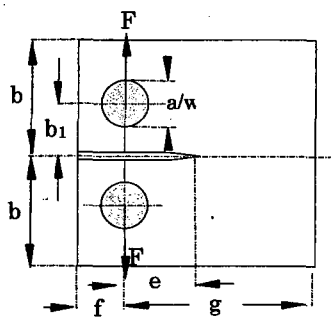

Figure A2- 11 Conventional CTS specimen as described by ASTM standard E399-90. Specimen geometry; b =0.6g, b1=0.275g, D =0.25g, c =0.25g, t =g/2

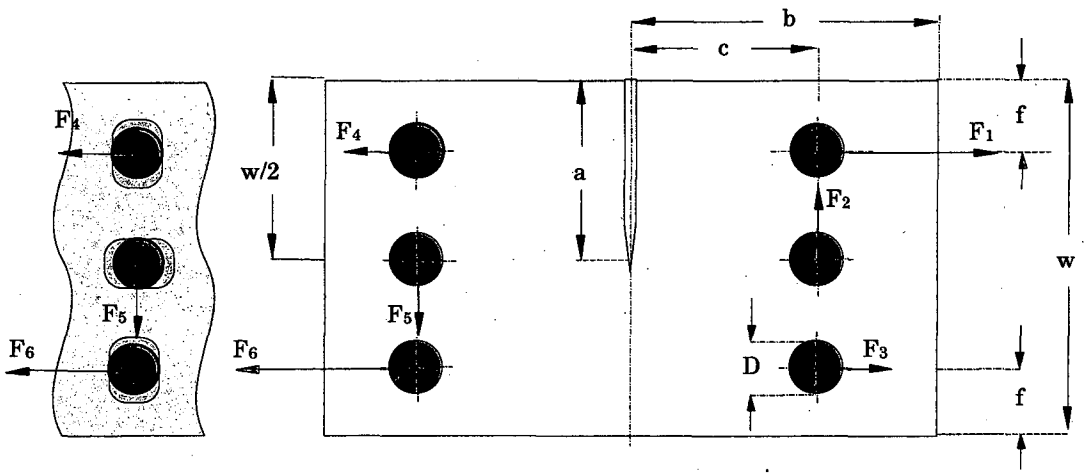

Figure A2- 12 Full mixed-mode CTS type specimen. Specimen geometry; $a \geq 0.5w$, $b=0.85w$, $c=0.6w$, $f=0.2w$, $t=0.5w$, $D=0.15w$

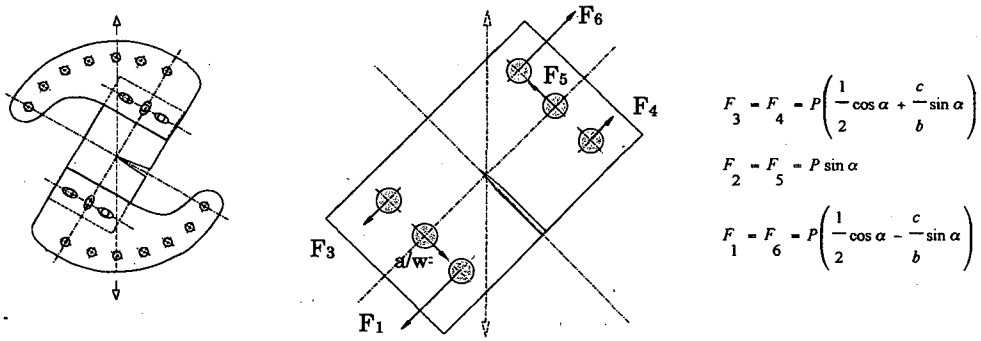

Figure A2- 13 Forces acting in mixed-mode loaded condition with 30°rotation of rig.

The load is then related to the crack-tip stresses through the established fracture toughness relationship

$$K_{I,II} = \frac{P\sqrt{\pi a}}{wt} F_{I,II} \qquad \textit{Equation A2- 2}$$

Where K_I and K_{II} represent the fracture toughness for modes I and II respectively, P the applied load, a the crack length, w the specimen width, and t the thickness (as represented in Figure A2- 12). $F_{I,II}$ in this equation are geometrical parameters respective to K_I and K_{II} which have been determined by Richard as:

$$F_I = \frac{\cos\alpha}{1-\frac{a}{w}}\sqrt{\frac{0.26+2.65\left(\frac{a}{w-a}\right)}{1+0.55\left(\frac{a}{w-a}\right)-0.08\left(\frac{a}{w-a}\right)^2}}$$

Equation A2- 3

$$F_{II} = \frac{\sin\alpha}{1-\frac{a}{w}}\sqrt{\frac{-0.23+1.40\frac{a}{w-a}}{1-0.67\left(\frac{a}{w-a}\right)+2.08\left(\frac{a}{w-a}\right)^2}}$$

Equation A2- 4

Where α is the angular rotation of the rig.

These geometrical parameters may be graphically represented with regard to the above for a range of a/w shown in below. It can be seen that for pure mode I loading, f_I is a maximum. With an increasing KII contribution for a higher mode, f_I diminishes until 0 for a pure mode II condition.

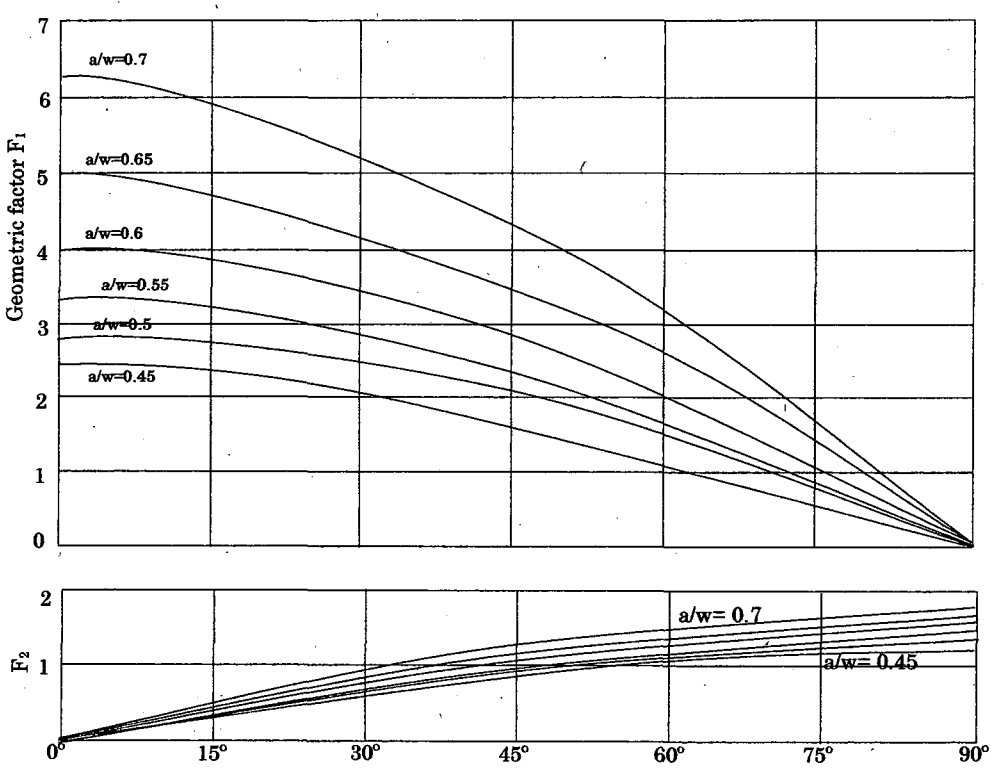

Figure A2- 14 Stress Intensity Factors in context of geometric factors for the CTS-type Specimen (6-pin) as a function of load application angle α and ratio a/w

2A.10 References applicable to the CTS-type rig

1. Richard, H.A., "Specimens for Investigating Biaxial Fracture and fatigue processes" Biaxial and Multiaxial Fatigue. EGF 3, Ed. Brown, M., Miller, K., 1989, Mechanical Engineering Publications., London, p217-229
2. Richard,H." Praxisgerechte Beurteilung von Bauteilen mit Rissen unter komplexer Beanspruchung", Proc. 7 symp. Vermorformung und Bruch, Magdeburg, Teil 1 1985, p181-186
3. Noury, P., Shenoi, R., Sinclair, I., "On Mixed-Mode Fracture of PVC Foam" Int. Journal of Fracture, vol.92, p131-151, 1998, Kluwer Academic Publishers
4. Benitz, K., Richard, H.A. "A Loading Device for the Creation of Mixed Mode in Fracture Mechanics" Int. Journal of Fracture, vol.22, p-R55-R58, 1983
5. Pirondi, A., Nicoletto, G. "Mixed Mode Fracture Envelop of a Structural Adhesive" Conf. Structural Adhesives and Industrial Applications-alternatives to traditional joining techniques., 11-12 Giugno 2001, Italy
6. Richard, H.A., "Some theoretical and experimental aspects of mixed mode fractures", Advances in Fracture Research, Proc. 6th Int. Conf. On Fracture (ICF6), vol.5. india, 4-10th Dec 1984., Pergamon Press, 1984, p3337-3344

Appendix Two-G

Damage Detection Techniques

Figure A2- 15 summarises a critical comparison of the most promising candidate techniques for damage detection and evaluation within a foam. The most applicable method available at eth time was TSA. The requirements complicit in selecting a method are as follows:

i. Quantitative data collection from a crack-tip for the analysis of critical stress factors.

ii. Ideally non-contact as the behaviour of foam core cell-walls is very sensitive and information of stress obtained around the crack-tip would be highly sought after. This effectively filters the candidate methods down to optical non-destructive testing techniques.

iii. Ideally a flexible method which could provide data on differing scales, both full-field to describe the bulk behaviour and zoomed into crack-tip for local stress information.

iv. Given the nature of the foam as a construction of cells, the method would ideally be capable of high resolution with attainable high levels of accuracy at this resolution.

v. The detection method would ideally have fast or real-time realisation of data, be simple to operate with low running costs and few consumables.

vi. Portability of equipment, robust technique that is sensitive for damage detection, but able to produce repeatable results without the need for strictly controlled lab conditions.

TECHNIQUE	DESCRIPTION
D-Sight	An image enhancement technique used for *flat*-surface inspection and dramatic visualisation of local effects and defects, allowing comprehensive surface inspection converting local variations in surface shape to light intensity. Operationally simple and real-time, but material types limited and defect classification is subjective.
Holography	Full field interferometric measurement of deformations. Electronic Speckle Pattern Interferometry ESPI uses CCD camera to compare 2 images of specimen at different instants wrt fixed reference point enabling quantitative strain and stress measurement. Is versatile, sensitive with real-time data measuring in mm range but is very sensitive to test environment and difficult to separate superposition effects and obtain reliable data.
Laser-Ultrasonics	Scans of complex materials and shapes possible by laser-generated ultrasound, and pulsed echo techniques. A laser beam modulated with ultrasound frequency is able to scan large surfaces. Light energy is converted into mechanical waves penetrating the object as a second beam is superimposed and measures the echoed ultrasound. Fast method, and signal can be superimposed on contour data, but is complex to operate, and limited in detection of vertical cracks.
Shearography	Used to locate internal cracks and defects in full-field complex materials. Simultaneous inspection of area illuminated by divergent laser. Interferometric comparison of 2 points over fixed distance for all points in lit area. Only deformation gradient measured as only local deformation observed and results interpretation difficult and defect location requires correction and is dependent on lateral shearing vector.
Thermography	Can locate full-field inner and surface defects from observation of thermal equilibrium after thermal disturbance by momentary energy pulse emitted from flash lamp, laser, heat guns/lamps. Is versatile, sensitive even to a few mm depth, simple operation, detailed data possible but must be calibrated regularly and accuracy is dominated by sensitivity factors.
Digital Image Correlation (DIC)	Tracks movement of natural or applied surface pattern using charge coupled camera device (CCD) for strain measurements. Has high accuracy, and is available with many lens attachments including coupling for SEM microscopy. Is portable and environmentally insensitive, but is new technique with little published information.
Thermoelastic Stress Analysis (TSA)	Locates sums of stresses and analyses crack propagation by recording temperature distributions generated by thermoelastic effect. Application of cyclic loading concentrates volumetric changes at high tensioned locations of loading force. Resulting local energy change registers as temperature distribution in real-time. Focal plane array detection is sensitive except for in-plane or global movement, but exhibits comparatively low environmental sensitivity.

Figure A2- 15 Comparison of promising candidate optical methods for NDT of foam core

Appendix Six-A

TSA CTS-type Rig Design

The up-scaled design of the CTS-type rig for TSA, underwent several changes during development to accommodate and remain flexible for testing cross-linked and linear foam type materials. The procedure was begun with a first estimate by up-scaling the size in consideration with the dimensions of the servo-hydraulic test machine, running a *blind-test* to establish the continuity of the specimen geometry with respect the original 6-pin version, before construction and experimental TSA testing. However it was subsequently found that despite supportive end-tabs adhered to the sensitive foam specimens, results improved for the cyclic frequencies used (order of 10Hz) when the pin design was further altered to larger flush-fitting pins distributed across the specimen width. This meant that the specific geometric factors used in the calculation of K_{IC} as re-evaluated by the blind-test were no longer applicable. The procedural steps taken are summarised by the flowchart shown in Figure A6- 7. TSA testing for the design of the rig was undertaken with the Deltatherm TSA detector, which is an older system than the Cedip, but the TSA operational principles are the same even though the data may be displayed differently. The thermoelastic / calibration constants are specific to the detector system used so signal magnitudes are not directly comparable between the two systems. Some excerpts obtained using the Deltatherm system may be presented here to serve as a relevant illustration, preferentially allocating this body of work into this Appendix, otherwise it is covered in earlier MPhil transfer work[1].

6A.1 Initial size estimate

The first size estimate made with respect to limitations imposed by the clearance tolerance of the Instron testing machine and by the requirement to

enable a crack-tip pattern to be contained within the specimen dimensions without the boundary of size or edge effects

The literature review indicated that linear elastic fracture mechanics (LEFM) is suitable to describe the fracture behaviour of foam. K_{IC} standards for plastics and metals are similarly described by an apparent crack initiation load P_Q with a 5% secant construction, where the load must be greater than 1.1 times the maximum load for the test to be valid, and where the specimen size requirements are as:

$$B, a \geq 2.5\left(\frac{K_Q}{\sigma_{YS}}\right)^2 \qquad \textit{Equation A6- 1}$$

$$0.45 \leq \frac{a}{W} \leq 0.55$$

where B = specimen thickness, a = crack length, W = specimen width

Anderson's key text on Fracture Mechanics[2] reports that the method often introduces an artificial size dependence for K_Q as demonstrated experimentally with rigid PVC and Polycarbonate (PC) and accentuated by any non-linearity in the load displacement curve. However, when specimen size is sufficient, stress intensity calculated using LEFM and J-integral become equal which Anderson showed in Figure A6- 1.

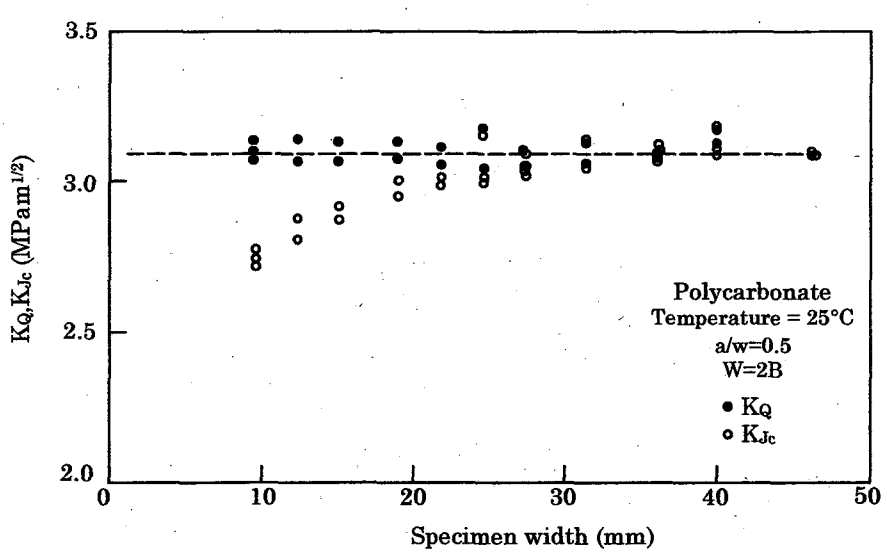

Figure A6- 1 Size dependence of K_Q and J-based fracture toughness for polycarbonate.

Initial TSA of mode I 60mm x 40mm x 1mm aluminium specimens with a central 10mm hole also allowed an indication of interference stresses from loading pins to be estimated and provided a conservative estimate for the minimum distance between loading pins and crack tip as approximately 3.5 times the hole diameter, and illustrated in Figure A6- 2. Parametric-matrix stress calculations in Excel converged to an optimal 100mm x 150mm panel with five loading points evenly distributed.

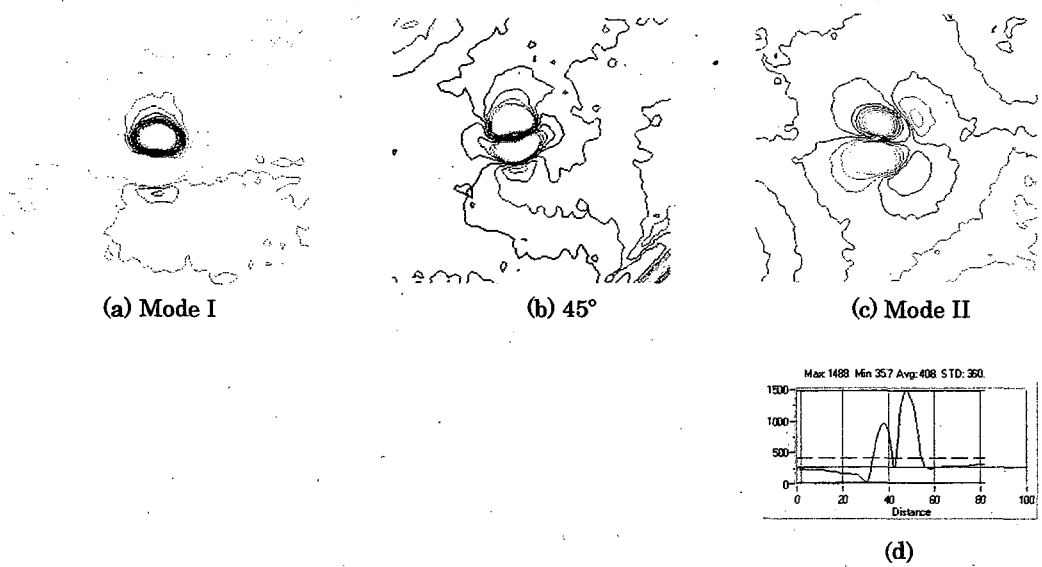

(a) Mode I (b) 45° (c) Mode II

(d)

Figure A6- 2 15 (a),(b),(c) DeltaTherm TSA contour plots of signal strength distribution away from hole edge. Drilled hole dimension of 10mm in aluminium 1mm thick.(d)TSA Signal Line plot across vertical mode II hole shows signal reaches a uniform average after a distance of between 3 and 3.5 times the hole diameter

6A.2 Resolution of Forces

The loading of the rig is such that the lines of force will intersect with the mid-point of the specimen as it rotates. Figure A6- 3 and Figure A6- 4 show the resolution of forces for the two configurations. Taking advantage of one of the most attractive features of the CTS-type design, loading angles of 10° and 80° were additionally formed to allow closer examination of near mode II. To maintain correct mass balance and structural strength, the rig was to be machined from a single aluminium block Figure A6- 5.

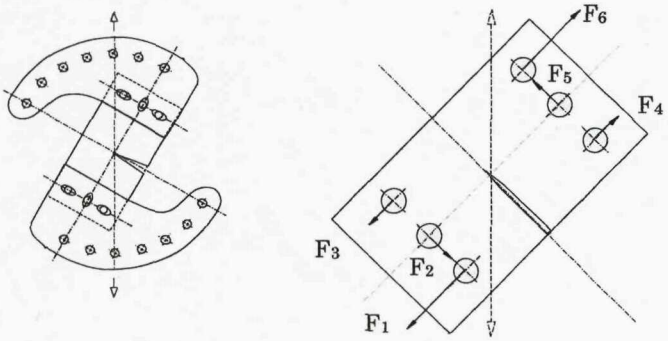

$$F_3 = F_4 = P\left(\frac{1}{2}\cos\alpha + \frac{c}{b}\sin\alpha\right)$$

$$F_2 = F_5 = P\sin\alpha$$

$$F_1 = F_6 = P\left(\frac{1}{2}\cos\alpha - \frac{c}{b}\sin\alpha\right)$$

Figure A6- 3 6-pin CTS-type specimen fixed into rig and loaded in a mixed mode condition

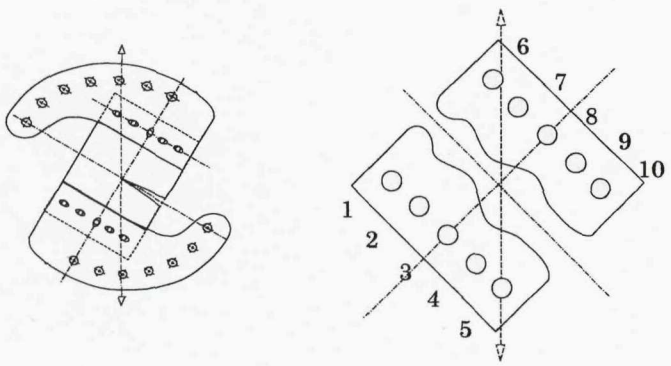

$$F_1 = F_{10} = P\left(\frac{1}{4}\cos\alpha - \frac{c}{2b}\sin\alpha\right)$$

$$F_2 = F_9 = P\left(\frac{1}{4}\cos\alpha - \frac{c}{b}\sin\alpha\right)$$

$$F_3 = F_8 = P\sin\alpha$$

$$F_4 = F_7 = P\left(\frac{1}{4}\cos\alpha + \frac{c}{b}\sin\alpha\right)$$

$$F_5 = F_6 = P\left(\frac{1}{4}\cos\alpha + \frac{c}{2b}\sin\alpha\right)$$

Figure A6- 4 Representation of a 10-pin specimen loaded in mixed mode condition (not to scale), showing loading points numbered.

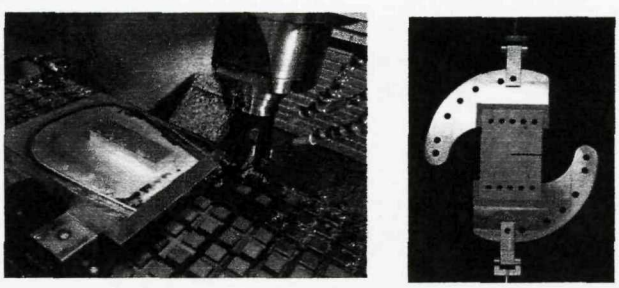

Figure A6- 5 Manufacture from single block aluminium and end product

6A.3 Blind Test

In using TSA to examine the crack-tip, a minimum estimate of the extent to which the stress extends would be useful, so with respect to flexibility of future specimen selection and testing, the most conservative estimate method

was taken, and used a J-intergal method for the parameter in Franc2D. The J-integral method was developed to accommodate non-linear behaviour in materials and is well detailed by Anderson. Franc2D is a numerical finite element modelling routine freely availability from Cornell University[3]. The routine was chosen for its user friendly and high profile successes by Boeing and NASA, and for the built-in J-integral method which has been used previously by Pirondi[4] to evaluate Richards criteria. The principles of the 6-pin CTS-type rig and the accompanying expressions for the geometrical factors developed by Richard have been previously validated by several authors[4,5,6], Franc2D was used to consider the deviation caused by the supplemental pins in the up-scaled 10-pin model.

The Richard expressions are used with the established fracture toughness relationship as described in Appendix A2 and used to commence a *blind test* to validate the expressions for the upscaled 10-pin model rig[7].

Arbitrary values for the parameters controlling mixity (ratio of K_{II}/K_I and K_{eq}), will be used to obtain a value for the ratio of crack length to width (a/w). The rotational angles are fixed by the rig as 0°, 10°, 30°, 45°, 60°, 80°, 90°, and the specimen dimensions have been fixed in the previous section. K_{II}/K_I , K_{eq} , and the newly determined value of a/w will be used as input values as shown in Table A6-1 and presents a comparison of the K_{II}/K_I and K_{eq} values obtained using Richard equations and those derived using a J-integral FEA approach.

It should be noted that the program is in US standard units and all input values must be converted to units of inches, ksi instead of MPa, and kips instead of kN. Details of the unit conversions are presented in Table 4 1. A screen-capture of the mesh model from CASCA is shown in Figure A6- 6, an associated package using Q8 elements which are eight node quadratic collapsed triangular elements in plane strain which could then be refined to emphasise features of interest such as loading points. The FEA model utilised the distribution of the globally applied load across the loading pins discerned as F1-10 in the diagram above. The selected calculation path in FRANC2D was a Pre-Process/Problem Type/Plane Strain in which a default value of unit thickness is used. As the software units are fixed, the default thickness is 1 inch, and must consequently by corrected to mm by assuming 25.4mm per

inch for a 20mm thick foam. The percentages in the final column indicate the percentage difference between K_{II}/K_I and K_{eq} as calculated using Richards geometrical factors, and the results developed from FEA. Some percentage difference was shown, though it was consistently below 2.5%. It was concluded that equations developed by Richard were feasible for use with the modified 10-pin specimen.

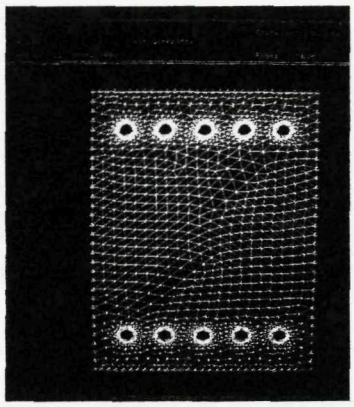

Figure A6- 6 Casca model used in Franc2D plot.

α°	Pmax (kN)	Pmax (kips)	F_6	F_7	F_8	F_9
0	8.966485	2.020616	0.50515	0.50515	0.000	0.50515
0	17.93297	4.041233	1.01031	1.01031	0.000	1.01031
0	26.89945	6.061848	1.51546	1.51546	0.000	1.51546
45	6.31274	1.422519	-0.1035	-0.4586	1.0059	0.96154
45	12.62552	2.845188	-0.2071	-0.9172	2.0118	1.92308
45	13.93828	4.267781	-0.3106	-1.3757	3.0177	2.88462
60	9.187274	2.07037	-0.3740	-1.0068	1.7929	1.52445
60	19.83745	4.47041	-0.7481	-2.0137	3.5859	3.0489
60	29.75618	6.66181	-1.1221	-3.0206	5.3789	4.57335

Table A6-1 Results of Excel determination of first approximation of a/w for selected KII/KI ratios. Conversion units 1 inch=25.4mm, 1kips =4.45kN, 1ksi = 6.897MPa, 1ksi√inch =1.1MPam-2. Specimen dimensions used: 100mm x 150mm x 20mm. Force calculations used converted units as w=3.937, b= 0.85w = 3.346, c = 0.6w = 2.362. Comparison to data from FRANC2D shown as shaded with %errors between the real input values and the calculated outputs.

F_{10}	a/w	Ksi√inch K_{1max}	Ksi√inch K_{2max}	MPa√m K_{1max}	MPa√m K_{2max}
0.50515	0.5	0.8857	0	4.947	0.0
1.01031	0.5	1.7608	0	9.833	0.0
1.51546	0.5	2.641	0	14.75	0.0
0.60650	0.64	0.86515	0.298	4.831	1.664
1.21301	0.64	1.729	0.596	9.660	3.328
1.81951	0.64	2.5947	0.894	14.49	4.992
0.89162	0.59	0.7468	0.5218	4.170	2.914
1.78325	0.59	1.4885	1.04	8.314	5.807
2.67488	0.59	2.2347	1.562	12.48	8.722

K_2/K_1	K_{eq}	%Error $\left(1-\frac{K_2/K_{1FRANC2D}}{K_2/K_{1INPUT}}\right)*100$	$\left(1-\frac{K_{eq_{FRANC2D}}}{K_{eq_{INPUT}}}\right)*100$
0	4.951	0	1.05
0.0	9.833	0	1.71
0.0	14.753	0	1.68
0.344	5.110	1.714	2.20
0.345	10.218	1.423	2.20
0.345	15.329	1.423	2.20
0.699	5.090	0.143	1.80
0.697	10.144	0.428	1.42
0.698	15.247	0.286	1.54

Table A6-1 Contd.

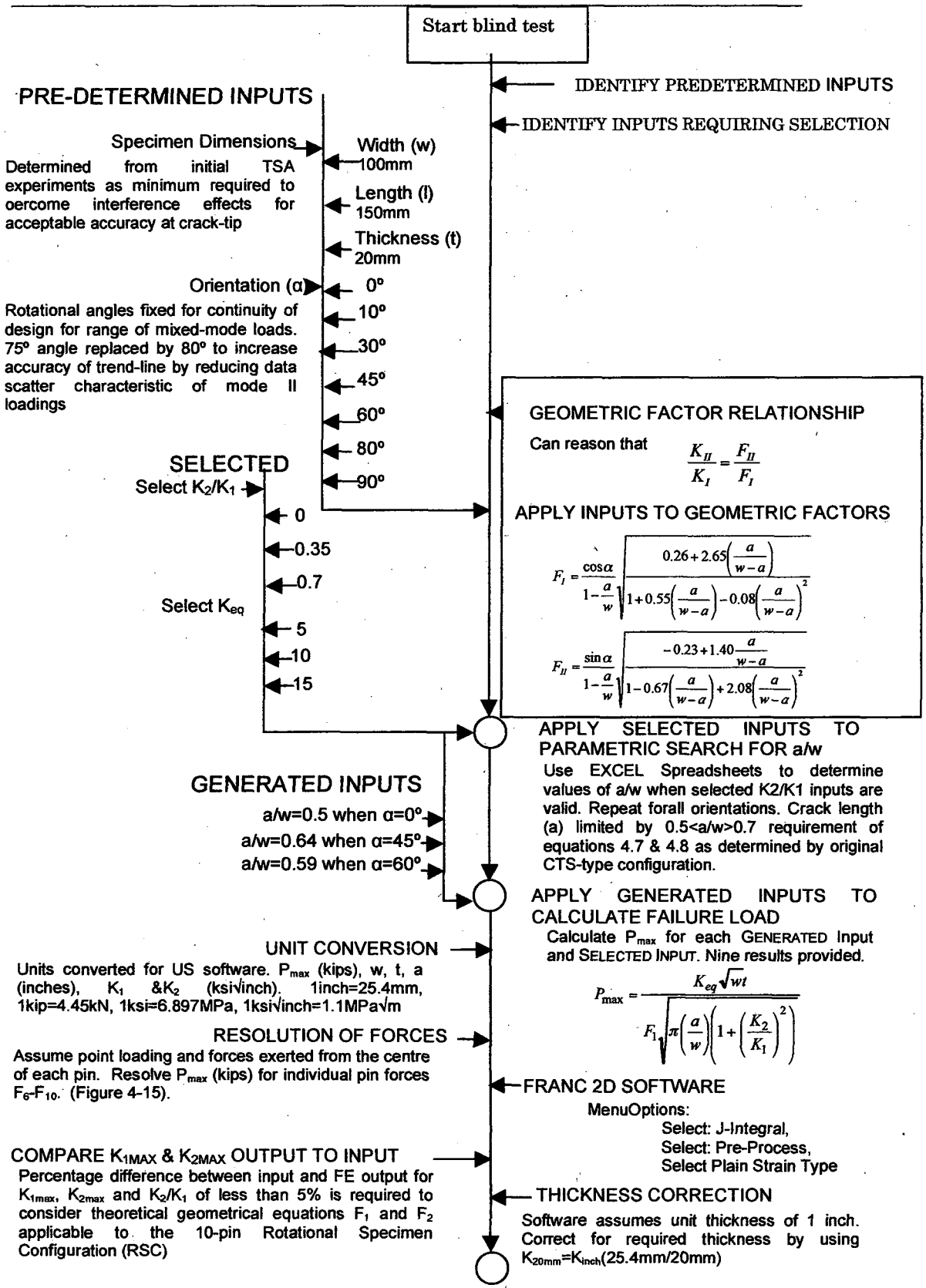

Figure A6- 7 Flow chart to summarise rig-design

References

[1] Lembessis,E., "Evaluation of SIF's for aged sandwich foam using TSA" MPhil transfer, 2006
[2] Anderson,T., "Fracture mechanics-fundamentals and applications" 3rd edition, Taylor and Francis Publishing Group, 2005.
[3] FRANC2D software http://www.cfg.cornell.edu/software/software.htm
[4] Pirondi, A., Nicoletto, G. "Mixed Mode Fracture Envelop of a Structural Adhesive" Conf. Structural Adhesives and Industrial Applications-alternatives to traditional joining techniques., 11-12 Giugno 2001, Italy
[5] Noury, P., Shenoi, R., Sinclair, I., "On Mixed-Mode Fracture of PVC Foam" Int. Journal of Fracture, vol.92, p131-151, 1998, Kluwer Academic Publishers
[6] Benitz, K., Richard, H.A. "A Loading Device for the Creation of Mixed Mode in Fracture Mechanics" Int. Journal of Fracture, vol.22, p-R55-R58, 1983
[7] Sinclair, I. "Blind-test" description from verbal communication and interview. University of Southampton